Construction of cross-layer linked G-octamer *via* conformational control: stable G-quadruplex in H-bond competitive solvent

Ying He[1], Yanbin Zhang[2], Lukasz Wojtas[1], Novruz G. Akhmedov[3], David Thai[1], Heng Wang[1], Xiaopeng Li[1], Hao Guo[2]* and Xiaodong Shi[1]*

[1]Department of Chemistry, University of South Florida, 4202 E. Fowler Avenue, Tampa, Florida 33620, United States.

[2]Department of Chemistry, Fudan University, 2005 Songhu Road, Shanghai, 200438, P. R. China.

[3]Department of Chemistry, West Virginia University, Morgantown, WV 26505, United States.

Electronic Supplementary Information

Table of Contents:

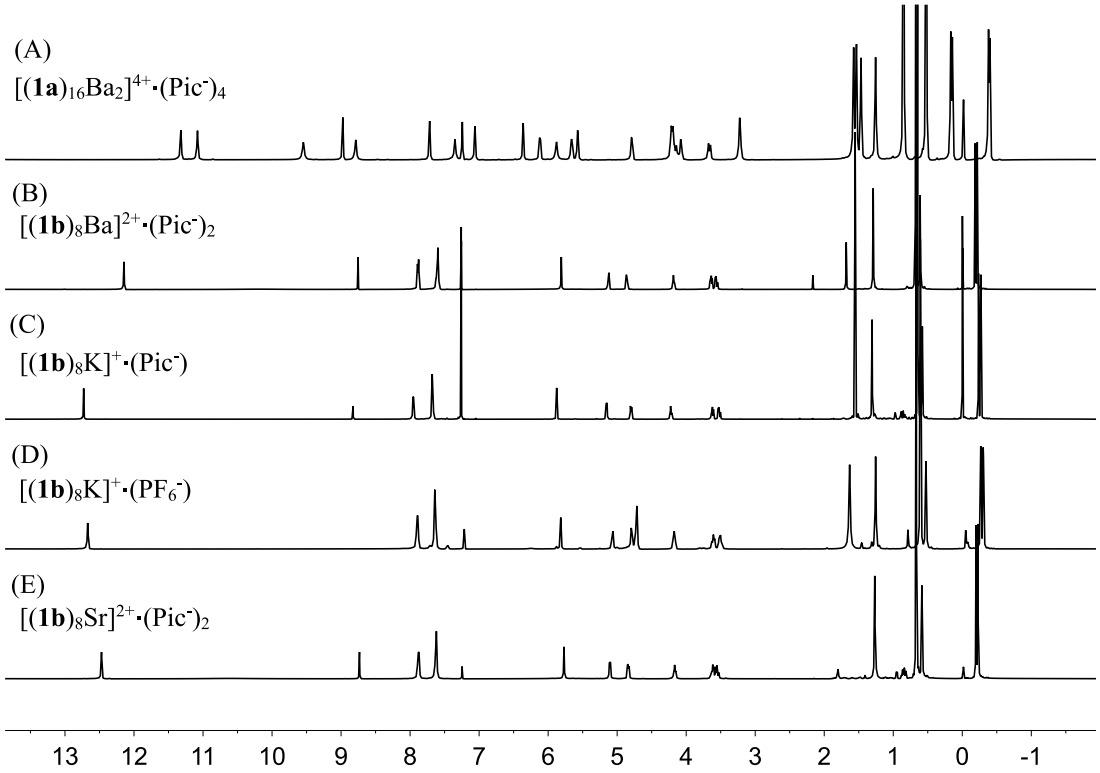

Figure S1. ^{1}H NMR spectra of (A) $[(\mathbf{1a})_{16}Ba_2]^{4+}\bullet(Pic^-)_4$; (B) $[(\mathbf{1b})_8Ba]^{2+}\bullet(Pic^-)_2$; (C) $[(\mathbf{1b})_8K]^{+}\bullet(Pic^-)$; (D) $[(\mathbf{1b})_8K]^{+}\bullet(PF_6^-)$; (E) $[(\mathbf{1b})_8Sr]^{2+}\bullet(Pic^-)_2$.

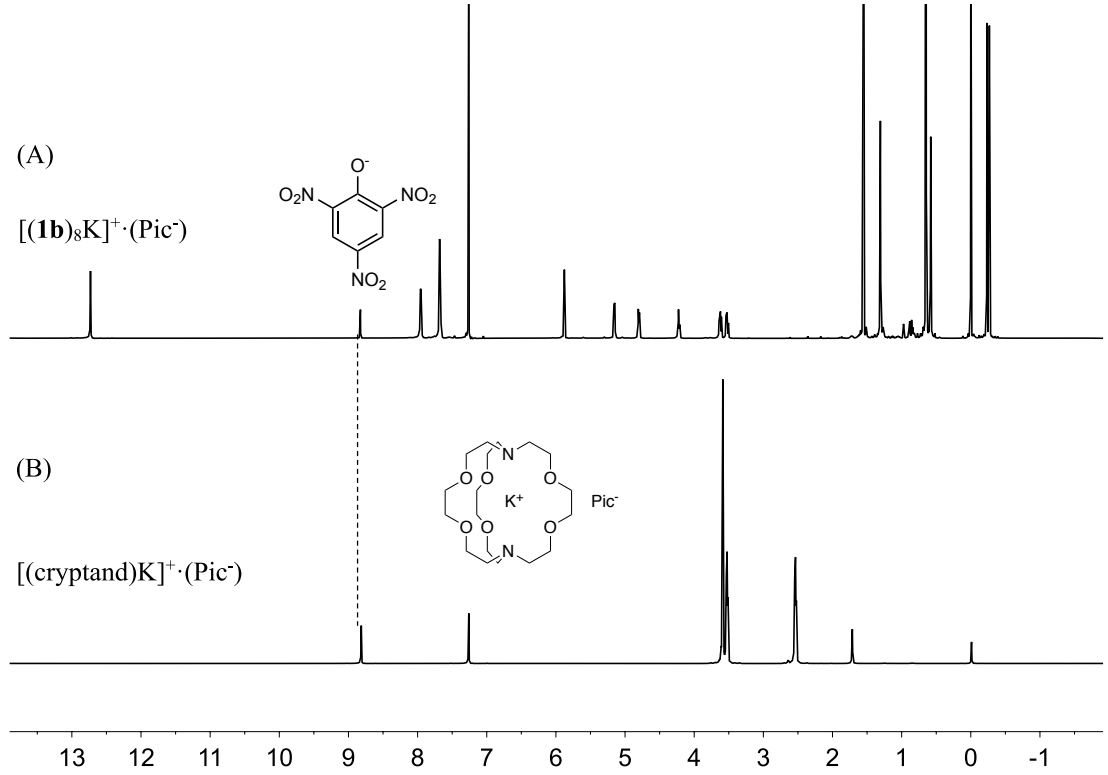

Figure S2. (A) ^{1}H NMR spectra of $[(\mathbf{1b})_8K]^{+}\bullet(Pic^-)$ and (B) ^{1}H NMR spectra of $\{([2.2.2]\text{-cryptand})K\}^{+}\bullet(Pic^-)$. The signal ascribed to free Picrate anion is observed at δ=8.83 ppm compared to picrate bridge at δ=9.00 ppm reported in $[(\mathbf{1a})_{16}Ba_2]^{4+}\bullet(Pic^-)_4$[1]

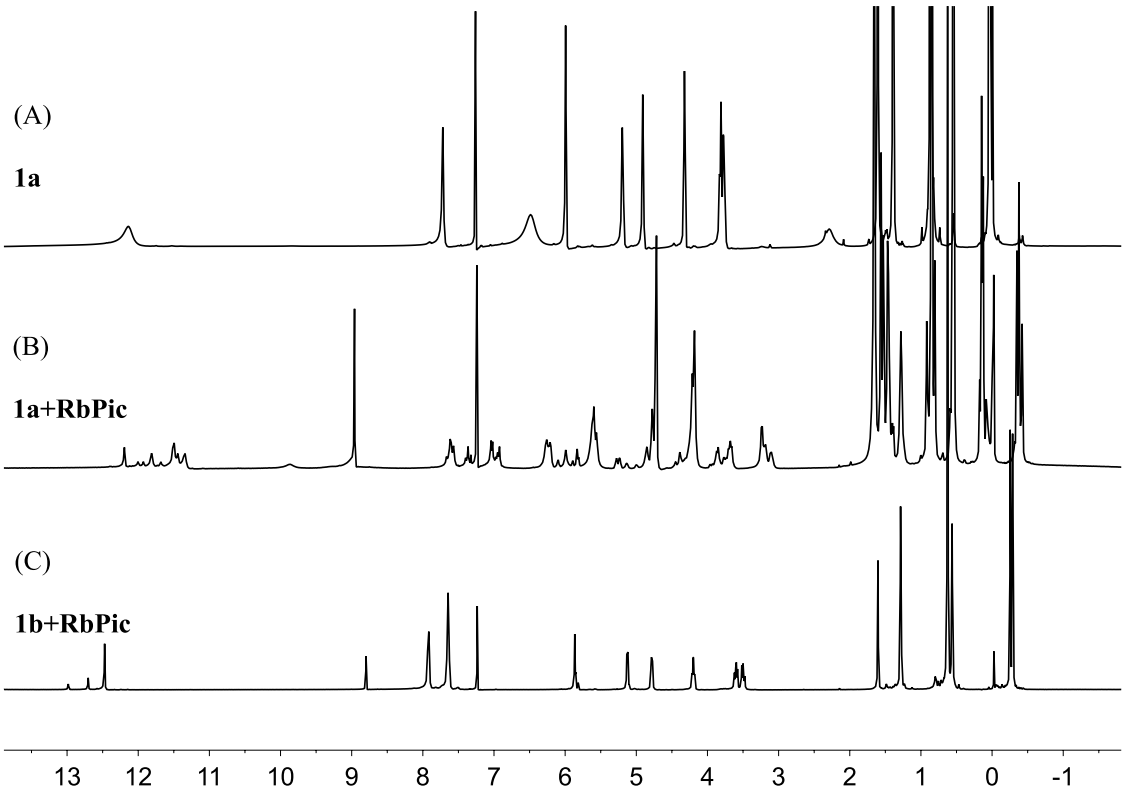

Figure S3. ^{1}H NMR spectra of Rb^{+} binding with guanosine derivatives in $CDCl_3$. (A) **1a** monomer (B) treating **1a** with RbPic yielded messy spectrum indicating no specific G-quadruplex formation. (C) treating **1b** with RbPic gave dominantly one set of signal suggesting the Rb binded G-octamer formation.

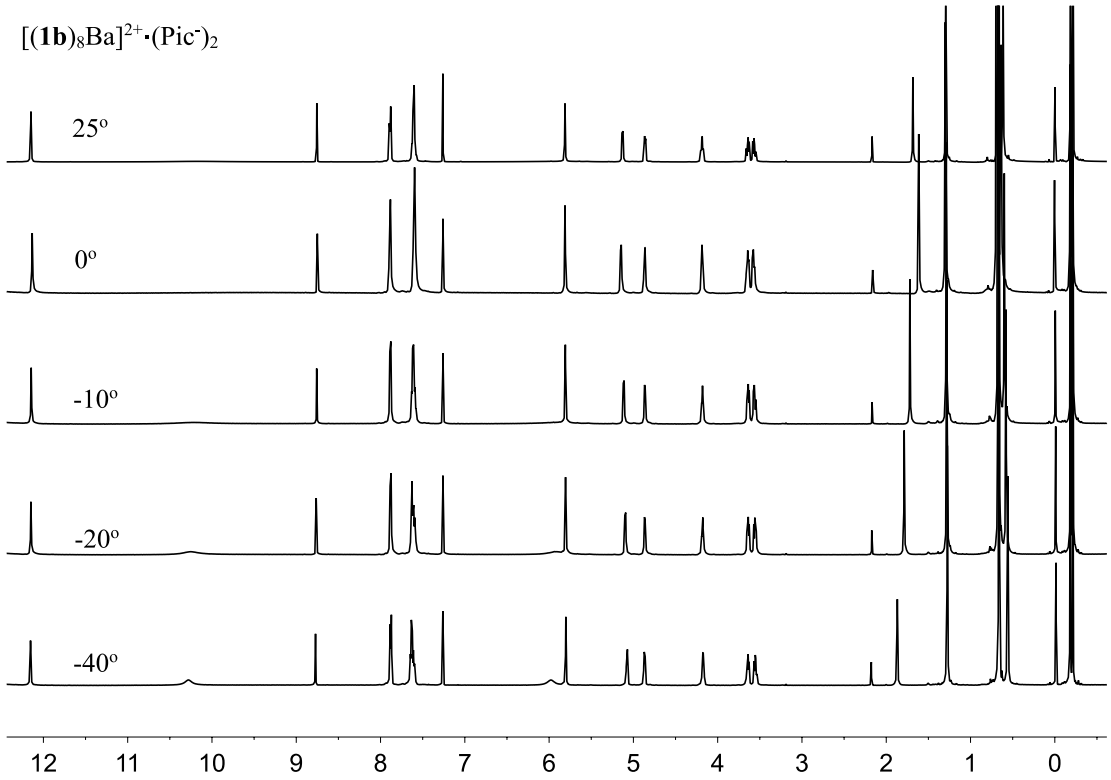

Figure S4. VT NMR spectra of $[(\mathbf{1b})_8Ba]^{2+}\bullet(Pic^{-})_2$ under temperature range from 25°C to -40°C. Two broad peaks of NH_2 showed up starting from 0°C at 10.28 ppm and 5.98 ppm respectively.

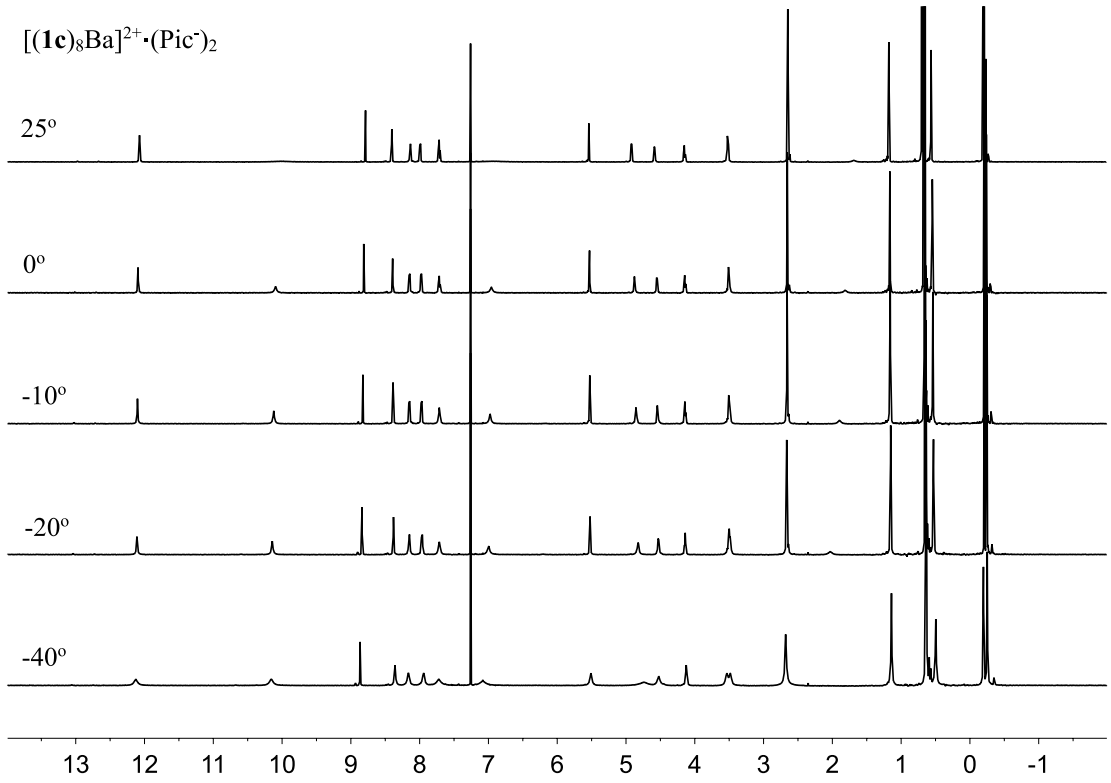

Figure S5. VT NMR spectra of $[(\mathbf{1c})_8Ba]^{2+}\bullet(Pic^-)_2$ under temperature range from 25°C to -40°C. Two broad peaks of NH_2 showed up starting from 0°C at 10.28 ppm and 7.25 ppm respectively.

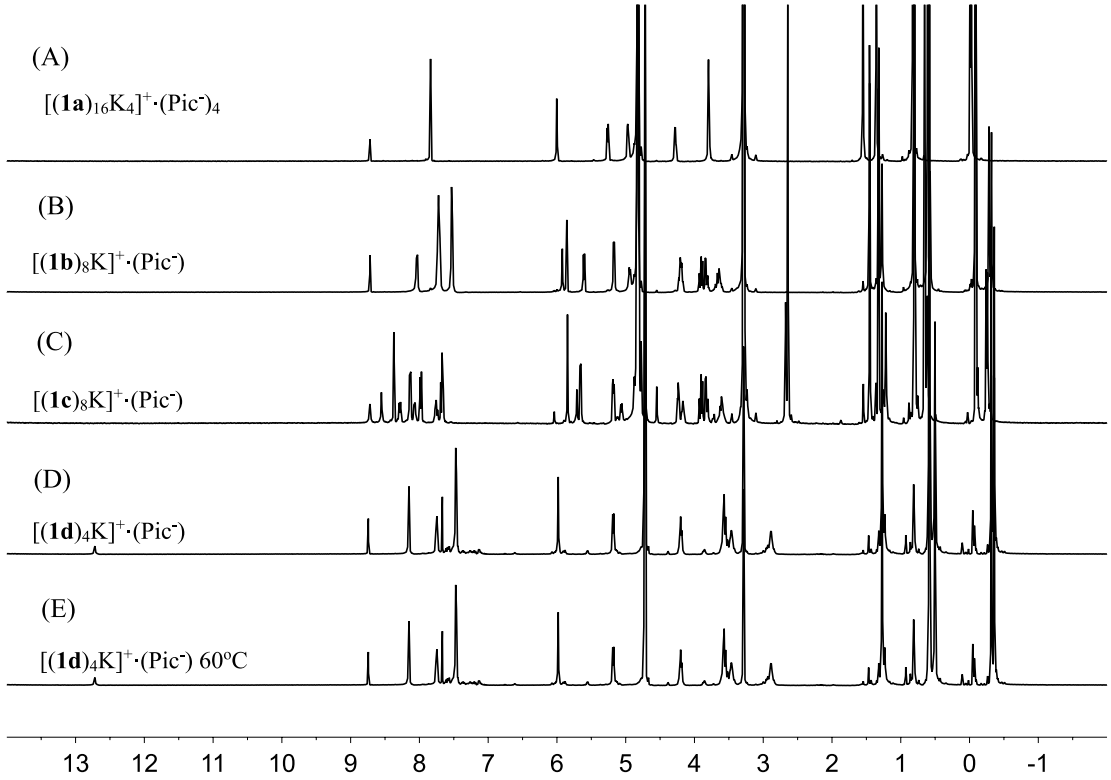

Figure S6. ^1H NMR spectra of G-quadruplex in CD_3OD. (A) $[(\mathbf{1a})_{16}K_4]^{4+}\bullet(Pic^-)_4$; (B) $[(\mathbf{1b})_8K]^+\bullet(Pic^-)$; (C) $[(\mathbf{1c})_8K]^+\bullet(Pic^-)$; (D) $[(\mathbf{1d})_4K]^+\bullet(Pic^-)$; (E) $[(\mathbf{1d})_4K]^+\bullet(Pic^-)$ at 60°C.

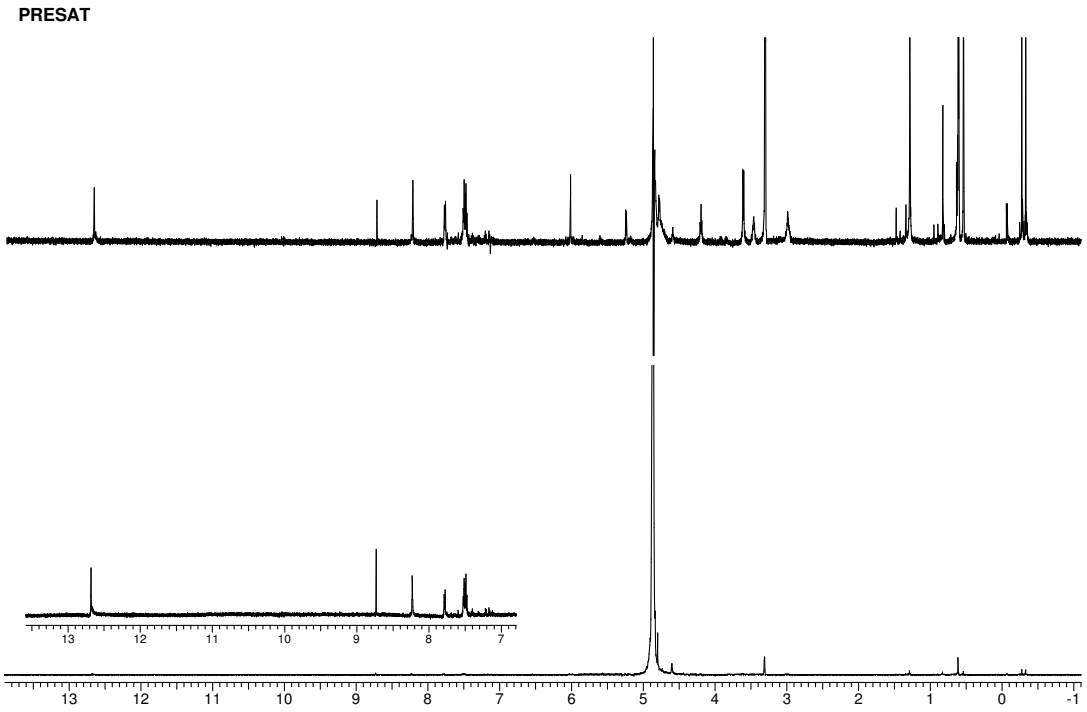

Figure S7. ^{1}H NMR spectra of $[(\mathbf{1d})_4K]^{+}\bullet(Pic^{-})$ in CD_3OH at 25^{o}C. Solvent signal suppression was applied. The peak at 12.7 ppm confirmed to be H1 of G-quadruplex in methanol.

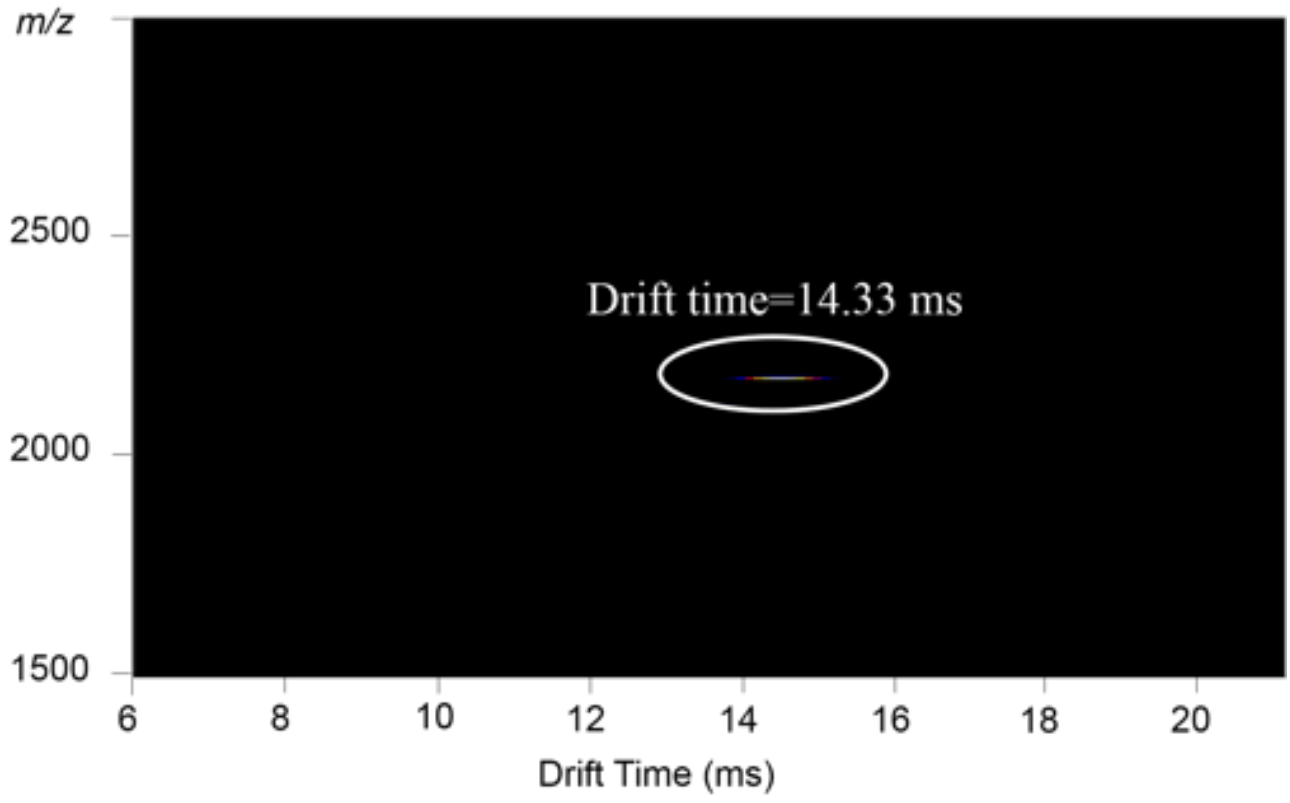

Figure S8. TWIM-MS of $[(\mathbf{1d})_4Ba]^{2+}\bullet(Pic^{-})_2$ in CH_3OH.

Table S1. Comparison of drift time of **1b**-**1d** G-octamer

G-octamer	Drift time (ms)
$[(\mathbf{1b})_8Ba]^{2+}\bullet(Pic^-)_2$ in $CDCl_3$	14.38
$[(\mathbf{1c})_8Ba]^{2+}\bullet(Pic^-)_2$ in $CDCl_3$	15.35
$[(\mathbf{1d})_4Ba]^{2+}\bullet(Pic^-)_2$ in $CDCl_3$	14.22
$[(\mathbf{1d})_4Ba]^{2+}\bullet(Pic^-)_2$ in CD_3OD	14.33

Drift time indicates the diffusion ability of the G-quadruplex, which is in correlation to hydrodynamic radius of the complex. As shown in **Table S1**, the drift time of **1b**-**1d** G-octamer in $CDCl_3$ falls between 14 ms~15 ms, while $[(\mathbf{1c})_8Ba]^{2+}\bullet(Pic^-)_2$ is slightly higher likely due to the acetyl group on aryl substituent. $[(\mathbf{1d})_4Ba]^{2+}\bullet(Pic^-)_2$ in CD_3OD showed similar drift time (14.33 ms) compared with other G-octamers, suggesting a similar hydrodynamic radius.

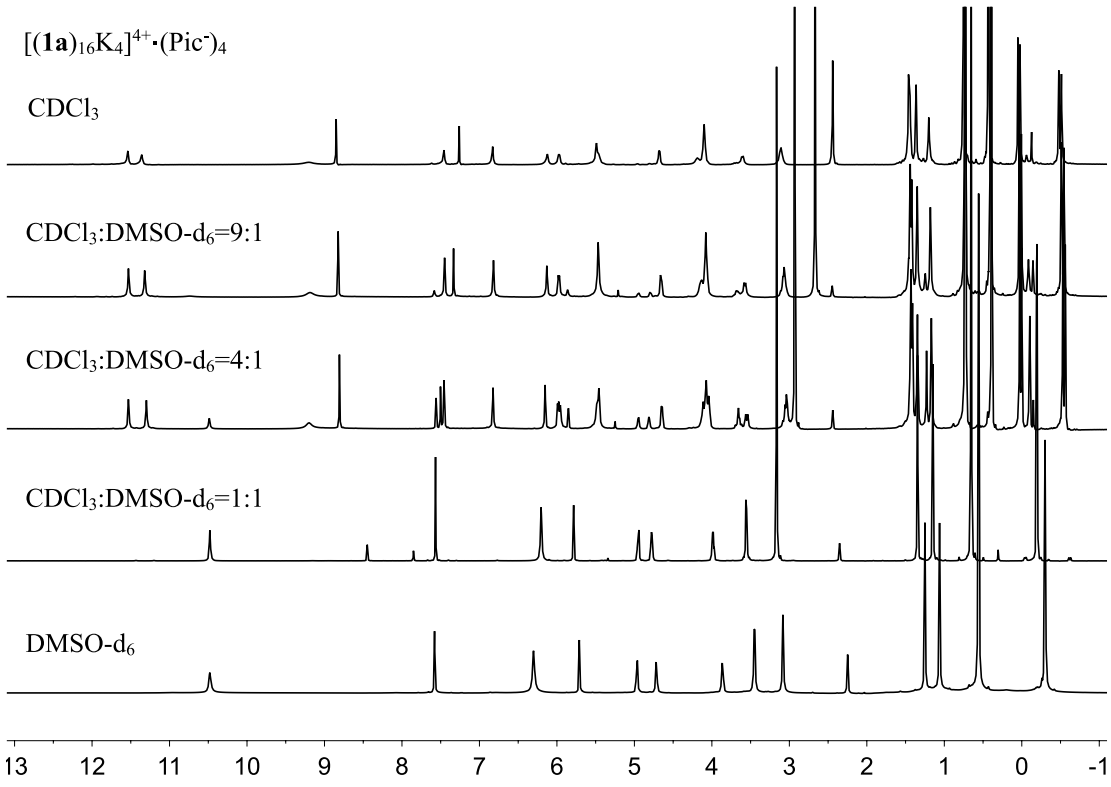

Figure S9. DMSO-d_6 titration: ^{1}H NMR spectra of $[(\mathbf{1a})_{16}K_4]^{4+}\bullet(Pic^-)_4$ in $CDCl_3$:DMSO-d_6 with different ratio.

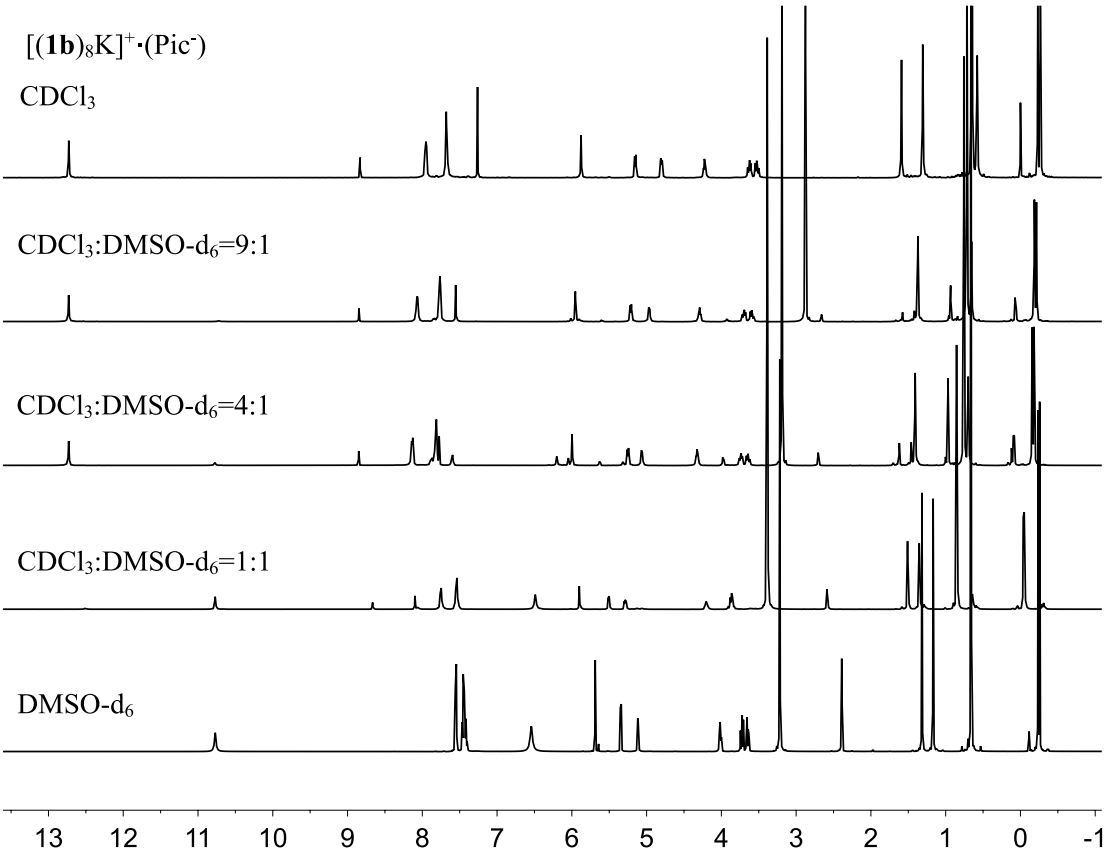

Figure S10. DMSO-d_6 titration: ^{1}H NMR spectra of [(**1b**)$_8$K]$^+$•(Pic$^-$) in $CDCl_3$:DMSO-d_6 with different ratio.

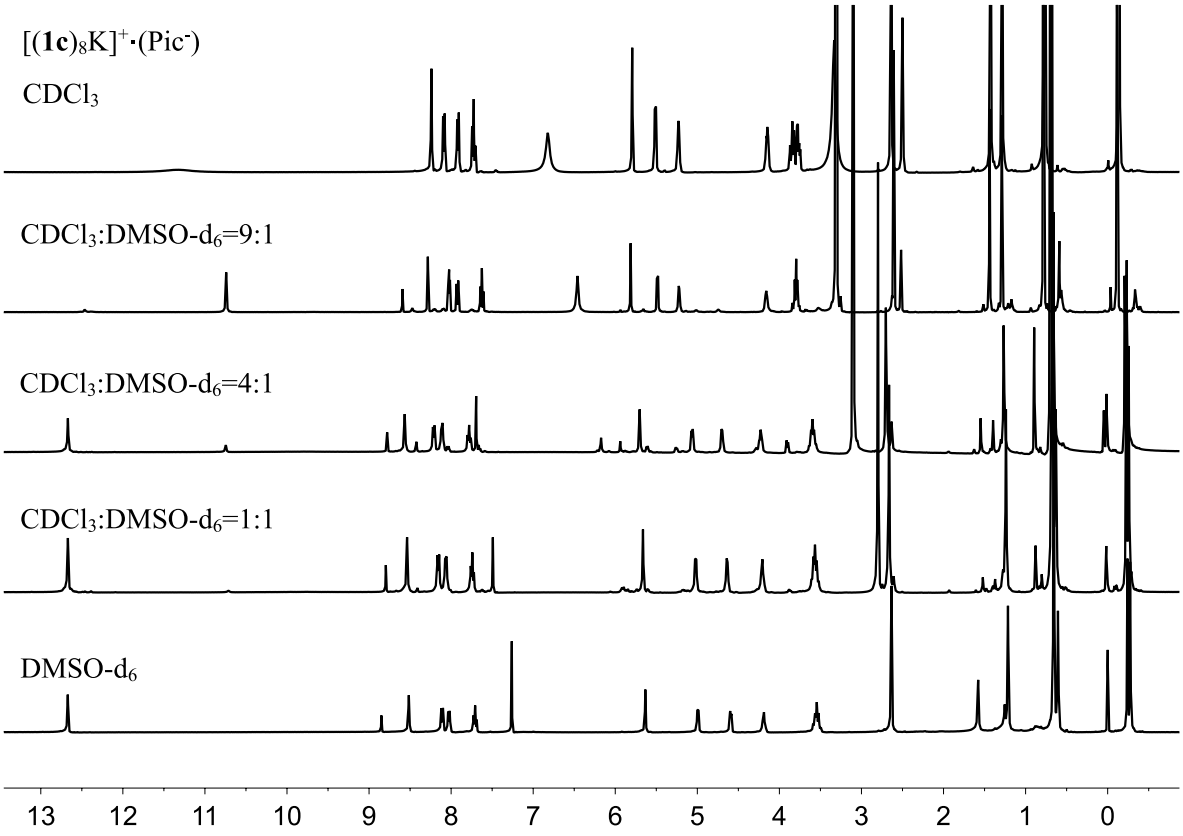

Figure S11. DMSO-d_6 titration: ^{1}H NMR spectra of [(**1c**)$_8$K]$^+$•(Pic$^-$) in $CDCl_3$:DMSO-d_6 with different ratio.

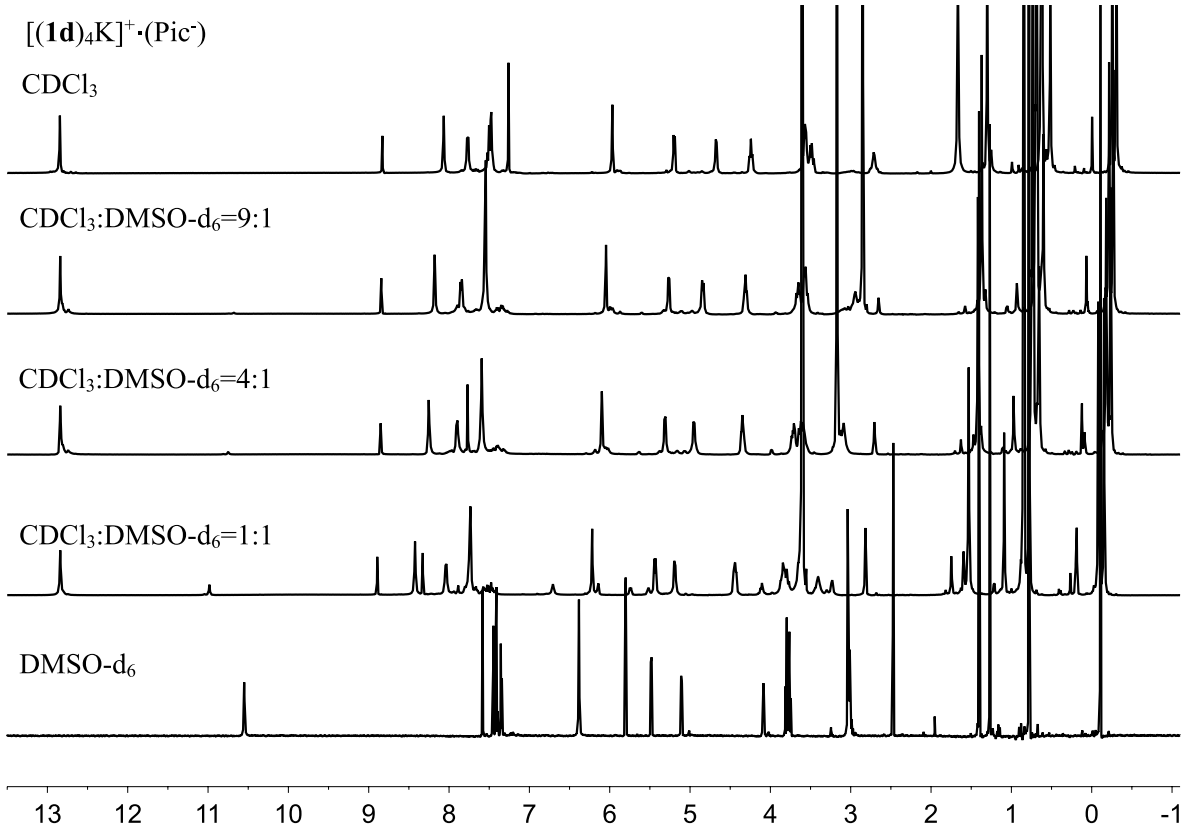

Figure S12. DMSO-d_6 titration: ^{1}H NMR spectra of [(**1d**)$_4$K]$^+$•(Pic$^-$) in $CDCl_3$:DMSO-d_6 with different ratio.

Table S2. Original data from VT ^{1}H NMR spectra of $[(\mathbf{1a})_{16}K_4]^{4+}\bullet(Pic^-)_4$

T(K)	Integration of H1		ln K_{dis}
	complex	monomer	
298.15	100	90.06	-113.94
303.15	100	104.25	-110.90
308.15	100	116.16	-108.67
313.15	100	126.24	-106.96
323.15	100	159.86	-102.17
328.15	100	192.06	-98.51
333.15	100	222.64	-95.62

Table S3. Original data from VT ^{1}H NMR spectra of $[(\mathbf{1b})_8K]^+\bullet(Pic^-)$

T(K)	Integration of H1		ln K_{dis}
	complex	monomer	
273.15	100	12.53	-63.91
288.15	100	21.17	-59.28
303.15	100	32.82	-55.44
308.15	100	38.82	-53.10
313.15	100	48.71	-52.04
318.15	100	58.86	-50.43
323.15	100	71.26	-48.83
328.15	100	85.82	-47.29

Table S4. Original data from VT ^{1}H NMR spectra of $[(\mathbf{1c})_8K]^+\bullet(Pic^-)$

T(K)	Integration of H1		ln K_{dis}
	complex	monomer	
288.15	100	25.24	-58.33
298.15	100	34.45	-55.62
303.15	100	40.01	-54.33
318.15	100	68.31	-49.78
323.15	100	78.03	-48.67
328.15	100	96.01	-46.96
333.15	100	113.92	-45.58

Table S5. Original data from VT ^{1}H NMR spectra of $[(\mathbf{1d})_4K]^+\bullet(Pic^-)$

T(K)	Integration of H1		ln K_{dis}
	complex	monomer	
298.15	100	4.99	-37.64
303.15	100	8.39	-35.08
308.15	100	8.81	-34.84
313.15	100	9.03	-34.72
323.15	100	9.03	-34.72
333.15	100	11.28	-33.62

Van't Hoff plots based on VT NMR spectra

1. For G_{16}-complex, $[(\mathbf{1a})_{16}K_4]^{4+}\bullet(Pic^-)_4$, four picrate anions were bonded with the complex as anion bridge in the solution based on ^{1}H NMR spectra integration. Thus, the equilibrium between complex (G_{16}) and monomer (G_m) was:

$$G_{16} \rightleftharpoons 16\ G_m + 3\ K^+ + 4\ Pic^-$$

Then,

$$K_{dis} = \frac{[G_m]^{16}\,[K^+]^3\,[Pic^-]^4}{[G_{16}]}$$

Freshly synthesized pure complex was applied for ^{1}H NMR study. Thus, for the equilibrium at a specific temperature:

$$[K^+] = 1/4\ [G_m] + [G_{16}];$$
$$[Pic^-] = 1/4\ [G_m]$$

2. For G_8-complexes, $[(\mathbf{1b})_8K]^+\bullet(Pic^-)$ and $[(\mathbf{1c})_8K]^+\bullet(Pic^-)$, as confirmed by ^{1}H NMR spectra and crystal structures, Pic^- was considered as "free" anion in G_8-octamers. Then the equilibrium between complex (G_8) and monomer (G_m) was:

$$G_8 \rightleftharpoons 8\ G_m + K^+$$

Then,

$$K_{dis} = \frac{[G_m]^8\,[K^+]}{[G_8]}$$

Freshly synthesized pure complex was applied for ^{1}H NMR study. Thus, for the equilibrium at a specific temperature:

$$[K^+] = 1/8\ [G_m]$$

3. For G_4-complex, $[(\mathbf{1d})_4K]^+\bullet(Pic^-)$, as confirmed by ^{1}H NMR spectra and crystal structures, Pic^- is considered as free anion in G_4-complex. Then the equilibrium between complex (G_4) and monomer (G_m) was:

$$G_4 \rightleftharpoons 4\ G_m + K^+$$

Then,

$$K_{dis} = \frac{[G_m]^4\,[K^+]}{[G_4]}$$

Freshly synthesized pure complex was applied for ^{1}H NMR study. Thus, for the equilibrium at a specific temperature:

$$[K^+] = 1/4\ [G_m]$$

The Van't Hoff equation is shown below:

$$\ln K_{dis} = -\frac{\Delta H}{R} * (1/T) + \frac{\Delta S}{R}$$

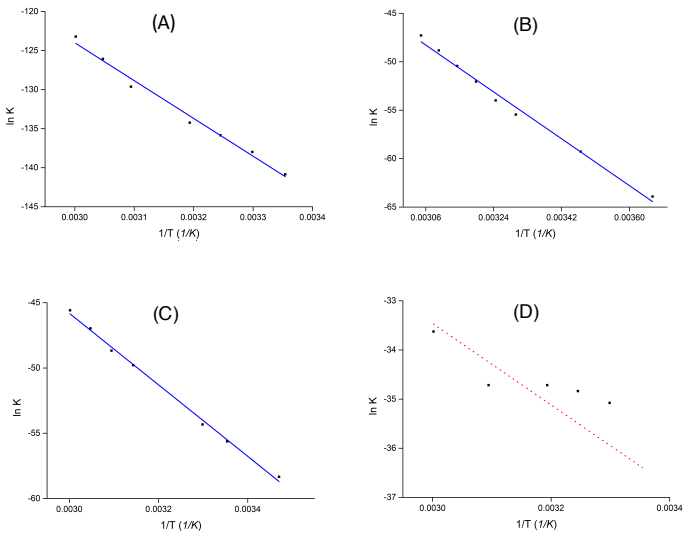

Figure S13. Van't Hoff plot (ln K_{dis} vs 1/T) of (A) $[(\mathbf{1a})_{16}K_4]^{4+}\bullet(Pic^-)_4$, (B) $[(\mathbf{1b})_8K]^+\bullet(Pic^-)$, (C) $[(\mathbf{1c})_8K]^+\bullet(Pic^-)$, (D) $[(\mathbf{1d})_4K]^+\bullet(Pic^-)$ in $CDCl_3$:DMSO-d_6 = 4:1.

Table S6. ΔH and ΔS of G-quadruplex dissociation to monomer

G-quadruplex	ΔH (kJ*mol^{-1})	ΔS (J*mol^{-1}*K^{-1})
$[(\mathbf{1a})_{16}K_4]^{4+}\bullet(Pic^-)_4$	402.70	177.16
$[(\mathbf{1b})_8K]^+\bullet(Pic^-)$	223.53	282.63
$[(\mathbf{1c})_8K]^+\bullet(Pic^-)$	227.58	301.85
$[(\mathbf{1d})_4K]^+\bullet(Pic^-)$	-	-

As shown in Table **S6**, $[(\mathbf{1a})_{16}K_4]^{4+}\bullet(Pic^-)_4$ gave highest absolute value of ΔH due to higher number of H-bond formation in hexadecamer: 1) twice numbers of H-bond within guanosine compared to G_8; 2) H-bond interaction between picrate anion and NH_2. The smaller absolute value of entropy suggests that G_{16}-hexadecamer is not a more organized conformation compared to G_8-octamer.

The absolute values of ΔH and ΔS are both slightly higher for $[(\mathbf{1c})_8K]^+\bullet(Pic^-)$ compared with $[(\mathbf{1b})_8K]^+\bullet(Pic^-)$. This result is in consistent with the observation of formation of cross-layer H-bond in $[(\mathbf{1c})_8K]^+\bullet(Pic^-)$, which is more favorable in regard to enthalpy. However, it could lock the free rotation of C8 substituents on guanosine, resulting in higher entropy loss in complex formation. Overall, the difference is negligible and the stability of the two complexes is comparable considering that cross-layer H-bond is very weak interaction.

For $[(\mathbf{1d})_4K]^+\bullet(Pic^-)$, no linear regression was obtained with the data taken from VT NMR spectra. This might due to the following reason: 1) the kinetic barrier for G-quadruplex $[(\mathbf{1d})_4K]^+\bullet(Pic^-)$ dissociation is so high that the complex remained intact without significant dissociation up to 60°C. 2) only one layer of the G-quadruplex dissociated and an intermediate of partially complexed guanosine was formed, making the process not suitable for the equilibrium equation derived above.

To confirm that kinetic exchange between complex and monomer is extremely slow for $[(\mathbf{1d})_4K]^+\bullet(Pic^-)$, NOESY experiment at 50°C was performed for $[(\mathbf{1b})_8K]^+\bullet(Pic^-)$, $[(\mathbf{1c})_8K]^+\bullet(Pic^-)$ and $[(\mathbf{1d})_4K]^+\bullet(Pic^-)$ and the results are shown below. Signals above 12 ppm corresponding to H1 in complex were chosen for excitation.

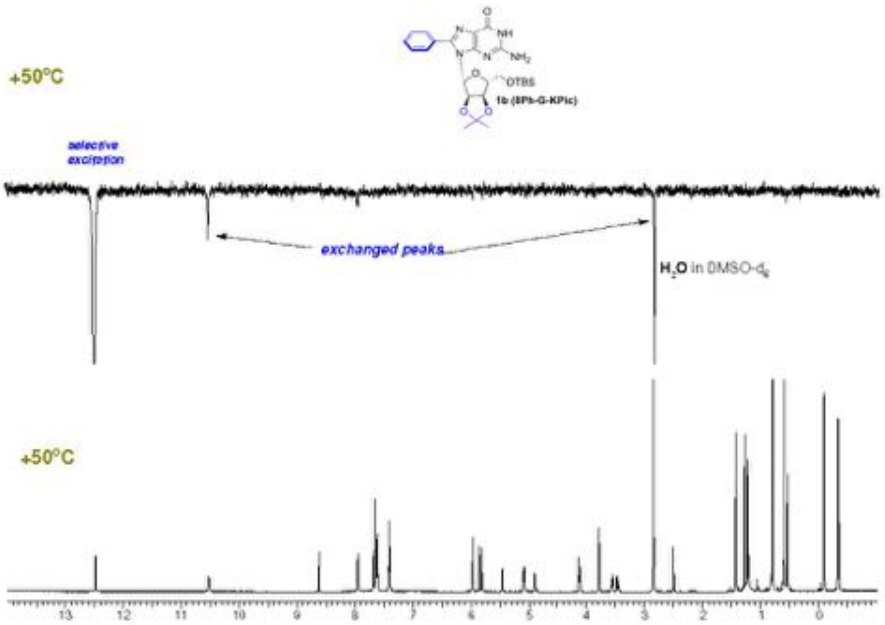

Figure S14. NOESY spectra of $[(\mathbf{1b})_8K]^+\bullet(Pic^-)$

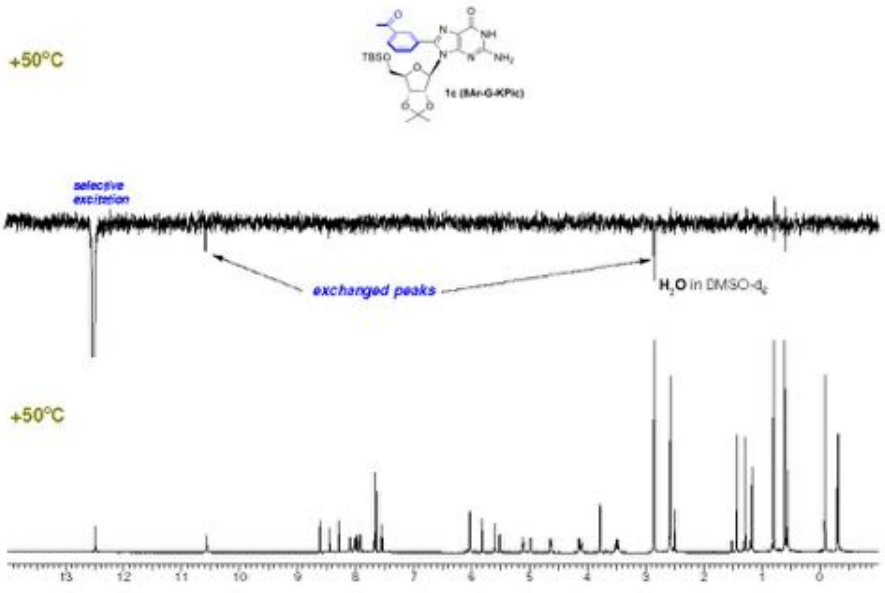

Figure S15. NOESY spectra of $[(\mathbf{1c})_8K]^+\bullet(Pic^-)$

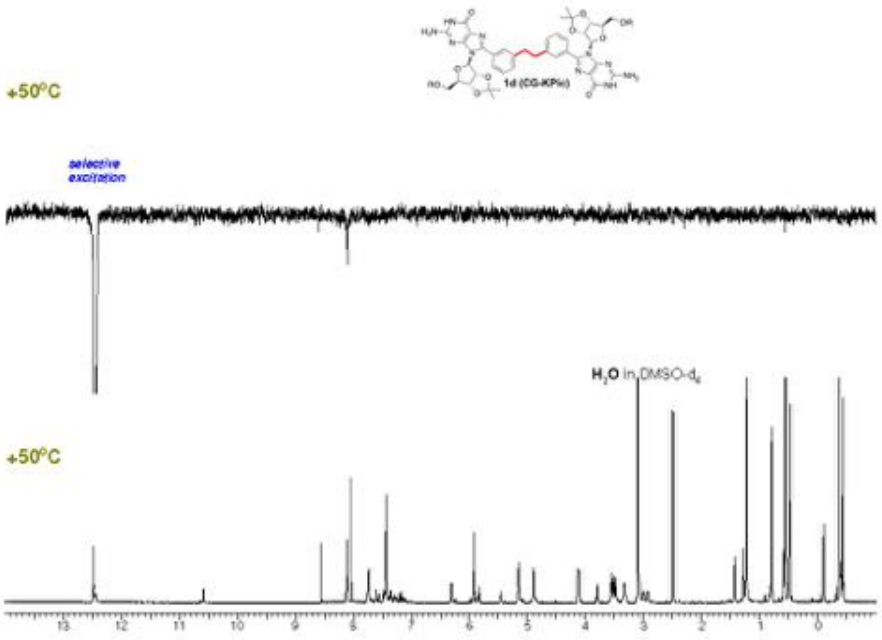

Figure S16. NOESY spectra of $[(\mathbf{1d})_4K]^+ \bullet (Pic^-)$

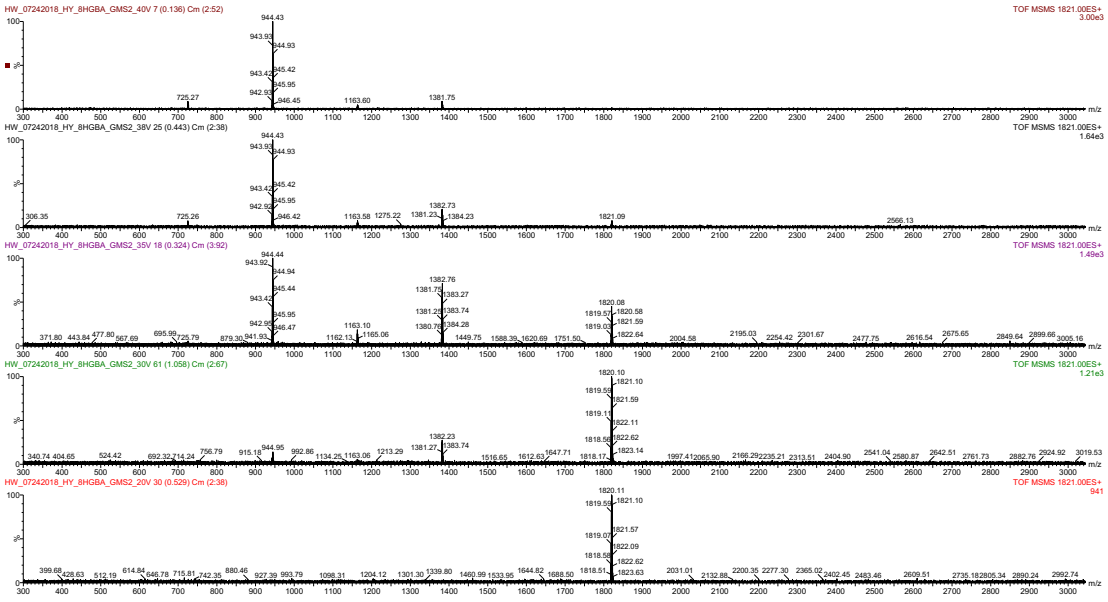

Figure S17. Tandem-MS recorded from $[(\mathbf{1a})_{16}Ba_2]^{4+}\bullet(Pic^-)_4$, corresponding to $[(\mathbf{1a})_8Ba]^{2+}$

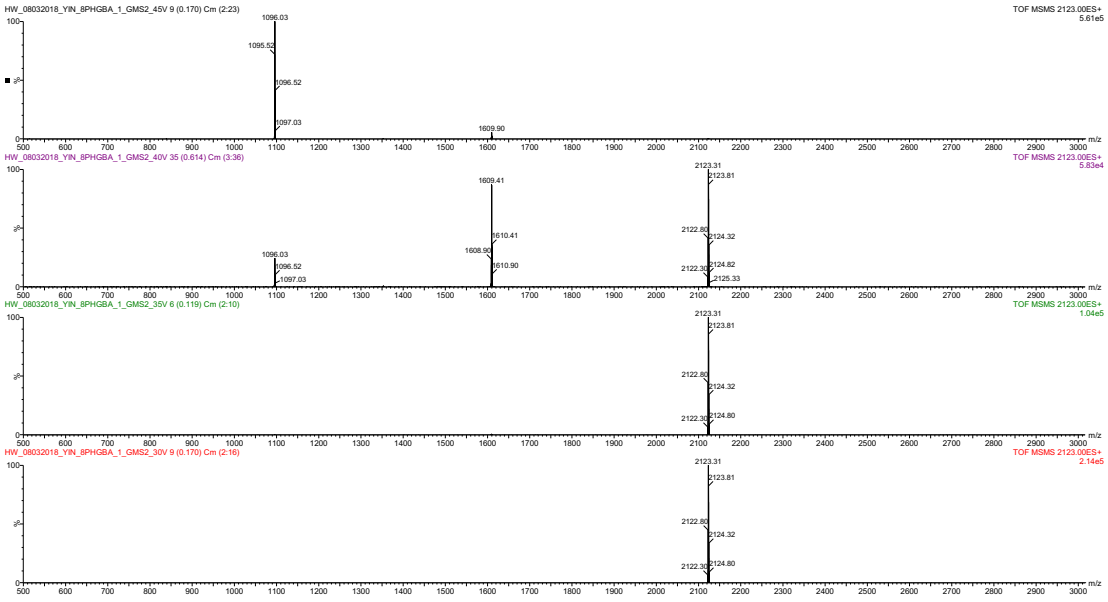

Figure S18. Tandem-MS recorded from $[(\mathbf{1b})_8Ba]^{2+}\bullet(Pic^-)_2$, corresponding to $[(\mathbf{1b})_8Ba]^{2+}$

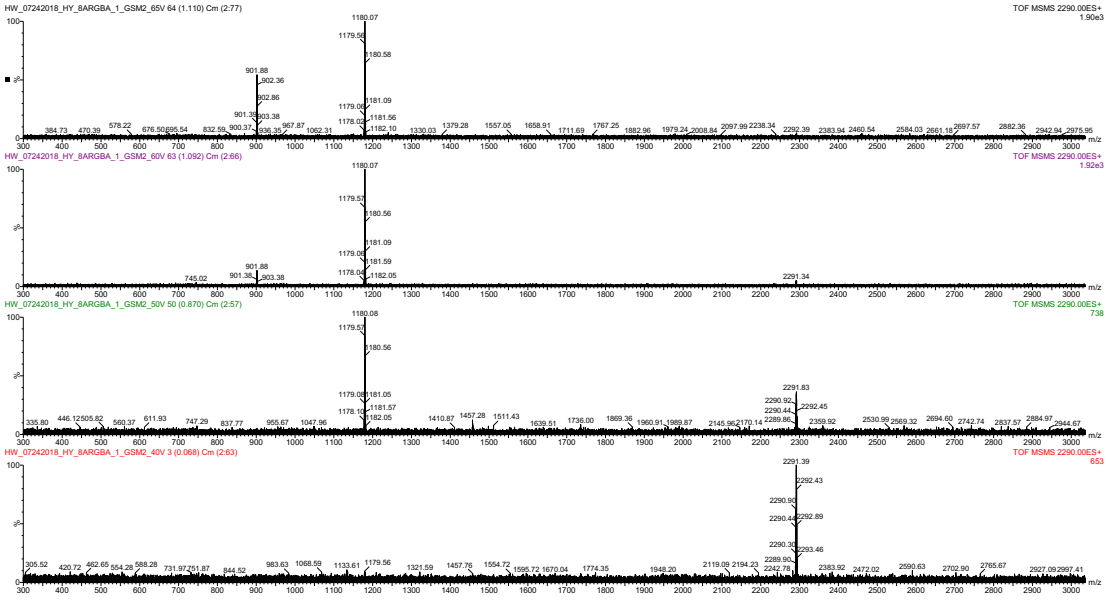

Figure S19. Tandem-MS recorded from $[(\mathbf{1c})_8Ba]^{2+}\bullet(Pic^-)_2$, corresponding to $[(\mathbf{1c})_8Ba]^{2+}$

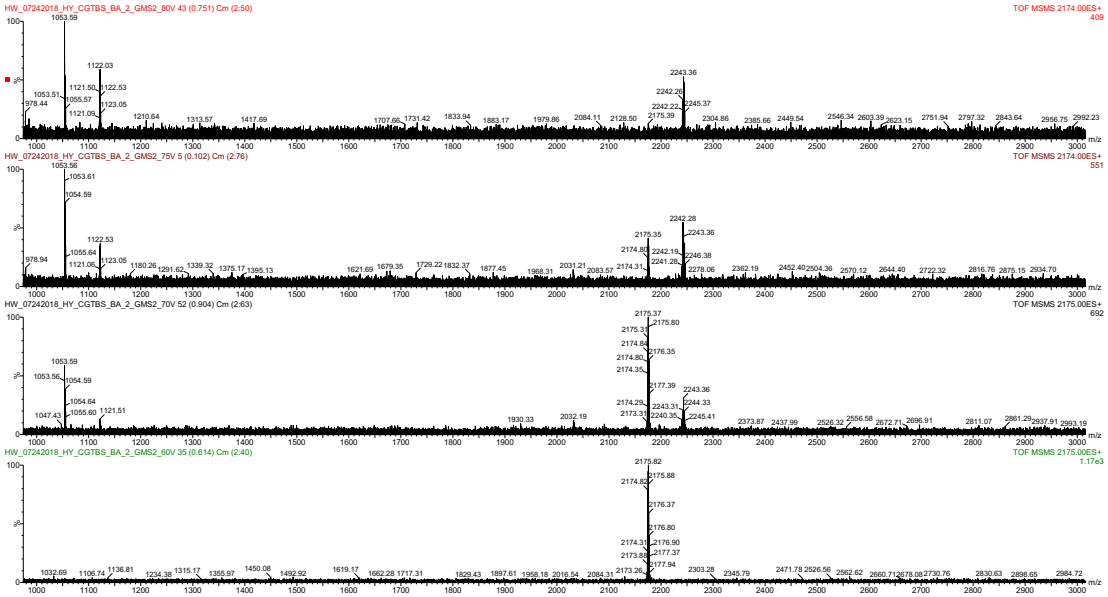

Figure S20. Tandem-MS recorded from $[(\mathbf{1d})_4Ba]^{2+}\bullet(Pic^-)_2$, corresponding to $[(\mathbf{1d})_4Ba]^{2+}$

Supplemental Experimental Procedures and Spectra

I. General Information

Unless otherwise noted, all reagents and solvents were obtained from a commercial provider and used without further purification. Flash column chromatography was performed on 230-430 mesh silica gel.

^{1}H NMR spectra of samples in $CDCl_3$ and DMSO-d_6 were recorded on Agilent 400 MHz spectrometers. ^{1}H NMR (600 MHz), ^{13}C NMR (151 MHz), H-H COSY and gHSQC spectra were acquired at 25^{o}C on a Varian INOVA 600 MHz spectrometer equipped with a triple-resonance z-axis pulsed field gradient 5 mm Probe. Chemical shifts were reported relative to internal tetramethylsilane (δ 0.00 ppm) or $CDCl_3$ (δ 7.26 ppm) or DMSO-d_6 (2.50 ppm) for ^{1}H NMR and $CDCl_3$ (δ 77.00 ppm), DMSO-d_6 (40.00 ppm) for ^{13}C NMR. HRMS were recorded on Agilent 6540 LC/QTOF spectrometer.

ESI-MS and TWIM-MS were recorded on Thermo Scientific Orbitrap Q Extractive Plus (Bremen,Germany) in the positive ion mode. We used the following conditions to perform TWIM-MS experiments: sample cone voltage, 30 V; extraction cone voltage, 3.0 V; ESI capillary voltage, 3 kV; source temperature, 80 ^{o}C; desolvation temperature, 100 ^{o}C; cone gas flow, 10 L/h; desolvation gas flow, 700 L/h (N2); source gas control, 0 mL/min; trap gas control, 2 mL/min; helium cell gas control, 100 mL/min; ion mobility (IM) cell gas control, 30 mL/min; sample flow rate, 5 μL/min; traveling wave height, 25 V; and traveling wave velocity, 1000 m/s.

II. Synthetic Procedure

2.1 Synthesis of S2[2]

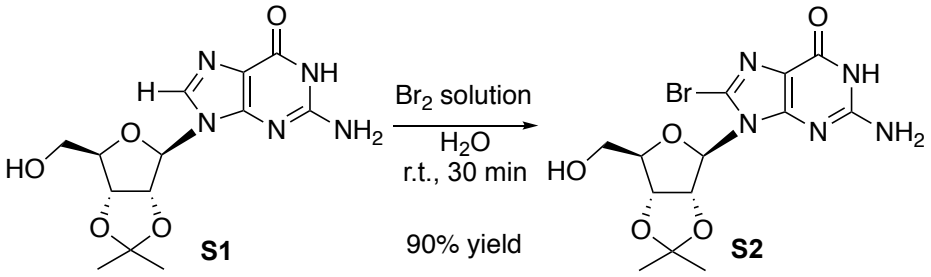

S1 was synthesized according to the literature procedure.[1]

S1 (5.0 g, 15.5 mmol) was suspended in distilled water (300 mL). Saturated Br_2 aqueous solution (300 mL) was added successively to the suspension under vigorous stirring until the yellow color of Br_2 maintained in the solution. After being stirred for an additional 30 min, the precipitate was filtered and washed with water and acetone to afford **S2** as a white solid (5.2 g, 90%).

^{1}H NMR (600 MHz, DMSO-d_6) δ 10.84 (s, 1H), 6.61 (s, 2H), 5.89 (d, J = 1.9 Hz, 1H), 5.76-4.74 (m, 2H), 4.41-3.81 (m, 1H), 3.54 (dd, J = 11.4, 5.8 Hz, 1H), 3.47 (dd, J = 11.5, 6.9 Hz, 1H), 1.52 (s, 3H), 1.32 (s, 3H).

^{13}C NMR (151 MHz, DMSO-d_6) δ 155.39, 153.61, 151.46, 120.17, 117.07, 113.04, 89.79, 88.21, 82.74, 81.48, 61.78, 27.03, 25.31.

HRMS (ESI) calcd. for $[C_{13}H_{16}BrN_5O_5+H]^+$ 404.0387, found 404.0383.

2.1 Synthesis of S3[2]

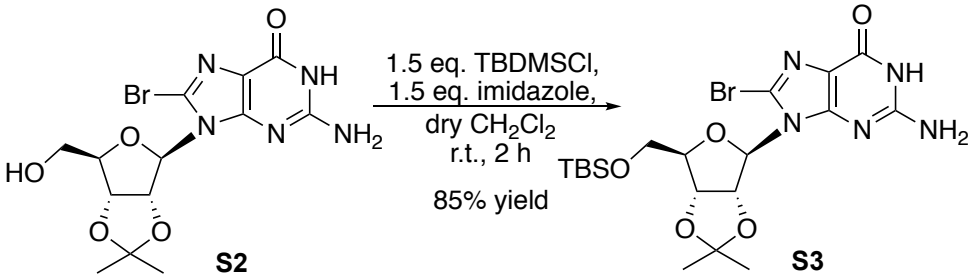

Suspension of **S2** (1.0 g, 2.5 mmol) in dry dichloromethane (40 mL, 0.2 M) was added imidazole (0.3 g, 3.8 mmol) and TBDMSCl (0.6 g, 3.8 mmol) subsequently. The reaction was left overnight. Upon the reaction completed, 1M HCl solution was added and extracted by DCM (3*40 mL). The combined organic layer was washed with saturated Na_2CO_3 solution then dried over $MgSO_4$. Removing the solvent under reduced pressure and recrystallization the pasty solid with dichloromethane and hexane yielded **S3** as white solid (1.1 g, 85%).

^{1}H NMR (600 MHz, DMSO-d_6) δ 6.85 (s, 2H), 5.91 (d, J = 1.4 Hz, 1H), 5.52 (dd, J = 6.3, 1.4 Hz, 1H), 5.15 (dd, J = 6.3, 3.5 Hz, 1H), 4.08 (ddd, J = 7.0, 5.7, 3.5 Hz, 1H), 3.71-3.64 (m, 2H), 1.51 (s, 3H), 1.33 (s, 3H), 0.77 (s, 9H), -0.12 (s, 3H), -0.14 (s, 3H).

^{13}C NMR (151 MHz, DMSO-d_6) δ 157.07, 154.73, 151.53, 119.92, 117.09, 112.81, 89.98, 88.67, 82.89, 81.49, 63.72, 26.90, 25.67, 25.33, 17.91, -5.51, -5.63.

HRMS (ESI) calcd. for $[C_{19}H_{30}BrN_5O_5Si]^+$ 518.1252, found 518.1254.

2.2 Synthesis of 1,2-bis(3-(4,4,5,5-tetramethyl-1,3,2-dioxaborolan-2-yl)phenyl)ethane[3]

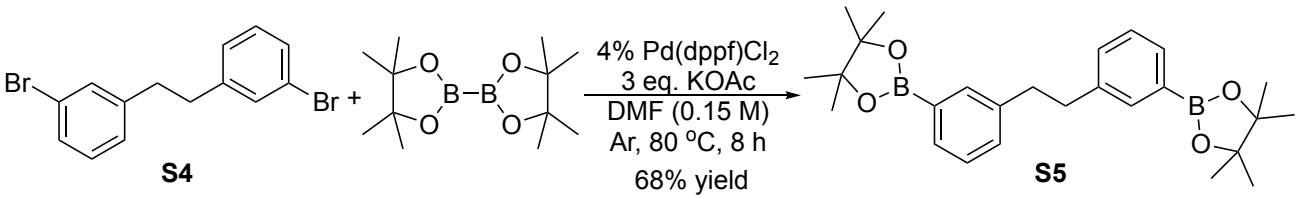

S4 **S5**

S4 was synthesized according to the literature procedure.[4]

To a Schlenk tube was added the **S4** (1.0 g, 2.9 mmol), 4,4,4',4',5,5,5',5'-octamethyl-2,2'-bi(1,3,2-dioxaborolane) (1.5 g, 6.1 mmol), Pd(dppf)Cl_2 (0.070 g, 0.1 mmol) and KOAc (0.88 g, 8.9 mmol). The mixture was evacuated and backfilled with argon for three times, followed by addition of dry DMF (20 mL, 0.15 M). Then the reaction mixture was heated to 80 °C and stirred for 8 h. Upon the completion monitored by TLC (hexane: ethyl acetate=20:1), the reaction mixture was quenched by 1 M HCl solution. After extraction by ether (3*40 mL), the organic layers were combined and dried over Na_2SO_4. The solvent was removed *in vacuo* to obtain crude solid, which was purified by column chromatography (hexane: ethyl acetate=20:1), resulting **S5** as a white solid (0.87 g, 68%).

^{1}H NMR (400 MHz, $CDCl_3$) δ 7.70 (s, 2H), 7.67-7.63 (m, 2H), 7.31-7.26 (m, 4H), 2.91 (s, 4H), 1.35 (s, 24H).

^{13}C NMR (101 MHz, $CDCl_3$) δ 141.19, 134.74, 132.35, 131.41, 127.75, 83.71, 38.22, 24.86.

HRMS m/z (ESI) calcd. for $[C_{26}H_{36}B_2O_4+H]^+$ 435.2872 found 435.2887.

2.3 General procedure to synthesize 8-substitued Guanosine[5]

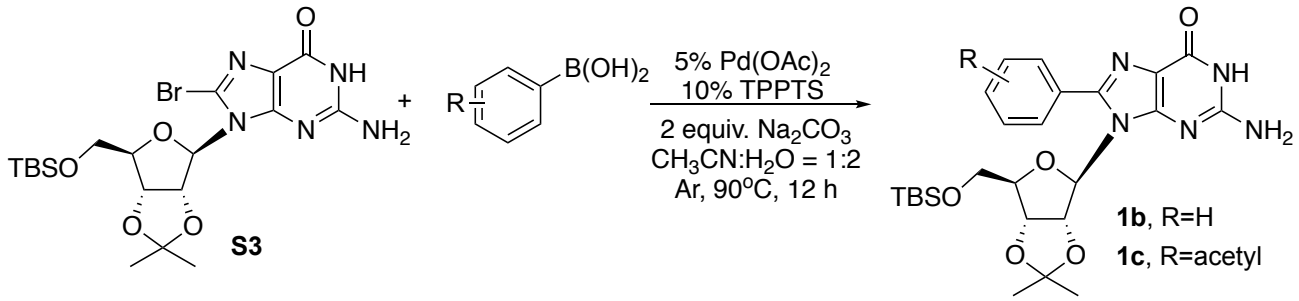

S3

S3 (1.0 g, 1.9 mmol), arylboronic acid (2.85 mmol), $Pd(OAc)_2$ (250 mg, 0.097 mmol), 3,3′,3″-Phosphanetriyltris trisodium salt (120 mg, 0.19 mmol), Na_2CO_3 (400 mg, 3.8 mmol), acetonitrile (3 mL) and water (6 mL) were added to a Schlenk tube under argon. The mixture was degassed by three freeze-pump-thaw cycles. Then the reaction was stirred at 90°C overnight till the completion monitored by LC-MS. 1M HCl solution was added and extracted by DCM (3*40 mL). The combined organic layer was washed with saturated Na_2CO_3 solution then dried over $MgSO_4$. The crude product was purified by column chromatography (DCM:MeOH=10:1). Further recrystallization can be realized using dichloromethane and methanol.

Synthesis of 1b

The reaction of **S3** (1.0 g, 1.9 mmol), phenylboronic acid (348 mg, 2.85 mmol), $Pd(OAc)_2$ (250 mg, 0.097 mmol), 3,3′,3″-Phosphanetriyltris trisodium salt (120 mg, 0.19 mmol), Na_2CO_3 (400 mg, 3.8 mmol), acetonitrile (3 mL) and water (6 mL) afforded **1b** as a white solid (820 mg, 82%).

^{1}H NMR (600 MHz, DMSO-d_6) δ 11.04 (s, 1H), 7.72-7.63 (m, 2H), 7.55 (dt, *J* = 14.9, 7.0 Hz, 3H), 6.68 (s, 2H), 5.80 (d, *J* = 1.2 Hz, 1H), 5.47 (dd, *J* = 6.1, 1.2 Hz, 1H), 5.22 (dd, *J* = 6.2, 3.3 Hz, 1H), 4.13 (ddd, *J* = 8.2, 4.7, 3.3 Hz, 1H), 3.84 (dd, *J* = 11.2, 8.2 Hz, 1H), 3.77 (dd, *J* = 11.3, 4.8 Hz, 1H), 1.43 (s, 3H), 1.28 (s, 3H), 0.78 (s, 9H), -0.12 (s, 3H), -0.14 (s, 3H).

^{13}C NMR (151 MHz, DMSO-d_6) δ 157.80, 154.21, 151.75, 146.68, 134.47, 130.24, 129.87, 129.36, 129.18, 127.73, 117.16, 112.98, 90.01, 89.56, 83.68, 82.38, 64.59, 27.30, 26.17, 25.72, 18.43, -4.97, -5.09.
HRMS m/z (ESI) calcd. for $[C_{25}H_{35}N_5O_5Si+H]^+$ 514.2480 found 514.2495 .

Synthesis of 1c

The reaction of **S3** (1.0 g, 1.9 mmol), (3-acetylphenyl)boronic acid (465 mg, 2.85 mmol), $Pd(OAc)_2$ (250 mg, 0.097 mmol), 3,3′,3″-Phosphanetriyltris trisodium salt (120 mg, 0.19 mmol), Na_2CO_3 (400 mg, 3.8 mmol) acetonitrile (3 mL) and water (6 mL) afforded **1c** as a white solid (801 mg, 76%)

^{1}H NMR (600 MHz, DMSO-d_6) δ 10.89 (s, 1H), 8.23 (s, 1H), 8.09 (d, *J* = 7.8 Hz, 1H), 7.91 (d, *J* = 7.4 Hz, 1H), 7.73 (t, *J* = 7.7 Hz, 1H), 6.68 (s, 2H), 5.79 (s, 1H), 5.49 (d, *J* = 6.2 Hz, 1H), 5.22 (dd, *J* = 6.2, 3.3 Hz, 1H), 4.21-4.08 (m, 1H), 3.85-3.81 (m, 1H), 3.78-3.74 (m, 1H), 2.64 (s, 3H), 1.42 (s, 3H), 1.28 (s, 3H), 0.77 (s, 9H), -0.13 (s, 3H), -0.14 (s, 3H).

^{13}C NMR (151 MHz, DMSO-d_6) δ 197.33, 156.68, 153.42, 151.29, 145.58, 137.18, 133.03, 130.16, 129.26, 129.04, 128.63, 116.79, 112.54, 89.64, 89.27, 83.20, 81.89, 64.08, 26.77, 25.70, 25.25, 17.96, -5.46, -5.57.
HRMS m/z (ESI) calcd. for $[C_{27}H_{37}N_5O_6Si+H]^+$ 556.2586 found 556.2601.

2.4 Synthesis of 1d' and 1d

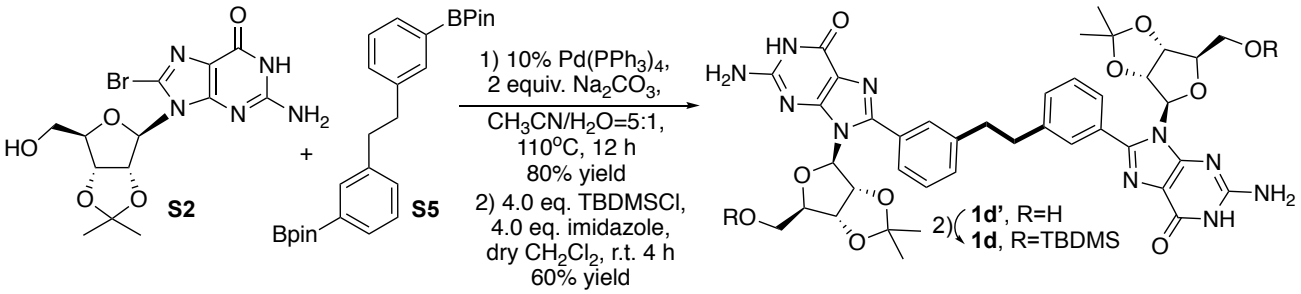

S2 (500 mg, 1.24 mmol), **S5** (267 mg, 0.62 mmol), $Pd(PPh_3)_4$ (143 mg, 0.124 mmol), Na_2CO_3 (262 mg, 2.48 mmol) was added to a 100 mL Schlenk tube. Mixture of acetonitrile and water (5:1, 24 mL) was added to the mixture under argon with vigorous stir. The reaction was heated to 110 °C for 12 h till completion as monitored by LC-MS. Then water (20 mL) was added before cooling the reaction in fridge for 1 h. The reaction mixture was filtered, and the residue was washed with water to give **1d'** as white solid (819 mg, 80%).

^{1}H NMR (400 MHz, DMSO-d_6) δ 10.91 (s, 2H), 7.61 (s, 2H), 7.51-7.31 (m, 6H), 6.62 (s, 4H), 5.80 (d, *J* = 2.1 Hz, 2H), 5.40 (dd, *J* = 6.2, 2.0 Hz, 2H), 5.16 (dd, *J* = 6.3, 3.6 Hz, 2H), 4.99-4.84(m, 2H), 4.20-3.96 (m, 2H), 3.73-3.61(m, 2H), 3.61-3.52 (m, 2H), 3.03 (s, 4H), 1.42 (s, 6H), 1.27 (s, 6H).
HRMS m/z (ESI) calcd. for $[C_{40}H_{44}N_{10}O_{10}+H]^+$ 825.3315 found 825.3318.

tert-Butyldimethylsilyl chloride (513 mg, 3.4 mmol) and imidazole (231 mg, 3.4 mmol) was added to **1d'** (700 mg, 0.85 mmol) in dry dichloromethane (5 mL) and stirred for 4 h. Upon the reaction completion, 1M HCl solution was added and extracted by DCM (3*40 mL). The organic layer was washed with saturated Na_2CO_3 solution then dried over $MgSO_4$. Solvent was removed under reduced pressure and the crude product was purified by column chromatography (DCM: MeOH=10:1) to yield **1d** as white solid (523 mg, 60%)

^{1}H NMR (600 MHz, DMSO-d_6) δ 10.82 (s, 1H), 7.87-7.83 (m, 1H), 7.72 (dt, *J* = 7.6, 1.5 Hz, 1H), 7.68 (t, *J* = 7.6 Hz, 1H), 7.62 (dt, *J* = 7.6, 1.5 Hz, 1H), 6.65 (s, 1H), 6.07 (d, *J* = 1.6 Hz, 1H), 5.75 (dd, *J* = 6.3, 1.6 Hz, 1H), 5.38 (dd, *J* = 6.3, 3.6 Hz, 1H), 4.35 (ddd, *J* = 7.6, 5.1, 3.6 Hz, 1H), 4.11-3.97 (m, 2H), 2.74 (p, *J* = 1.9 Hz, 2H), 1.67 (s, 3H), 1.54 (s, 3H), 1.04 (s, 9H), 0.16 (s, 3H), 0.16 (s, 3H).

^{13}C NMR (151 MHz, DMSO-d_6) δ 156.21, 152.95, 150.98, 146.29, 141.55, 129.61, 129.13, 128.69, 128.19, 126.22, 116.55, 112.45, 89.42, 88.33, 82.75, 81.66, 63.82, 36.33, 26.58, 25.36, 25.08, 17.55, -5.76, -5.84. HRMS m/z (ESI) calcd. for $[C_{52}H_{72}N_{10}O_{10}Si_2+H]^+$ 1053.5044 found 1053.5055.

2.5 General procedure for $(1)_8M^{n+}X^-_n$ complex preparation

To a solution of **1** (10 mg) in $CDCl_3$ (1 mL) was added the MCl_n (0.125 equiv.) and NaX (equivalents depend on the cation M^{n+} charge) in deionized H_2O (1 mL). After stirring for 2 h, the organic layer was separated and washed with deionized H_2O (2*1 mL). Removing the solvent by slow evaporation gave the crystalline G-quadruplex.

III. NMR Characterization of compounds

1. **1b**

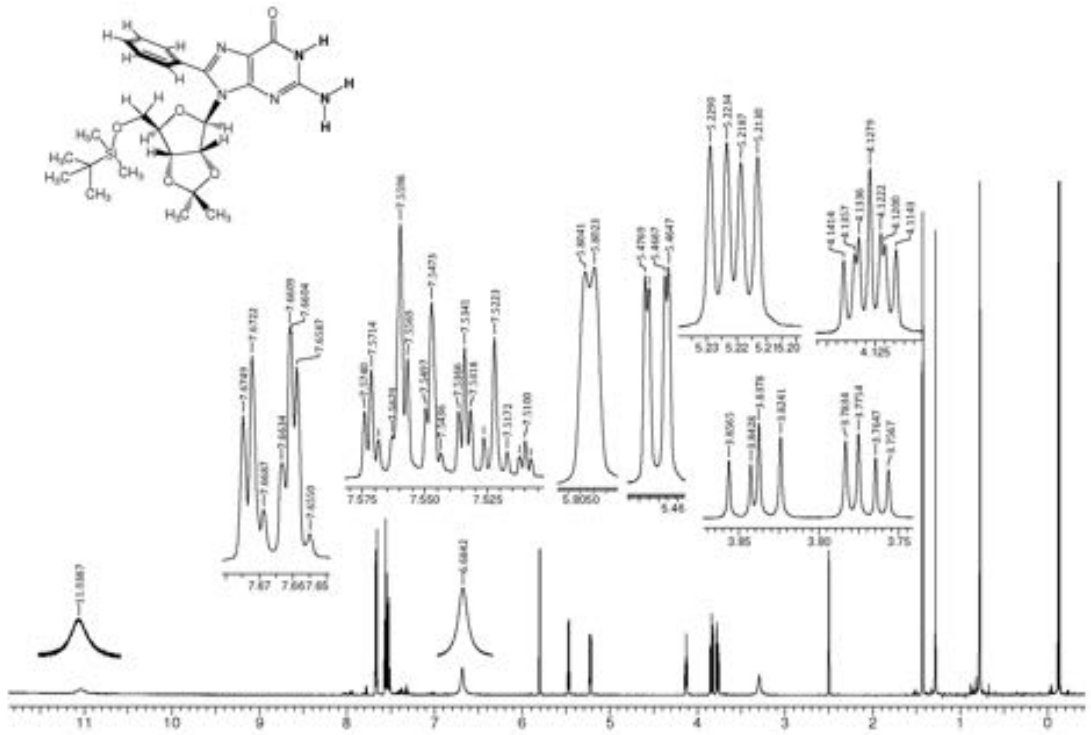

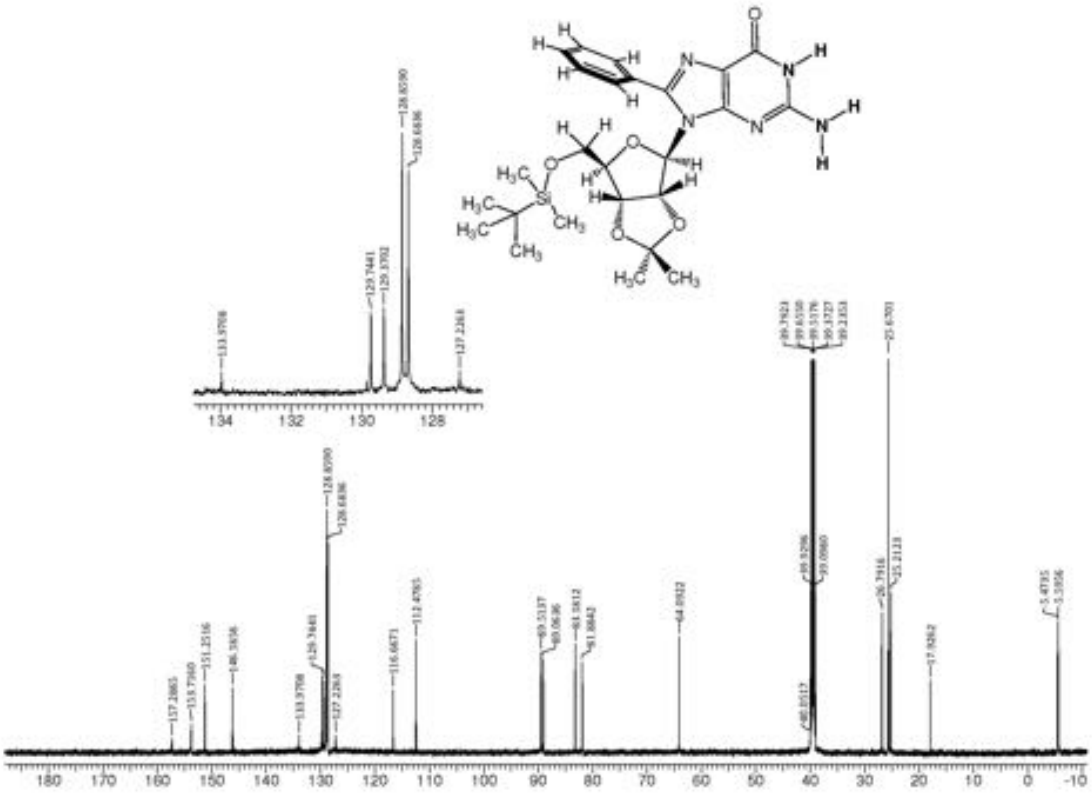

2. **1c**

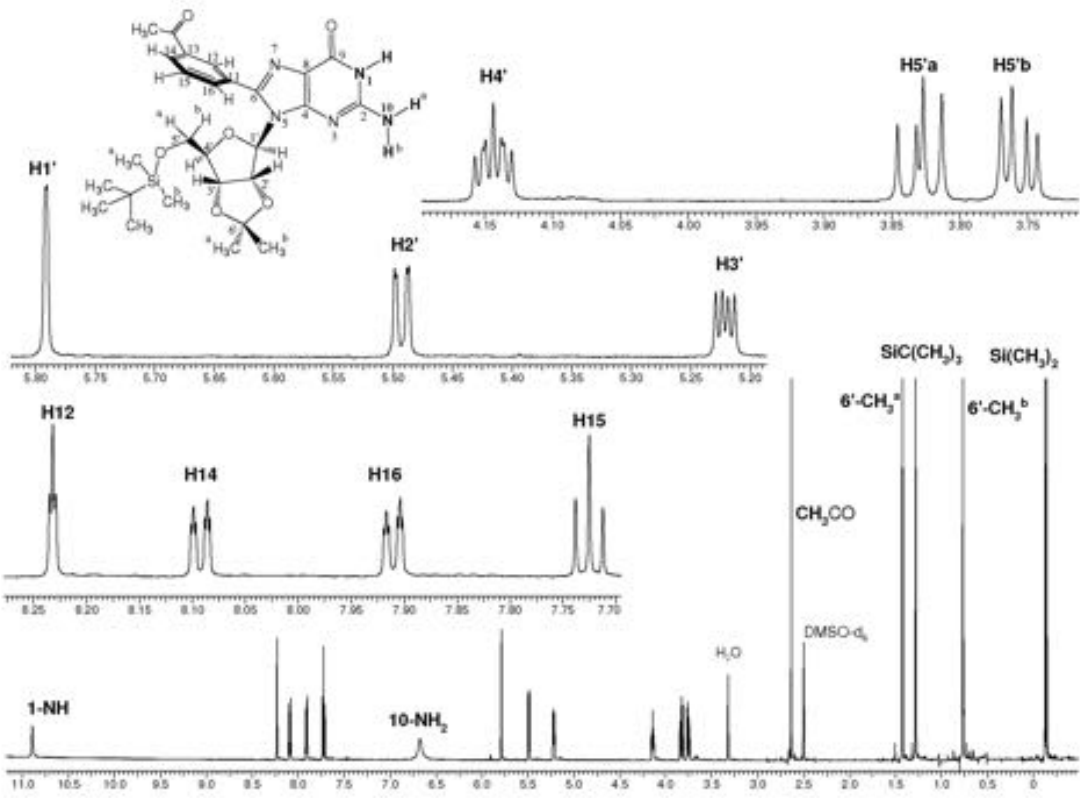
H1'
H4'
H5'a
H5'b
H2'
H3'
H12
H14
H16
H15
SiC(CH3)3
Si(CH3)2
6'-CH3a
6'-CH3b
CH3CO
DMSO-d6
H2O
1-NH
10-NH2

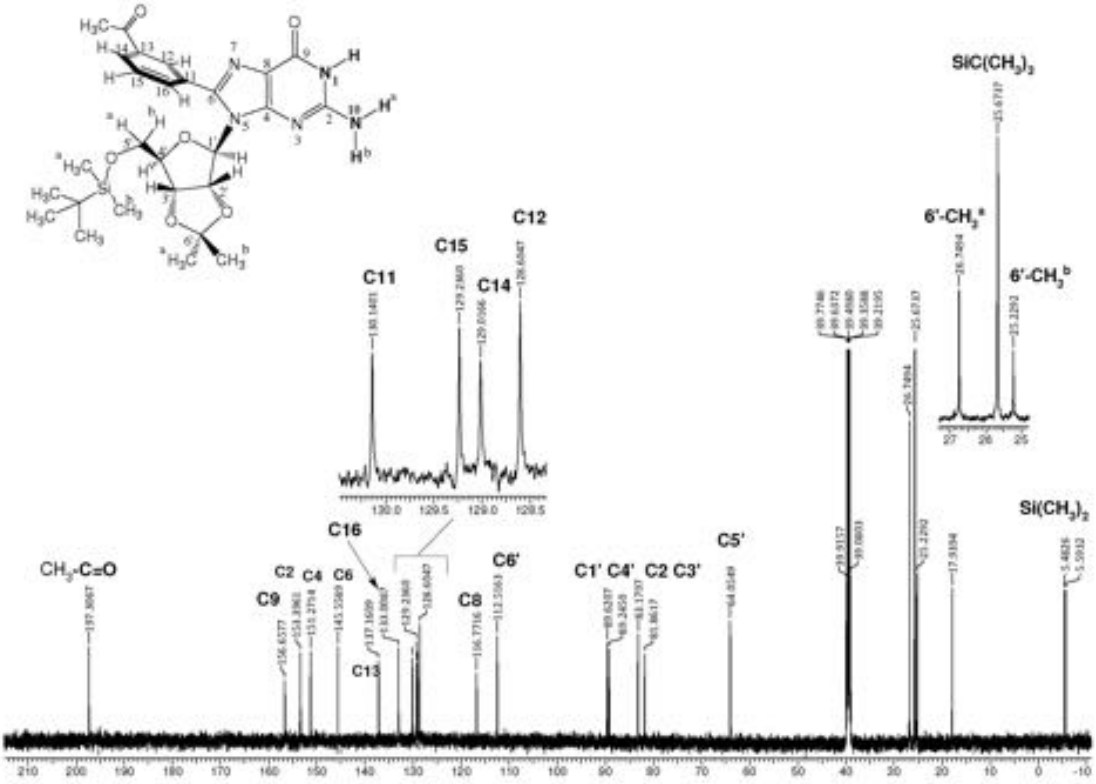
C11
C15
C14
C12
SiC(CH3)3
6'-CH3a
6'-CH3b
Si(CH3)2
C16
C2
C4
C6
C9
C13
C8
C6'
C1' C4' C2 C3'
C5'
CH3-C=O

3. **1d'**

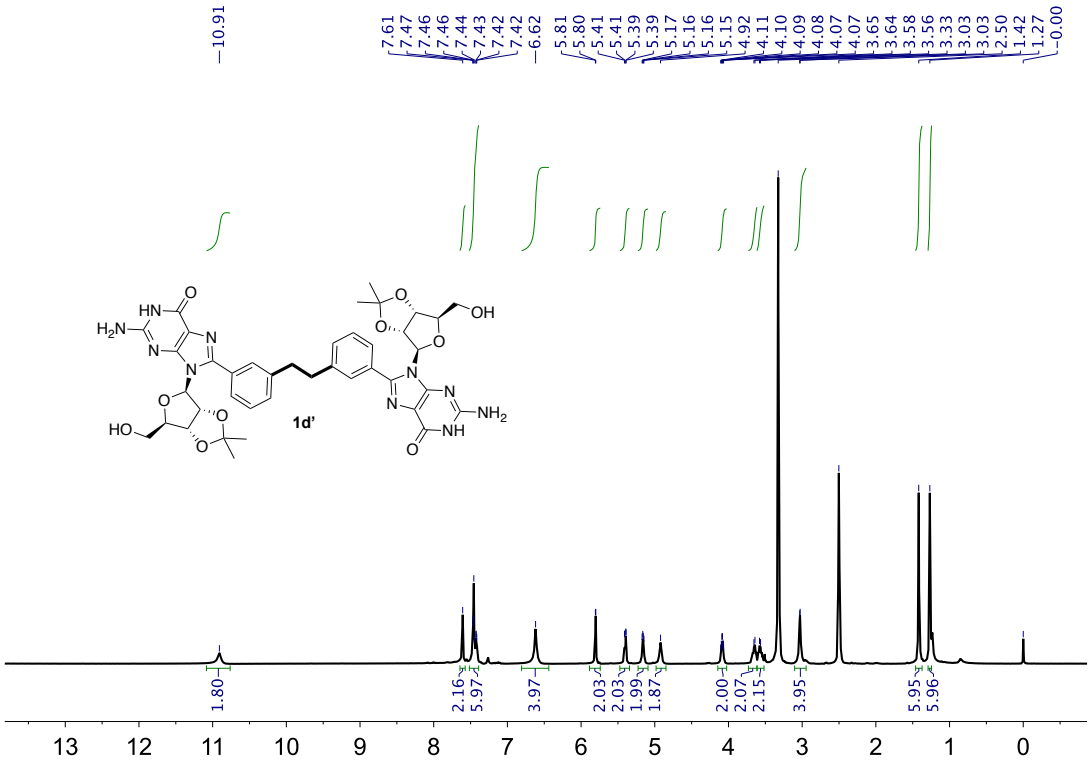
10.91
7.61
7.47
7.46
7.46
7.44
7.43
7.42
7.42
6.62
5.81
5.80
5.41
5.41
5.39
5.39
5.17
5.16
5.16
5.15
4.92
4.11
4.10
4.09
4.08
4.07
4.07
3.65
3.64
3.58
3.56
3.33
3.03
3.03
2.50
1.42
1.27
0.00
1d'
1.80
2.16
5.97
3.97
2.03
2.03
1.99
1.87
2.00
2.07
2.15
3.95
5.95
5.96
13
12
11
10
9
8
7
6
5
4
3
2
1
0

1d

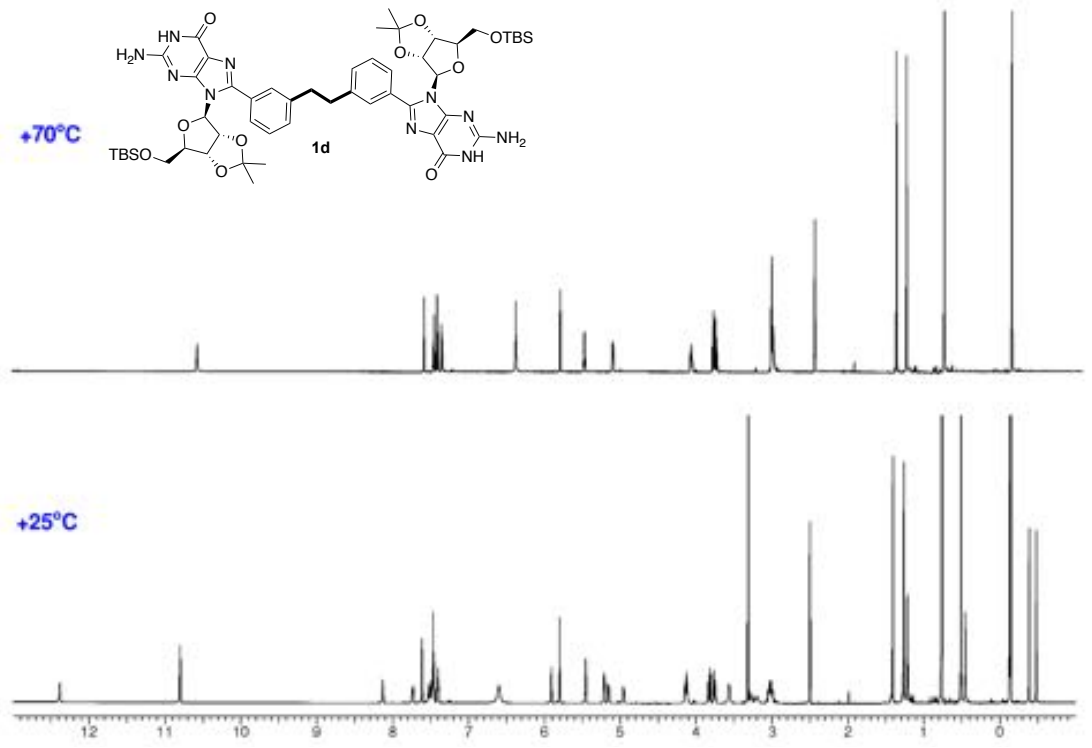
+70°C
1d
+25°C
12
11
10
9
8
7
6
5
4
3
2
1
0

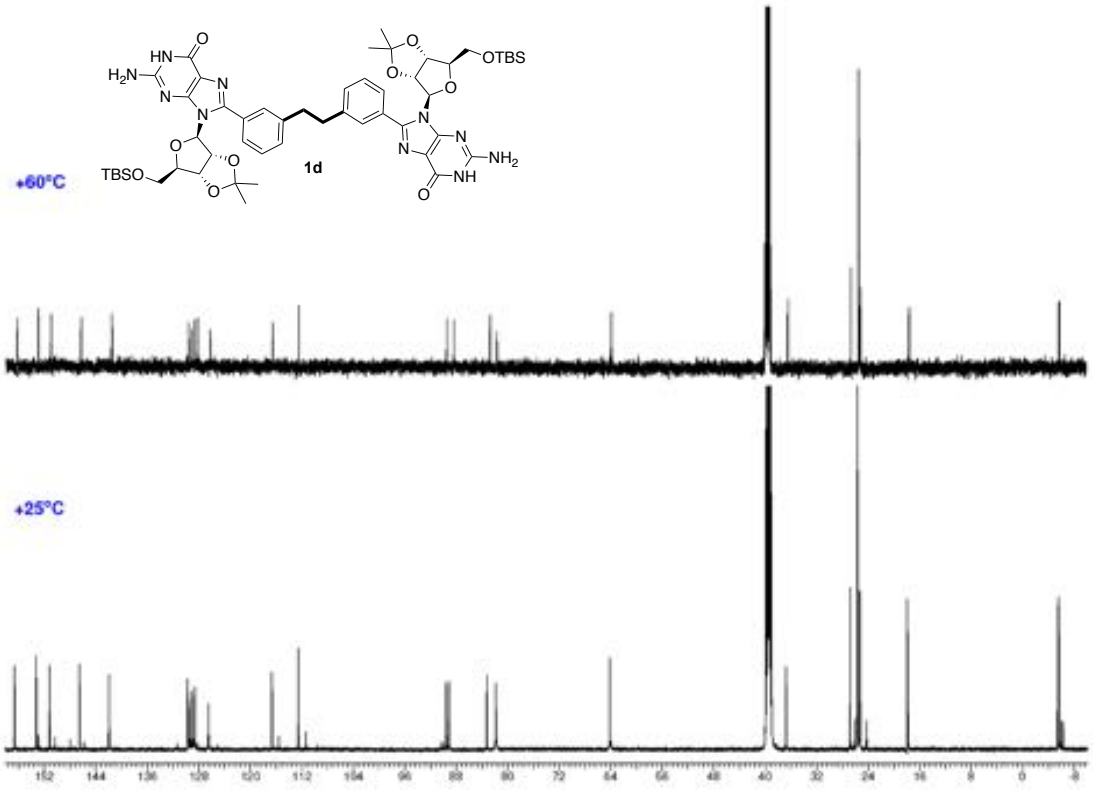
+60°C
+25°C
1d
TBSO
OTBS
HN
O
H2N
N
NH2
NH

4. **S2**

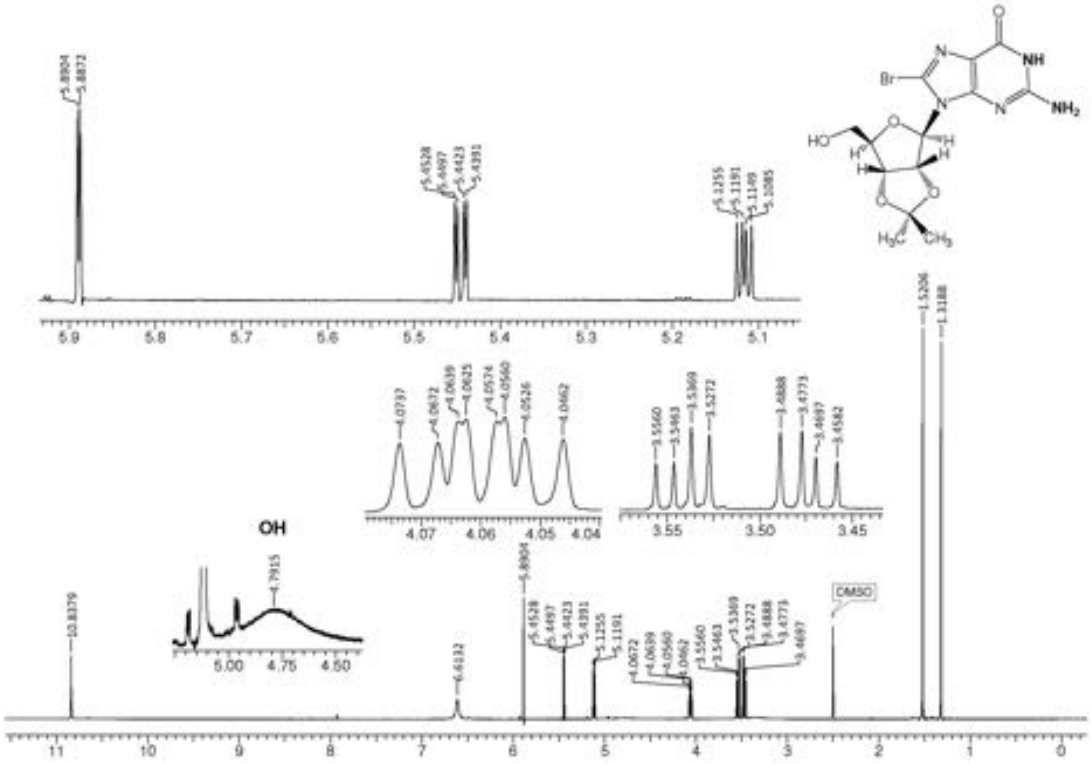

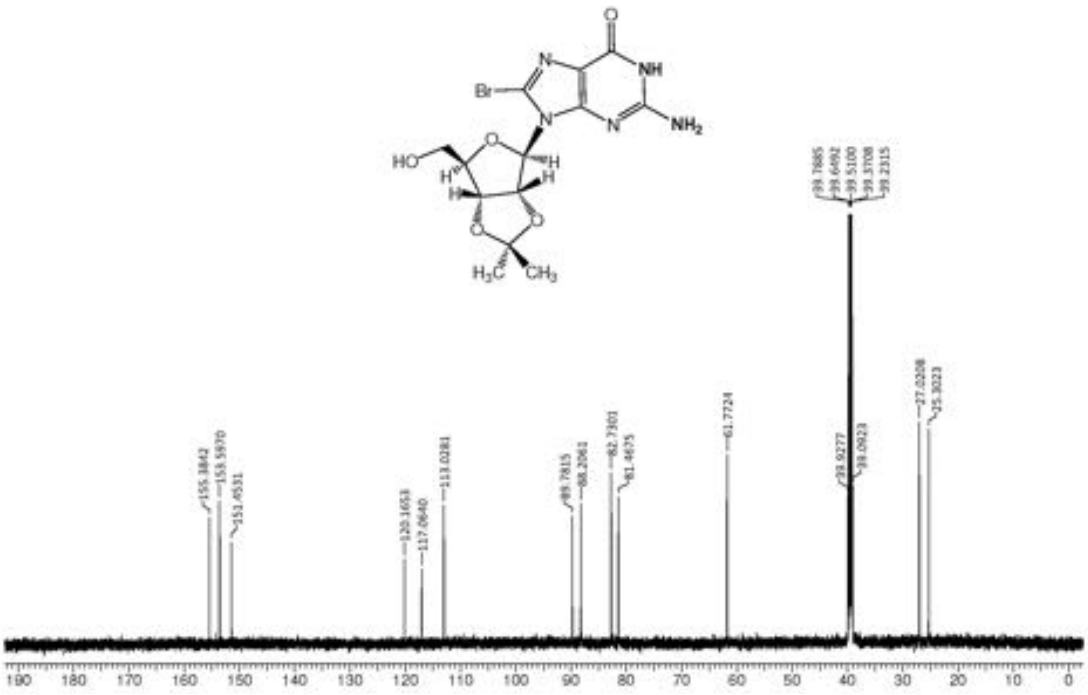

5. **S3**

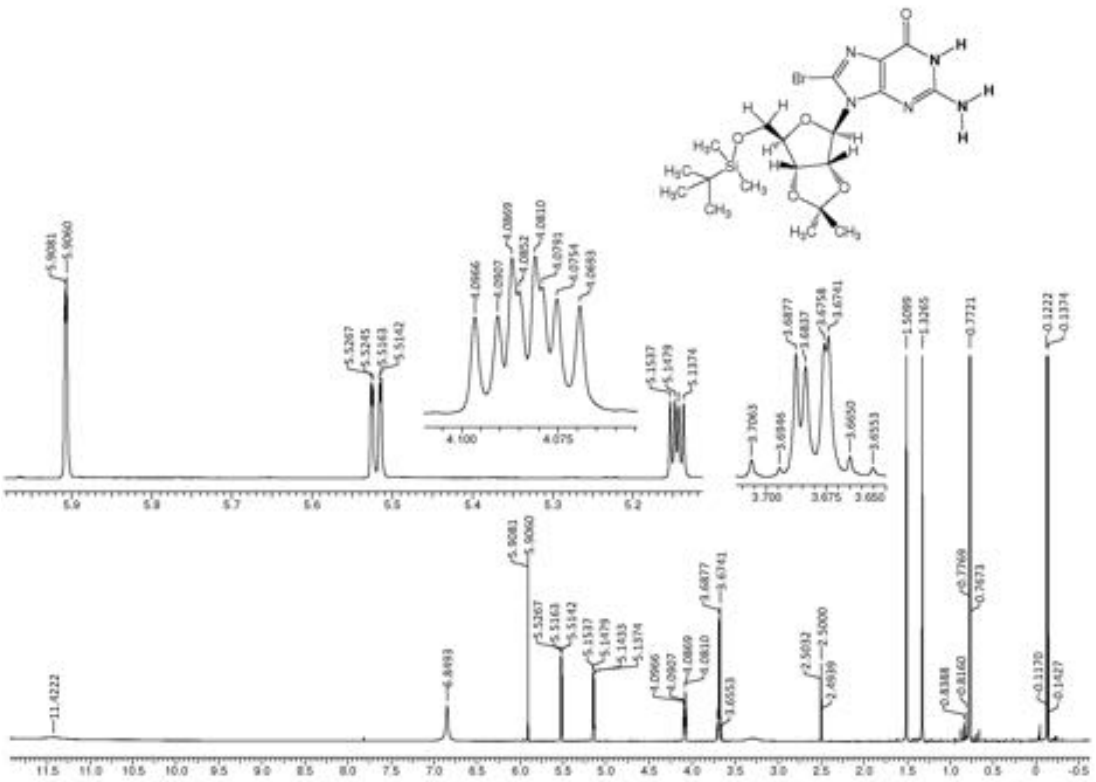

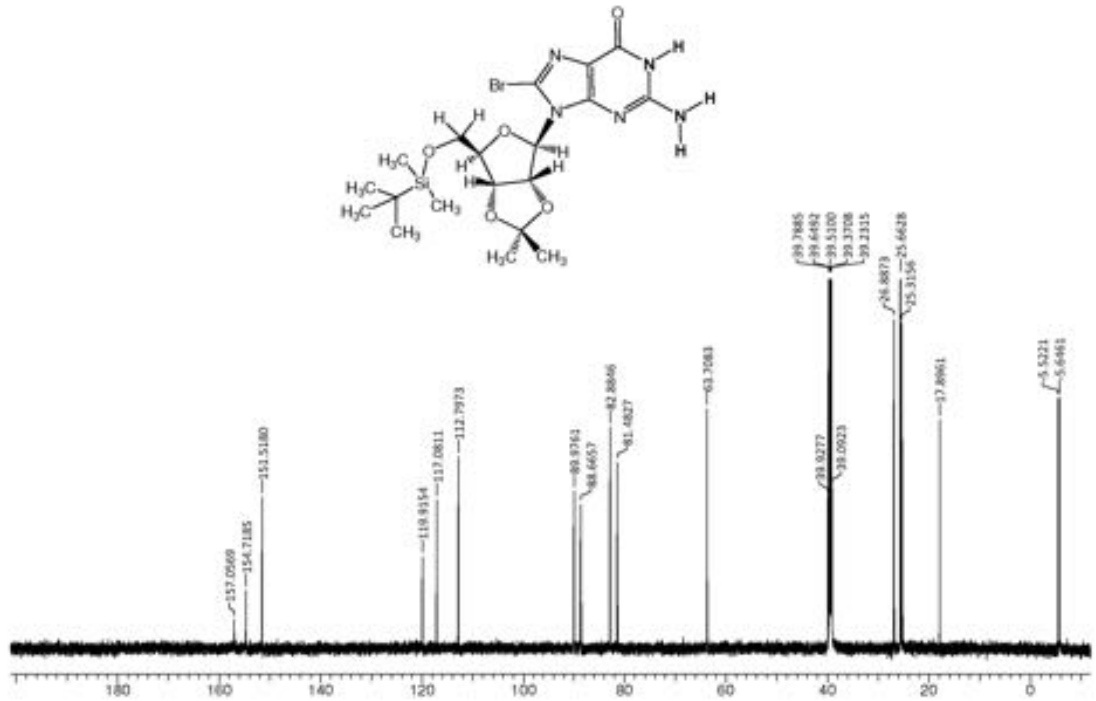

6. S5

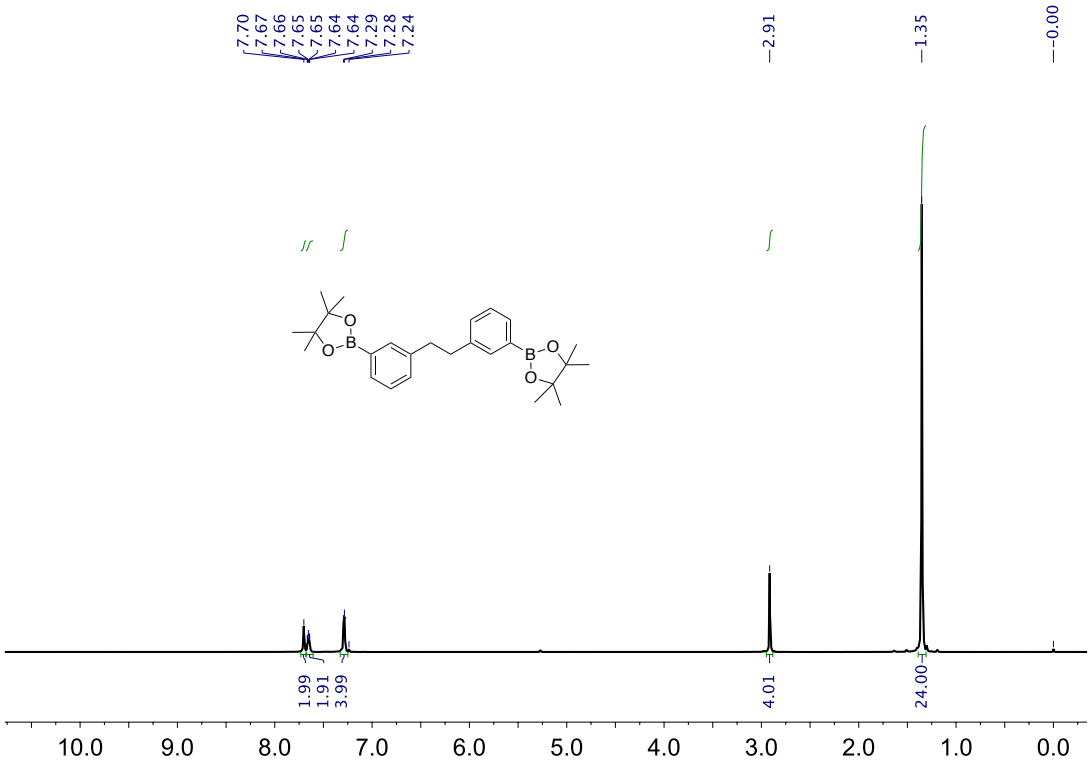
7.70
7.67
7.66
7.65
7.65
7.64
7.64
7.29
7.28
7.24
2.91
1.35
0.00
1.99
1.91
3.99
4.01
24.00
10.0
9.0
8.0
7.0
6.0
5.0
4.0
3.0
2.0
1.0
0.0

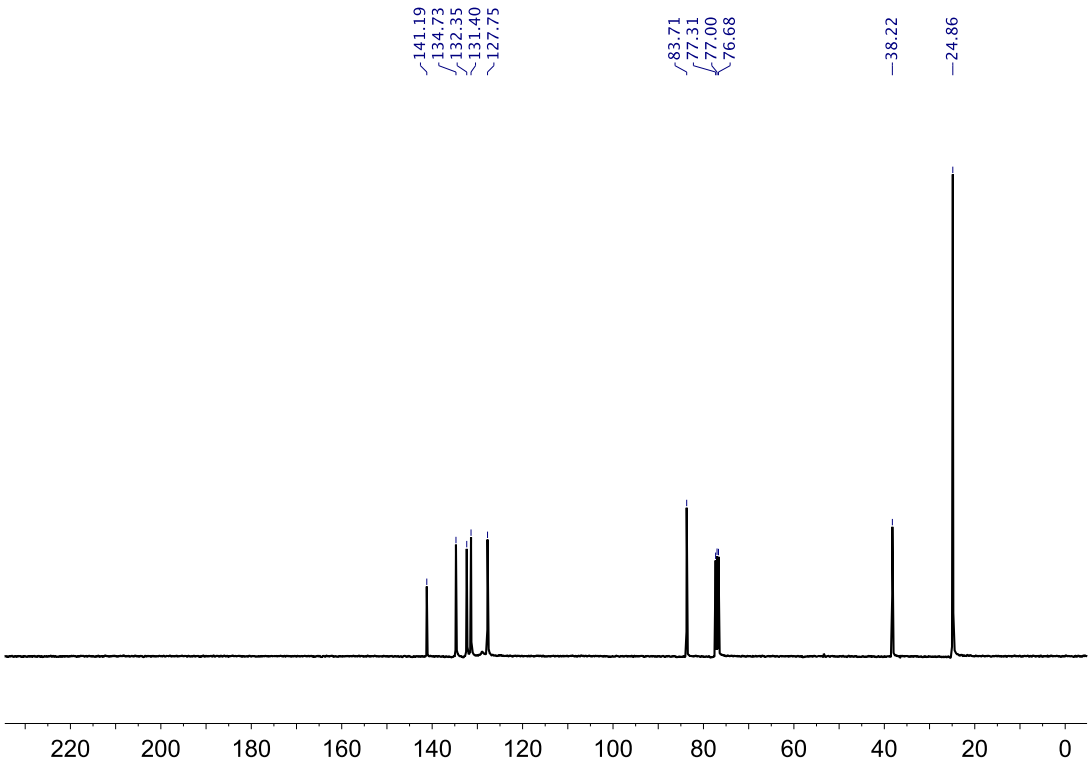
141.19
134.73
132.35
131.40
127.75
83.71
77.31
77.00
76.68
38.22
24.86
220
200
180
160
140
120
100
80
60
40
20
0

7. $[(\mathbf{1b})_8Ba]^{2+}\bullet(Pic^-)_2$

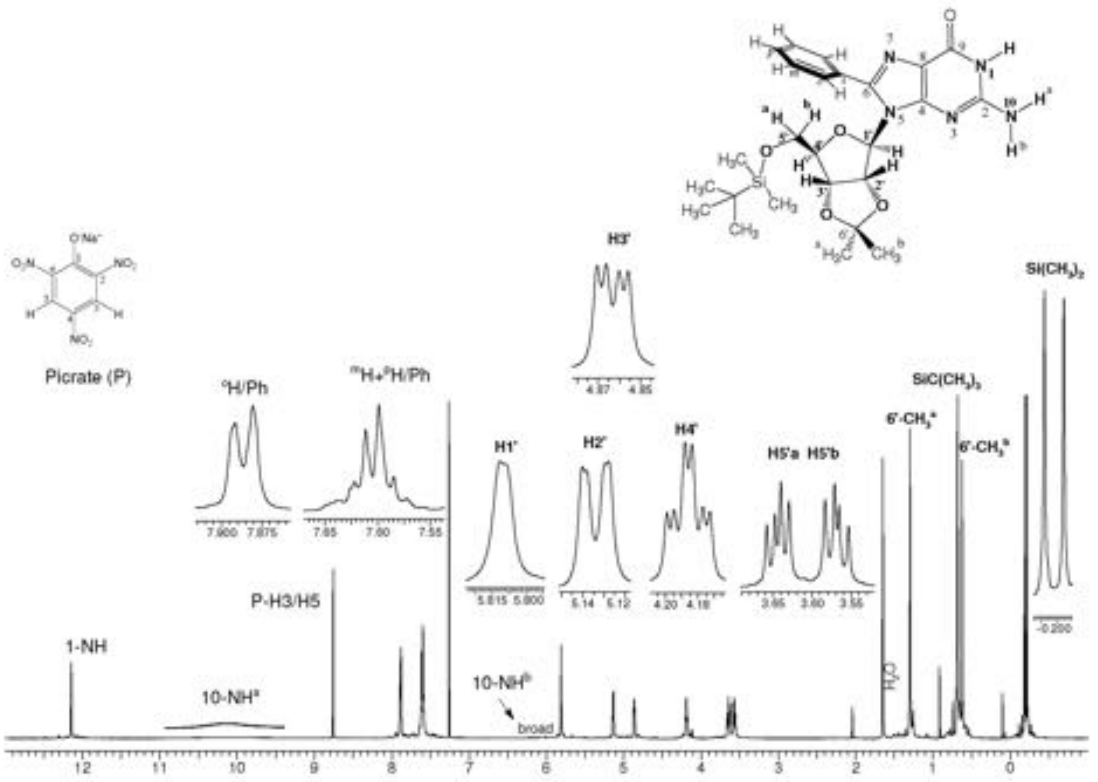

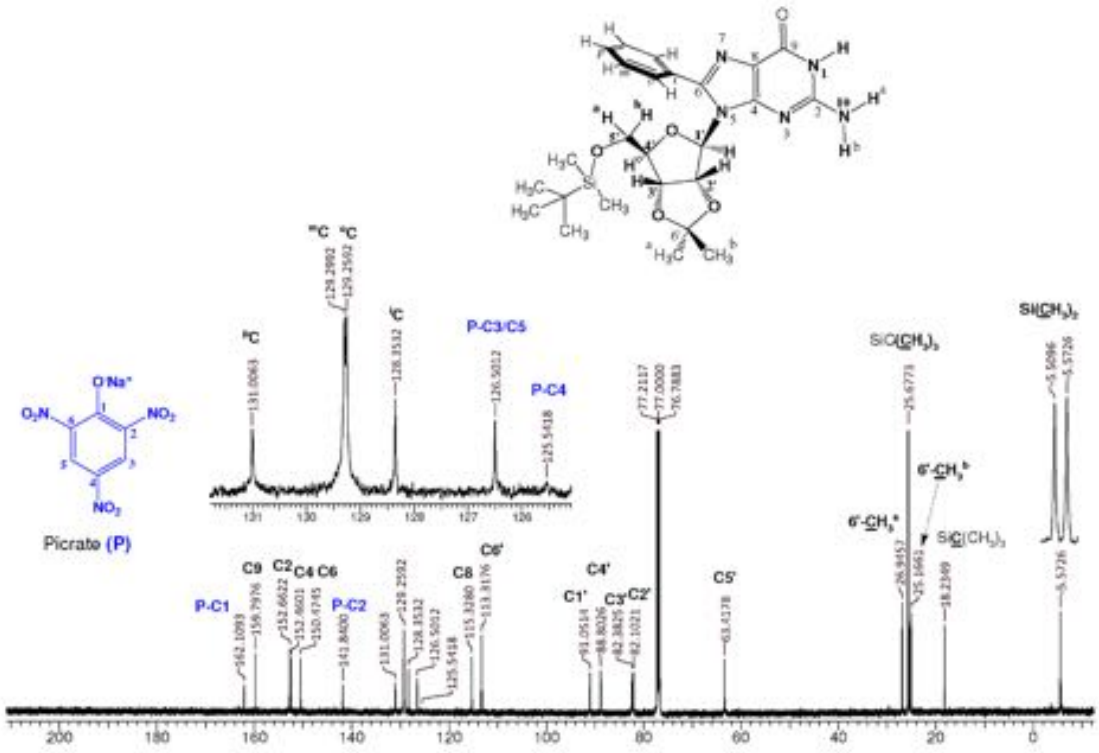

8. $[(\mathbf{1b})_8Sr]^{2+}\bullet(Pic^-)_2$

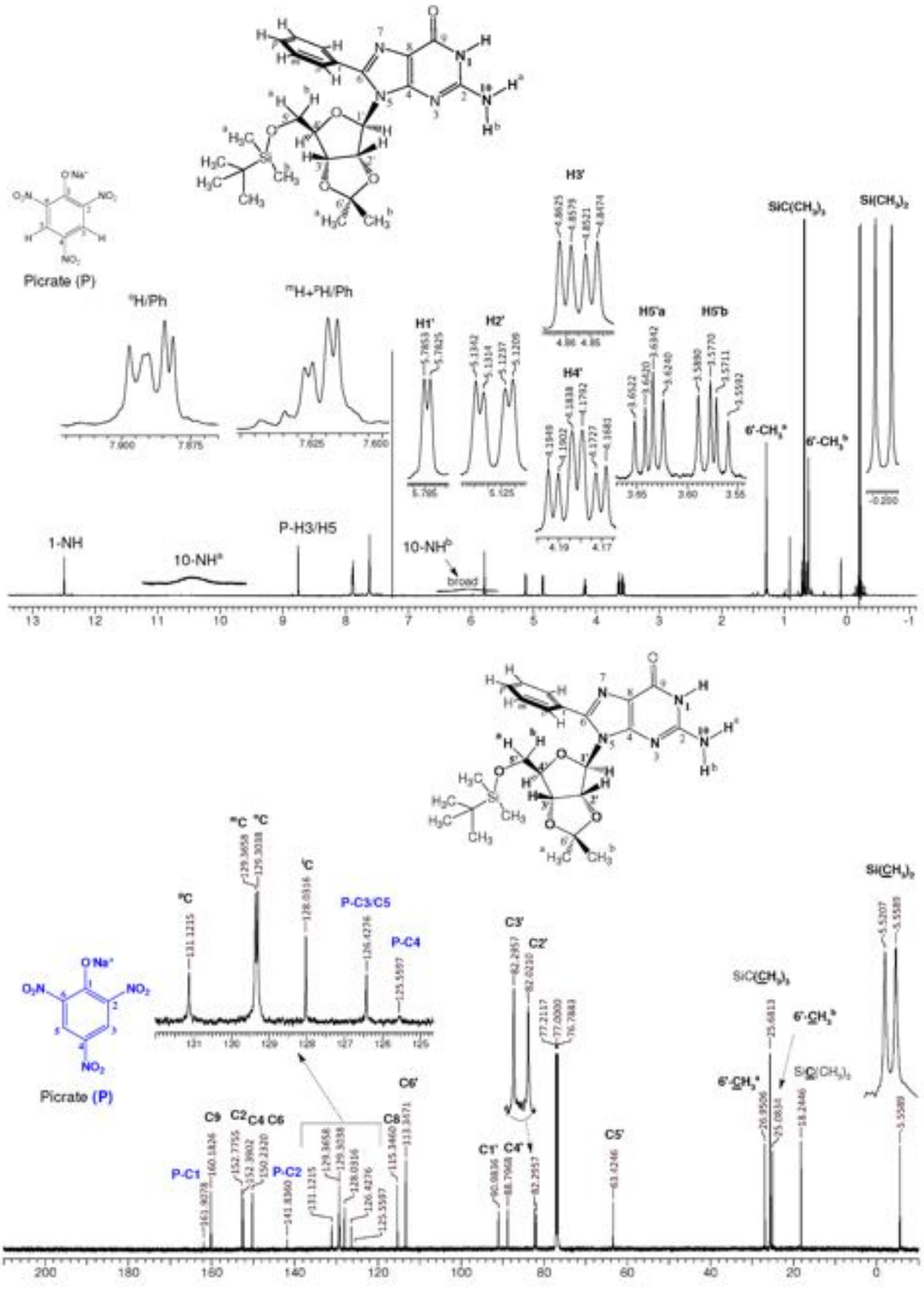

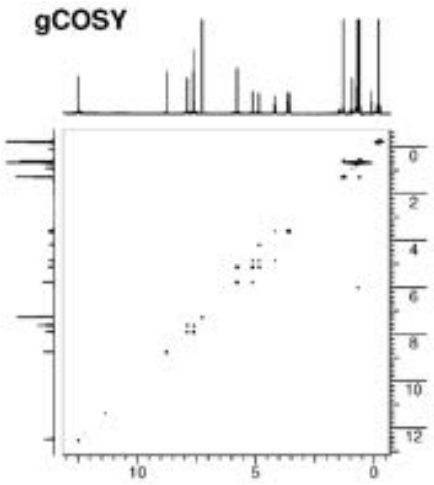
gCOSY

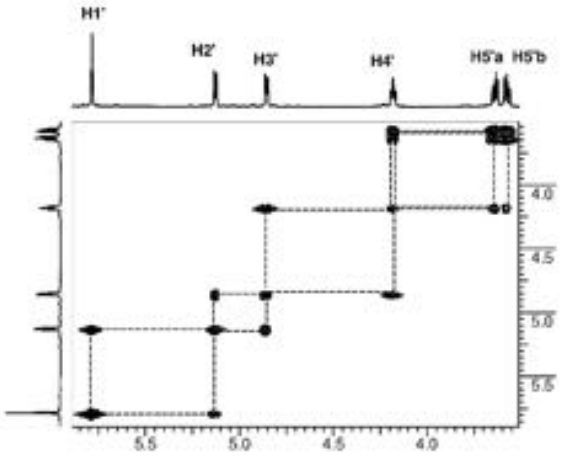
H1'
H2'
H3'
H4'
H5'a
H5'b

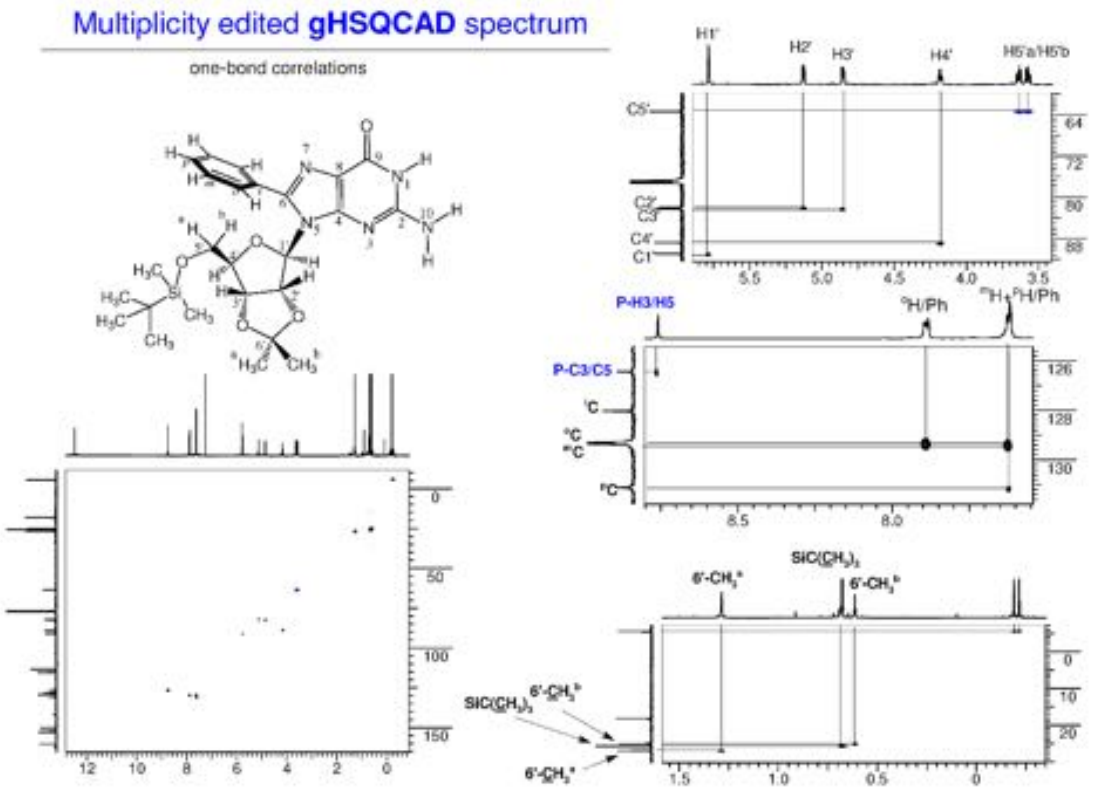
Multiplicity edited gHSQCAD spectrum
one-bond correlations
H1'
H2'
H3'
H4'
H5'a/H5'b
C5'
C2'
C3'
C4'
C1'
P-H3/H5
P-C3/C5
SiC(CH3)3
6'-CH3a
6'-CH3b

9. $[(\mathbf{1b})_8K]^+\bullet(PF_6^-)$

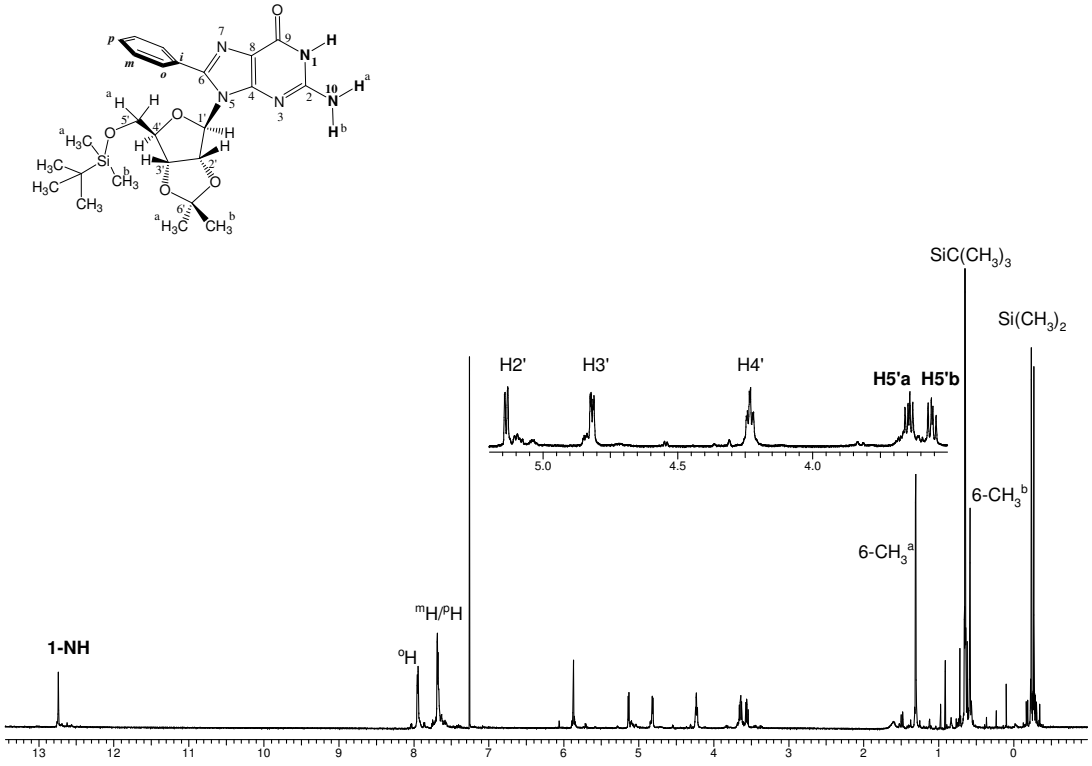

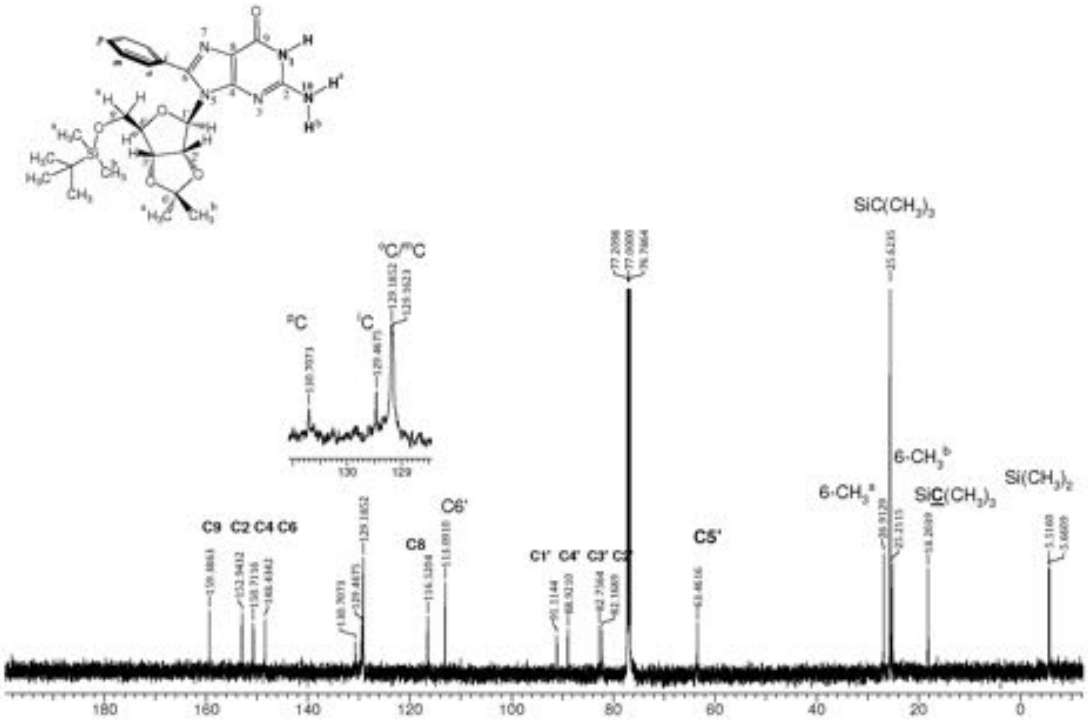

^{19}F NMR spectrum

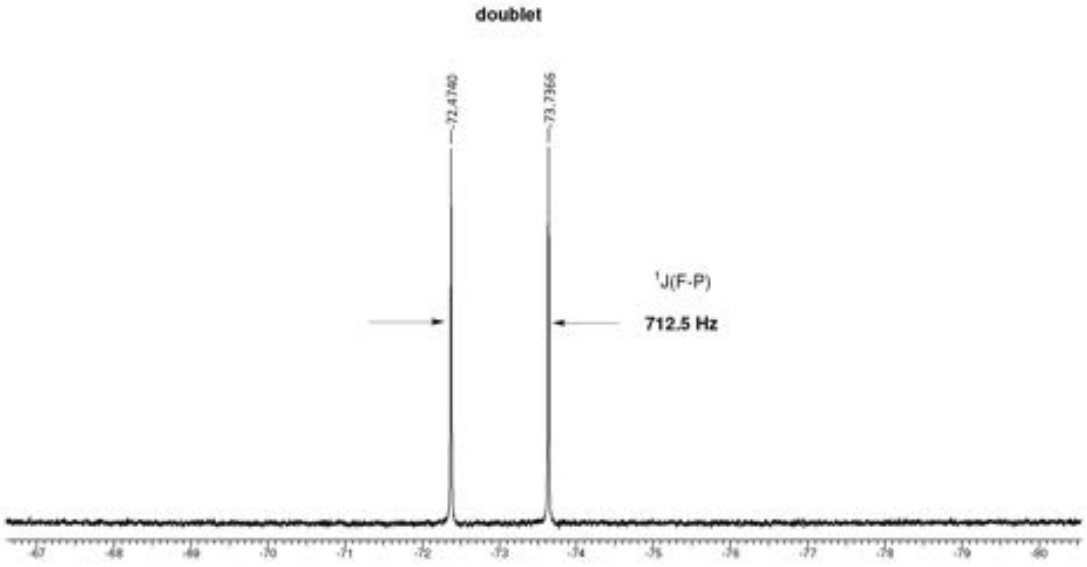

^{31}P NMR spectrum of KPF_6 in $CDCl_3$

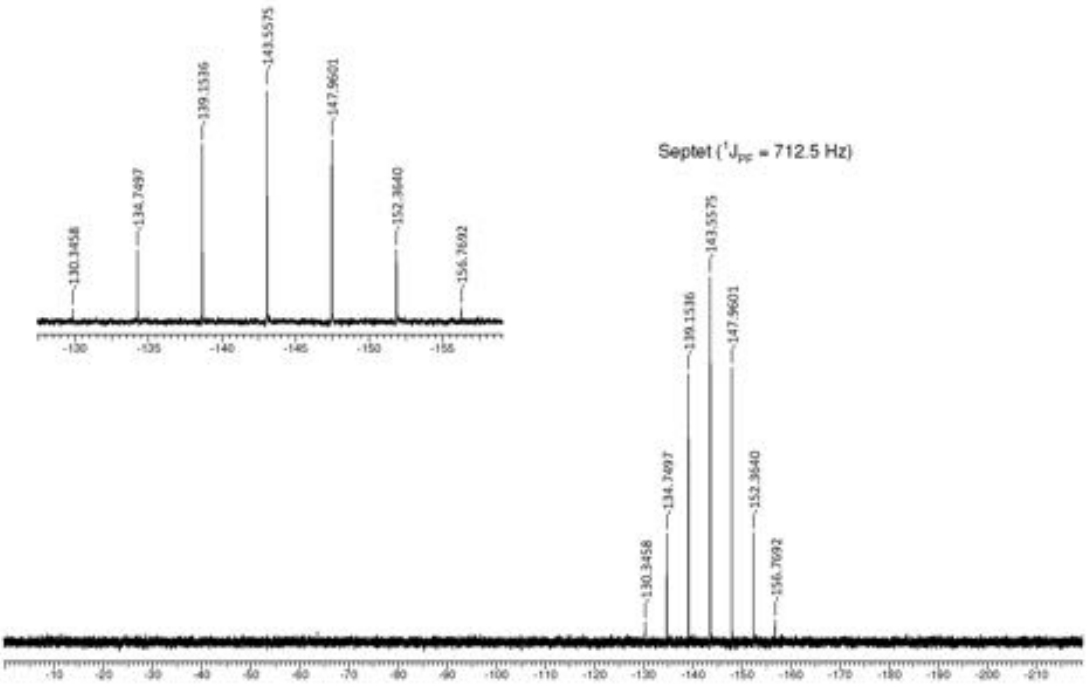

gHSQCAD

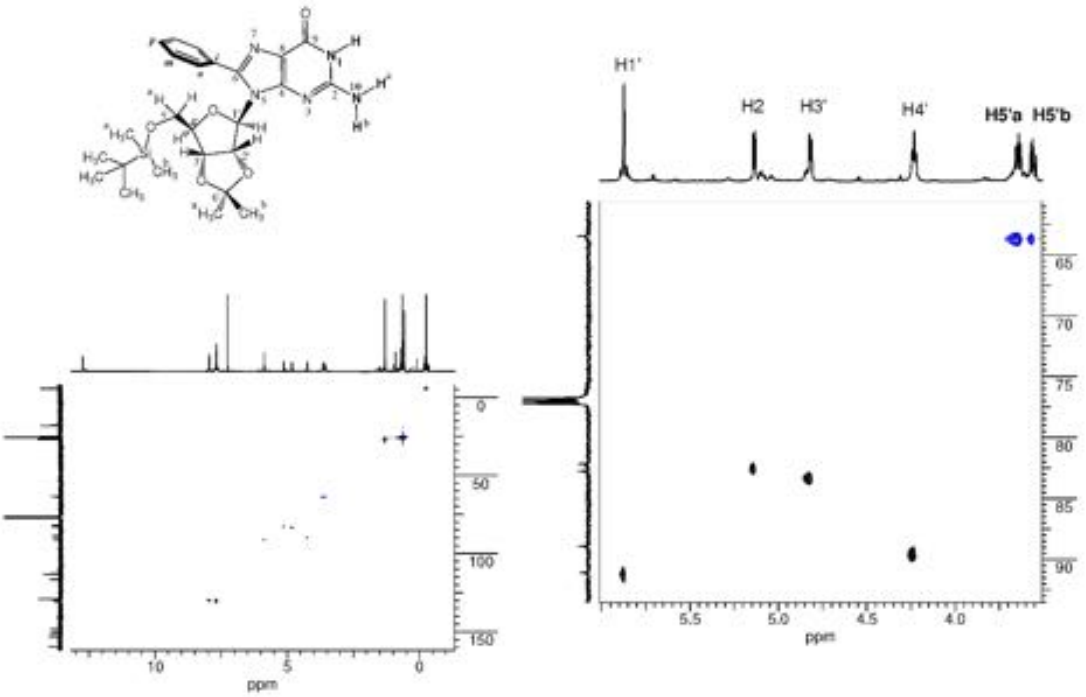

gCOSY

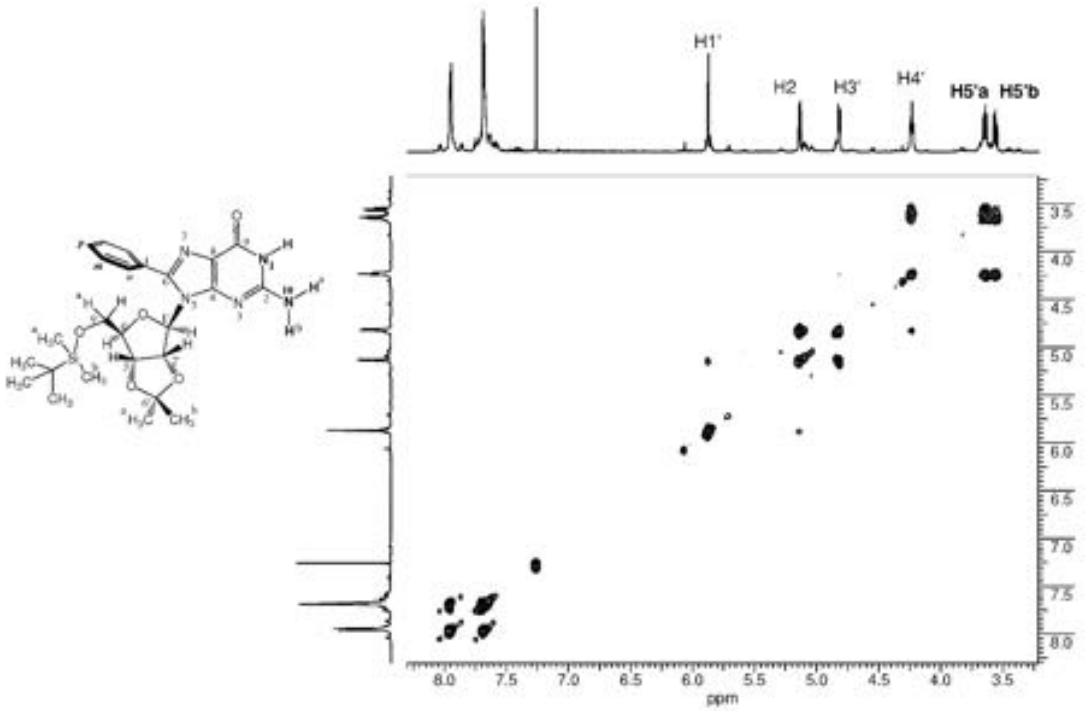

10. $[(\mathbf{1c})_8Ba]^{2+}\bullet(Pic^-)_2$

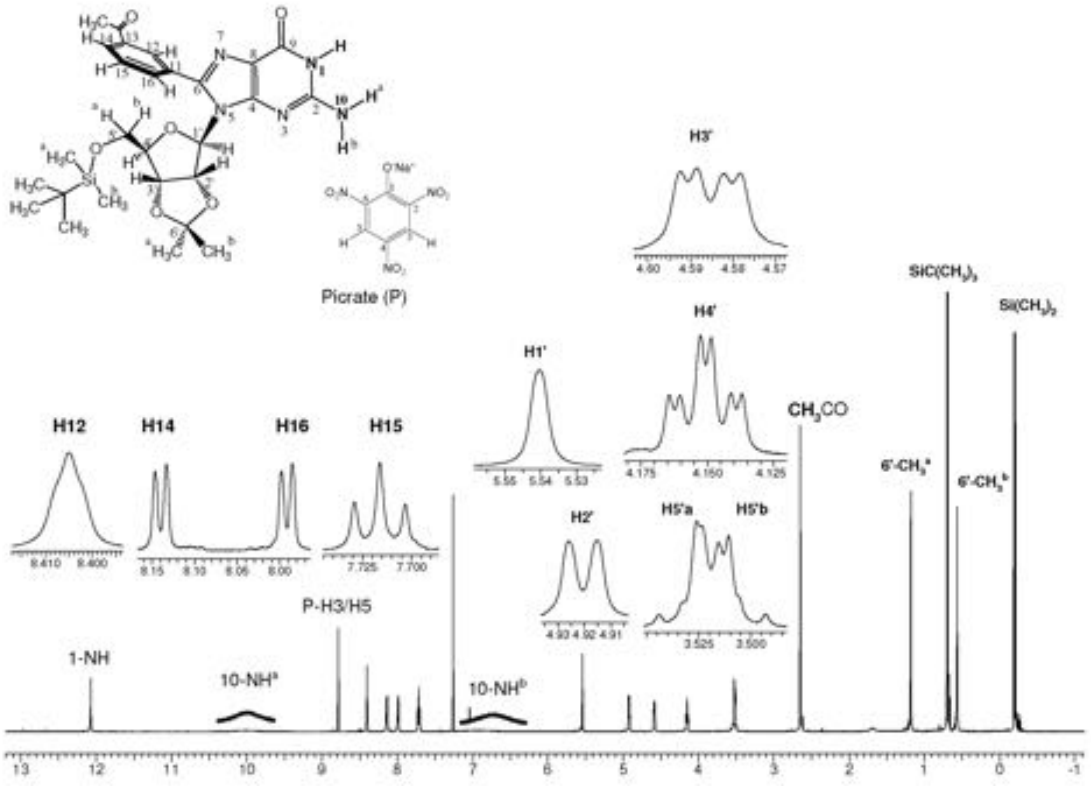

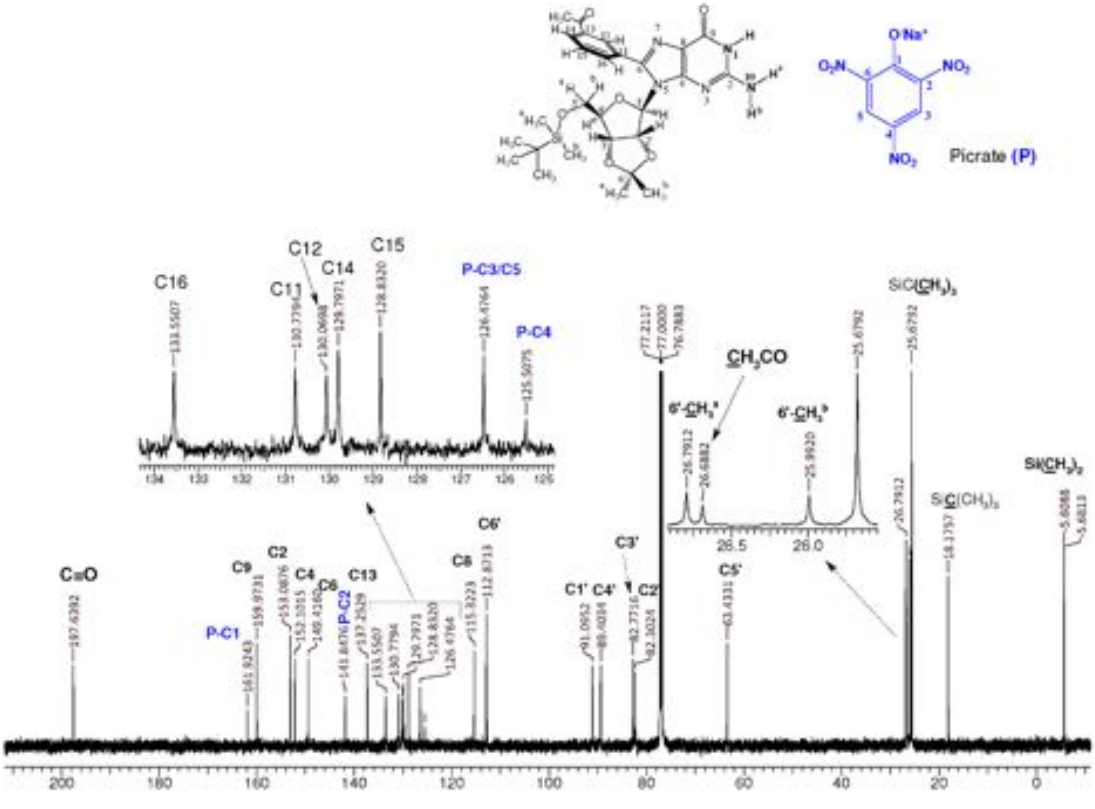

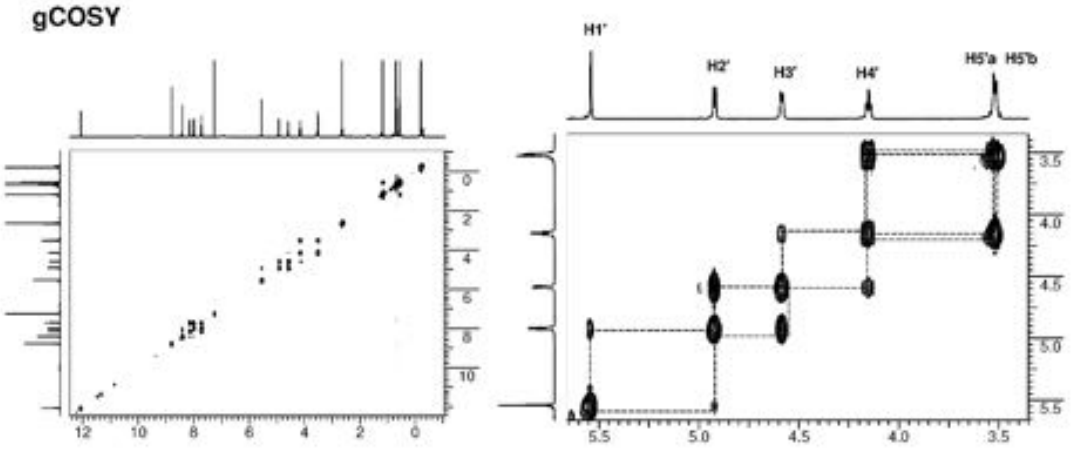
gCOSY
H1'
H2'
H3'
H4'
H5'a H5'b

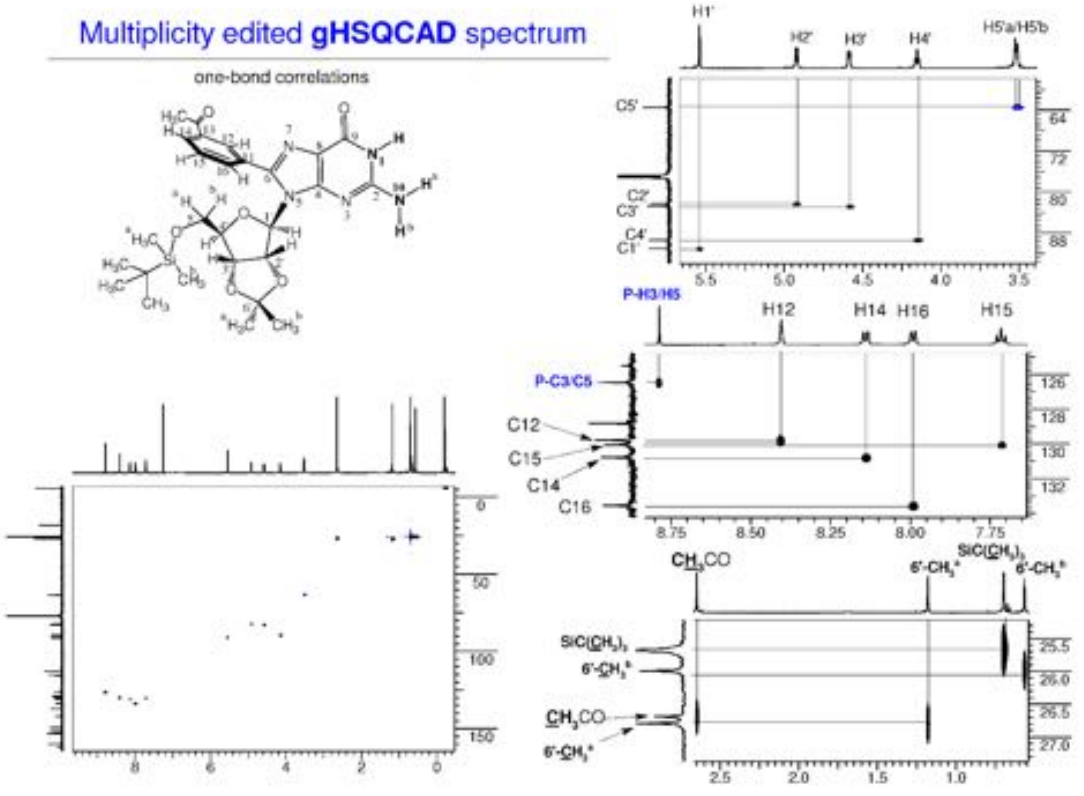
Multiplicity edited gHSQCAD spectrum
one-bond correlations
H1'
H2'
H3'
H4'
H5'a/H5'b
C5'
C2'
C3'
C4'
C1'
P-H3/H5
H12
H14
H16
H15
P-C3/C5
C12
C15
C14
C16
CH3CO
6'-CH3a
SiC(CH3)3
6'-CH3b

11. $[(\mathbf{1c})_8K]^+\bullet(Pic^-)$

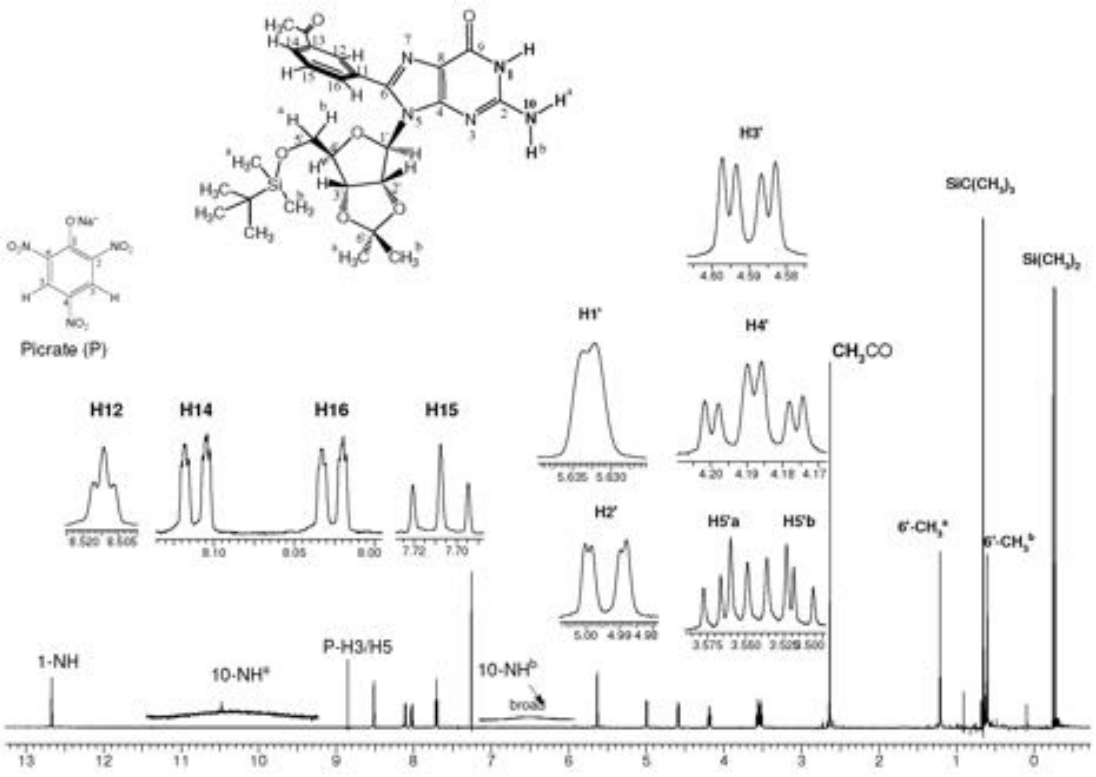

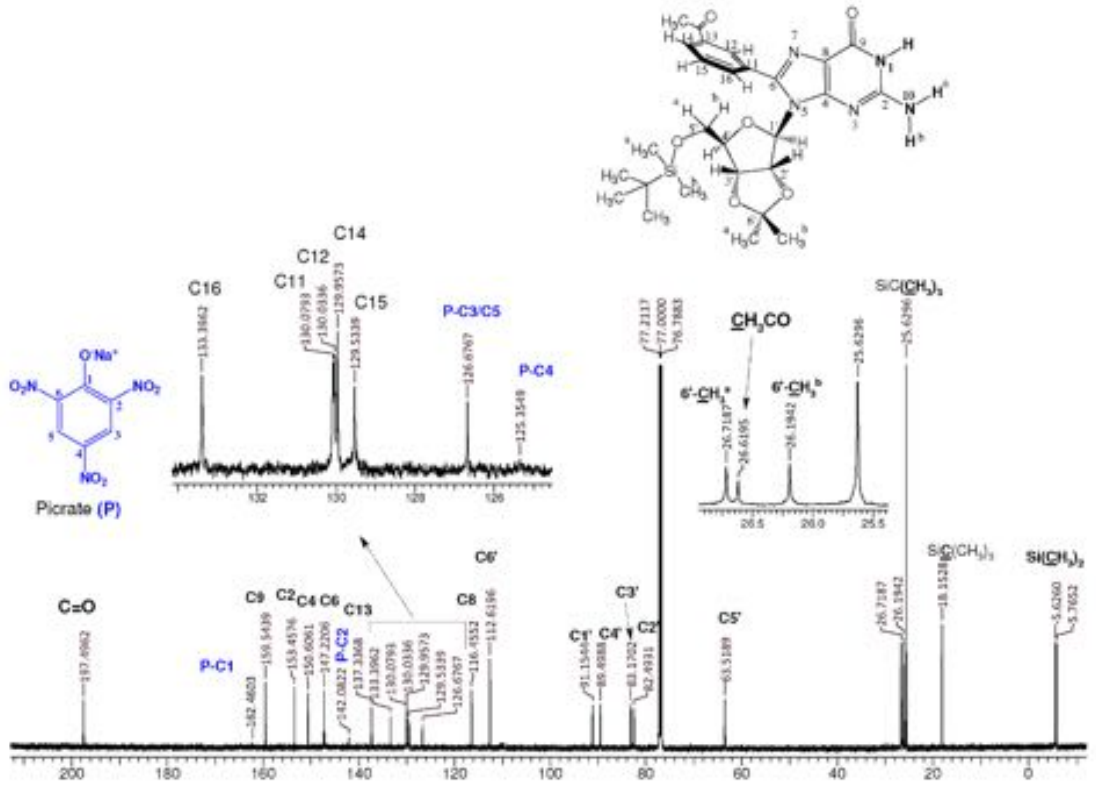

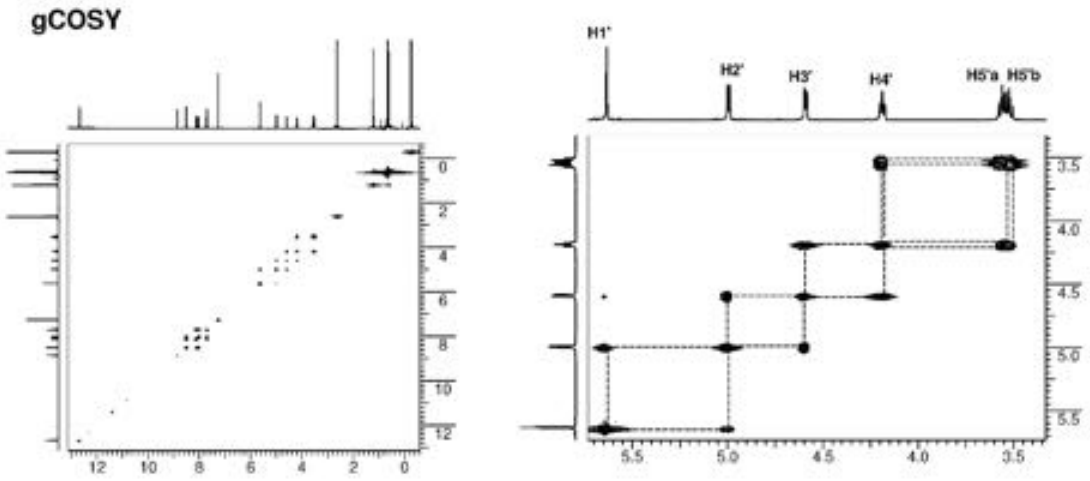
gCOSY
H1'
H2'
H3'
H4'
H5'a H5'b

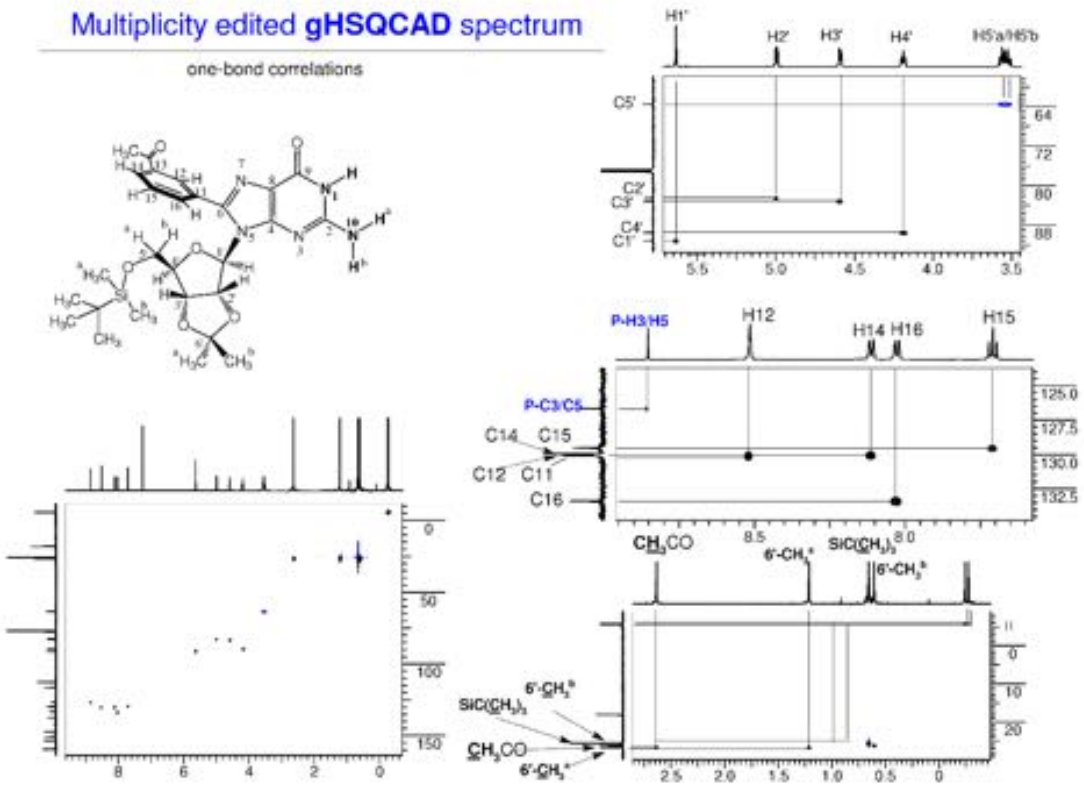
Multiplicity edited gHSQCAD spectrum
one-bond correlations
H1'
H2'
H3'
H4'
H5'a/H5'b
C5'
C2'
C3'
C4'
C1'
P-H3/H5
H12
H14 H16
H15
P-C3/C5
C14 C15
C12 C11
C16
CH3CO
6'-CH3a
SiC(CH3)3
6'-CH3b

12. $[(\mathbf{1d})_4K]^+\bullet(Pic^-)$

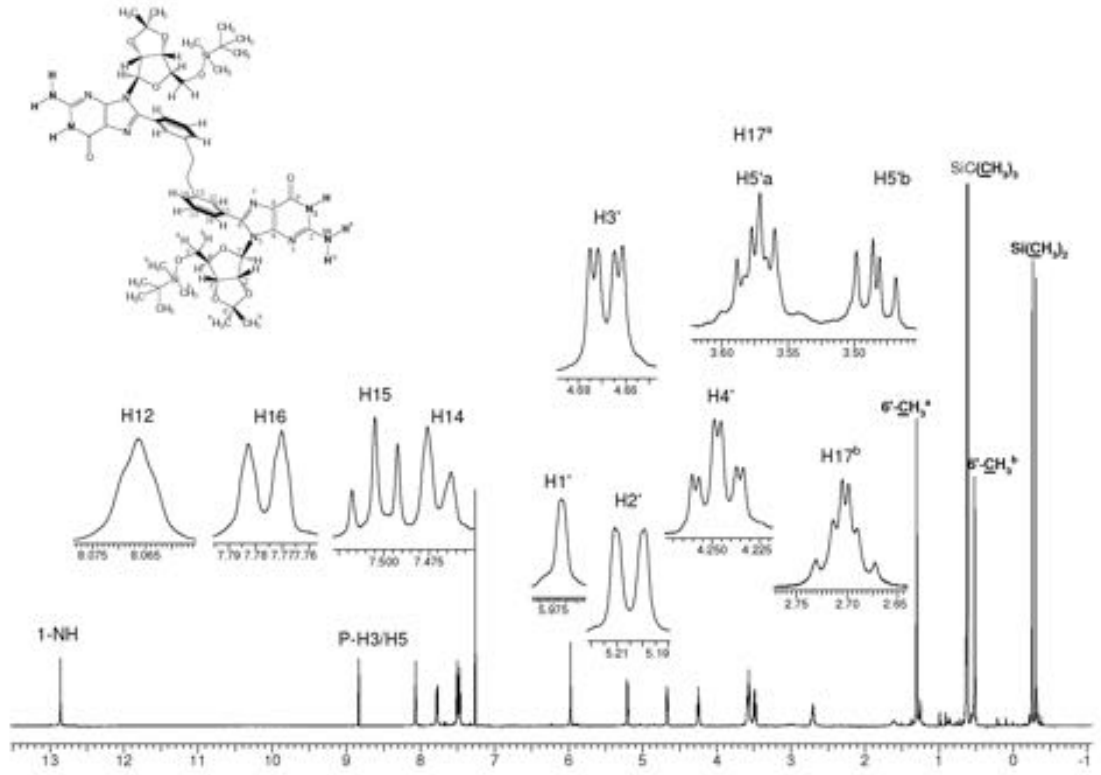

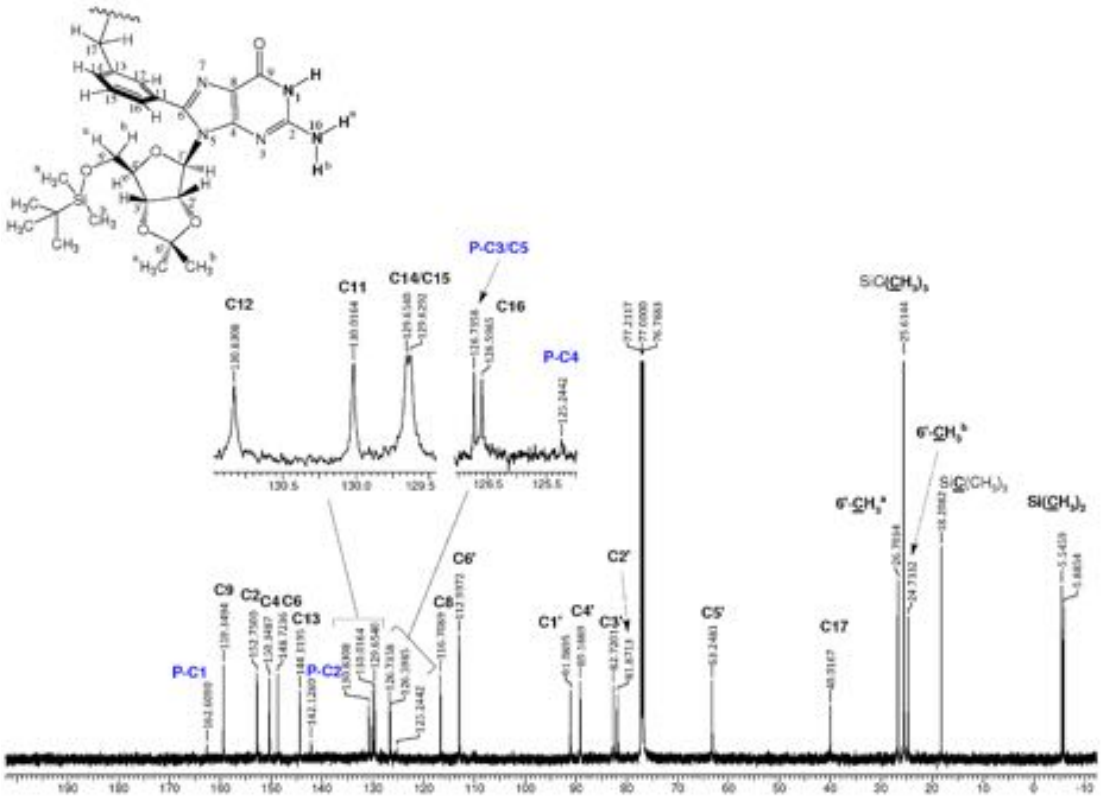

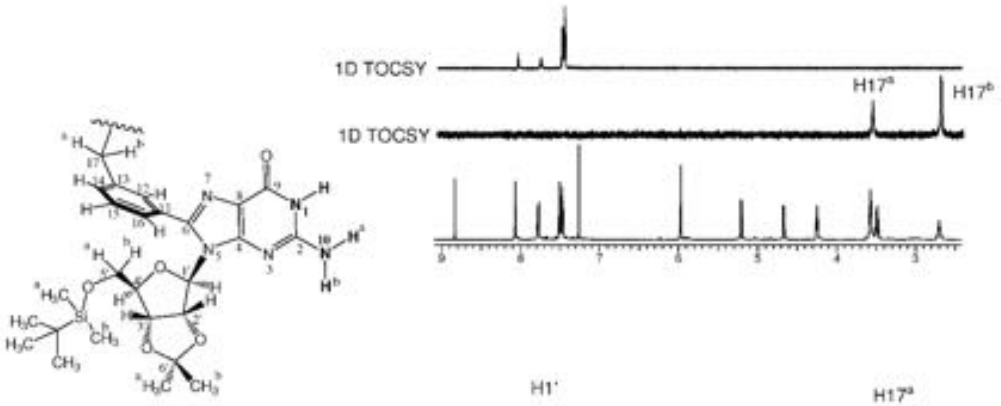
1D TOCSY
1D TOCSY
H17a
H17b

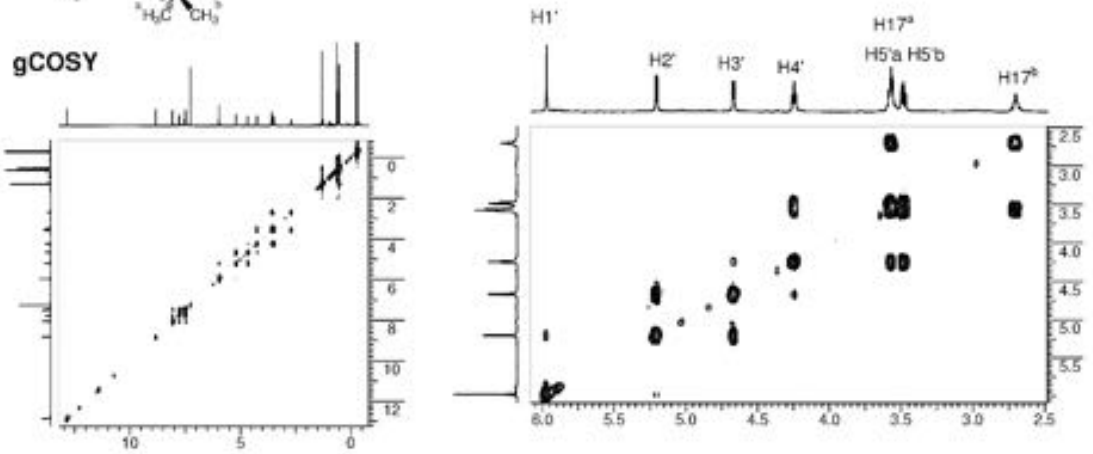
gCOSY
H1'
H2'
H3'
H4'
H17a
H5'a H5'b
H17b

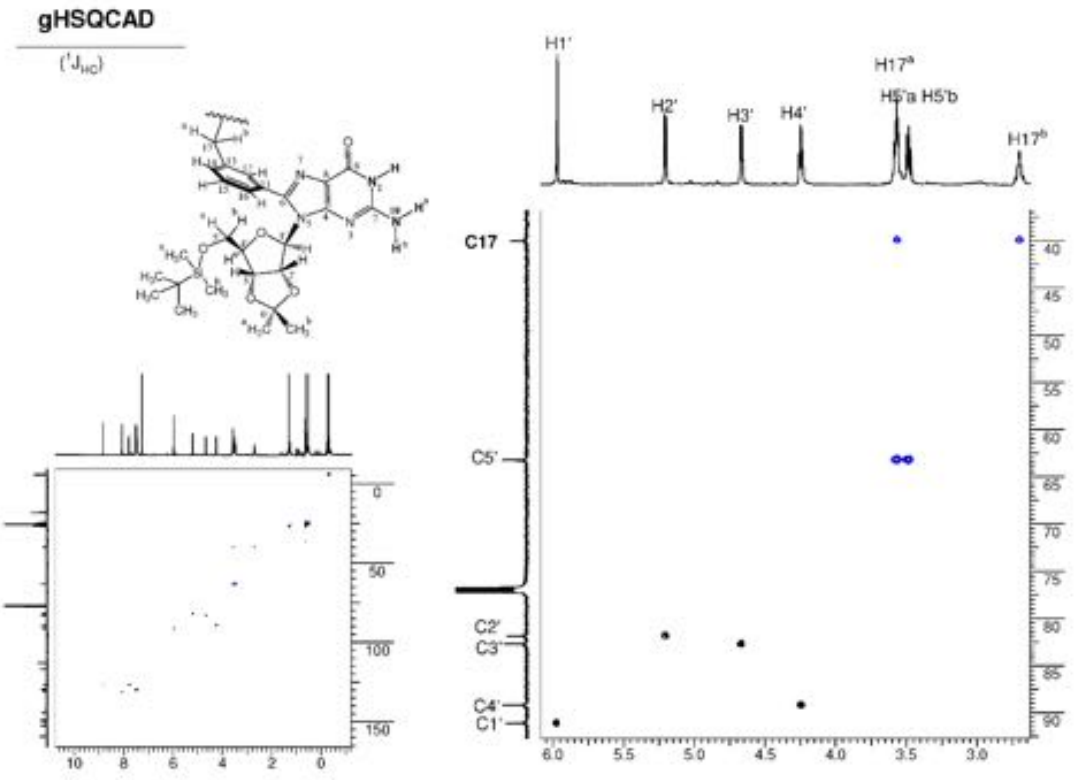
gHSQCAD
(1JHC)
H1'
H2'
H3'
H4'
H17a
H5'a H5'b
H17b
C17
C5'
C2'
C3'
C4'
C1'

IV. ESI-MS and TWIM-MS spectra data of complex

1. ESI-MS of $[(\mathbf{1b})_8Ba]^{2+}\bullet(Pic^-)_2$

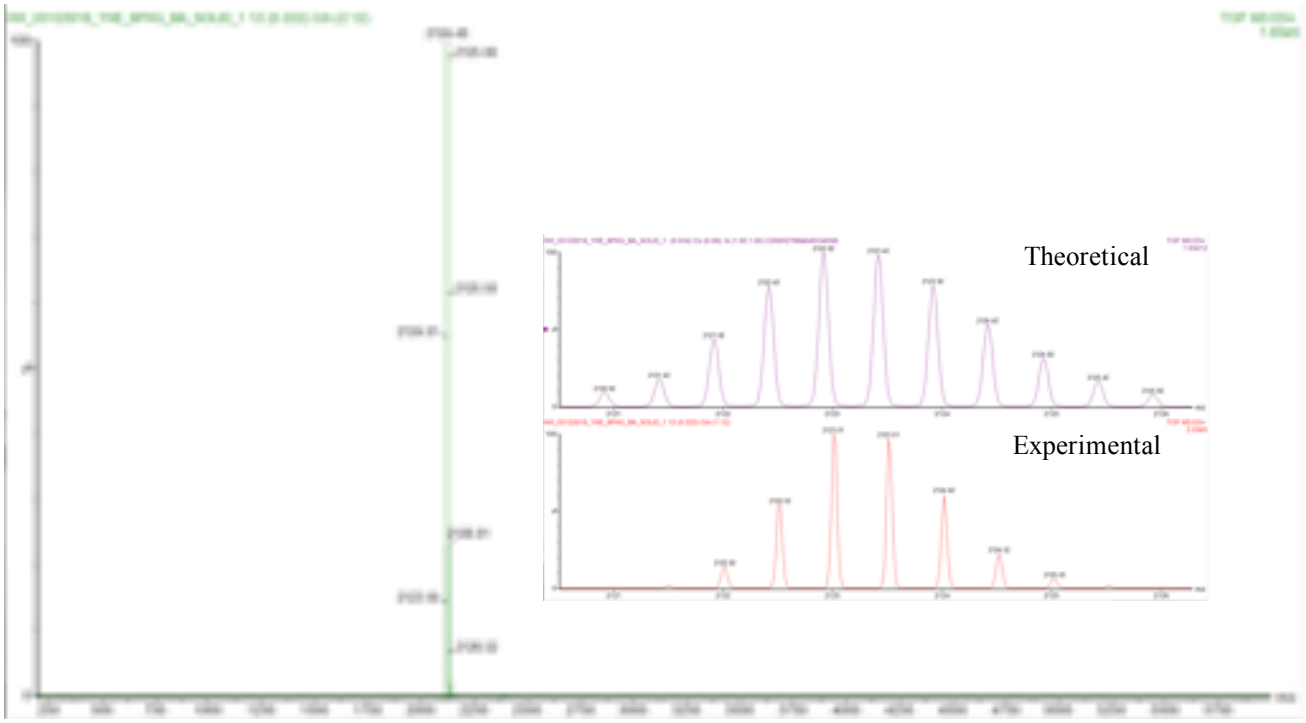

TWIM-MS of $[(\mathbf{1b})_8Ba]^{2+}\bullet(Pic^-)_2$

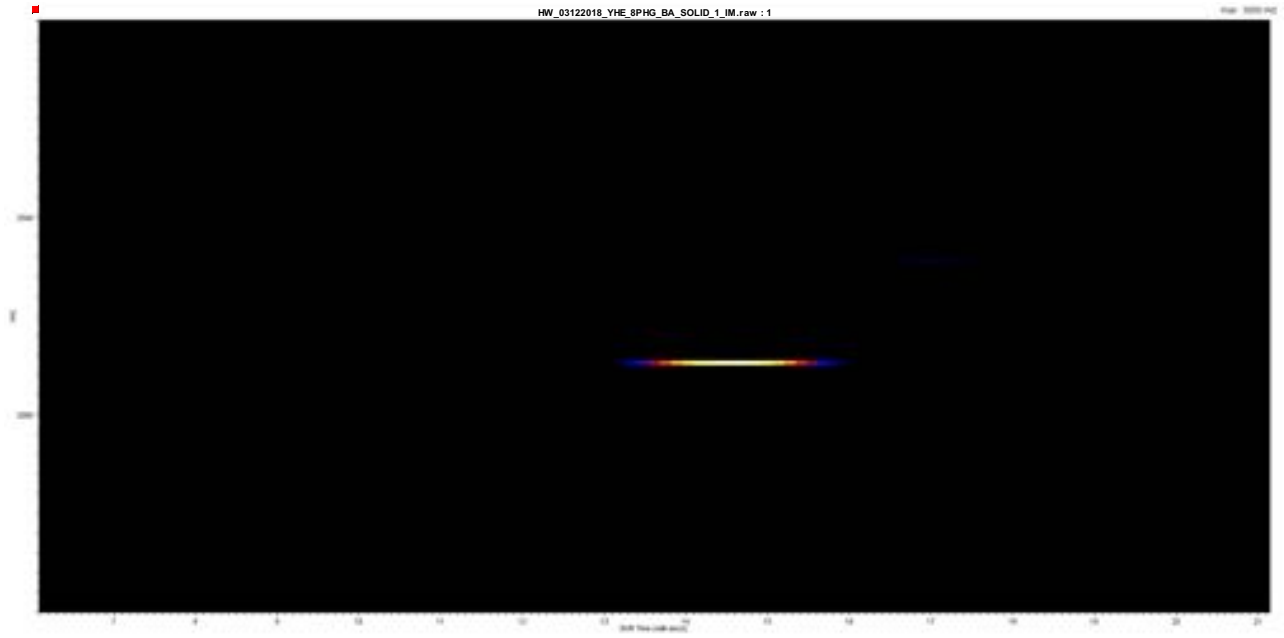

2. ESI-MS of $[(\mathbf{1b})_8K]^+ \bullet (Pic^-)$

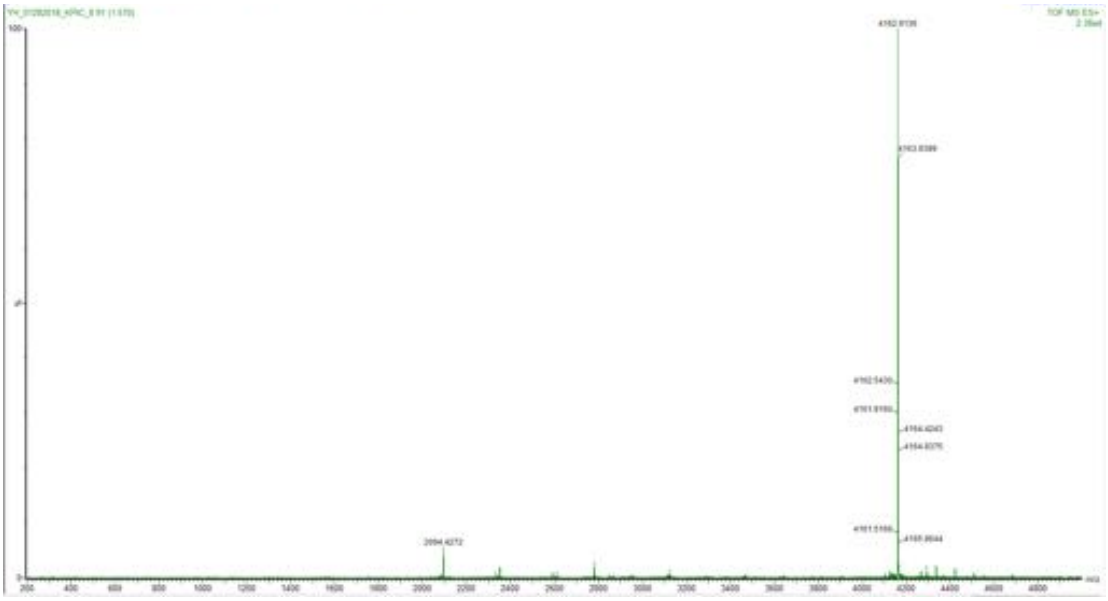

3. ESI-MS of $[(\mathbf{1b})_8K]^+ \bullet (PF_6^-)$

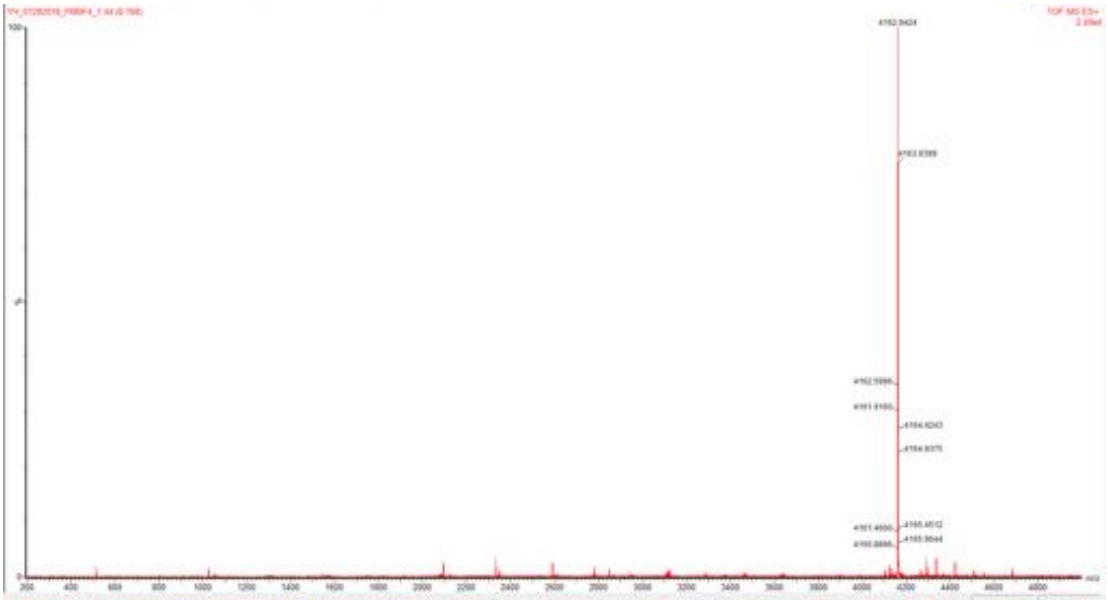

4. ESI-MS of $[(\mathbf{1c})_8Ba]^{2+}\bullet(Pic^-)_2$

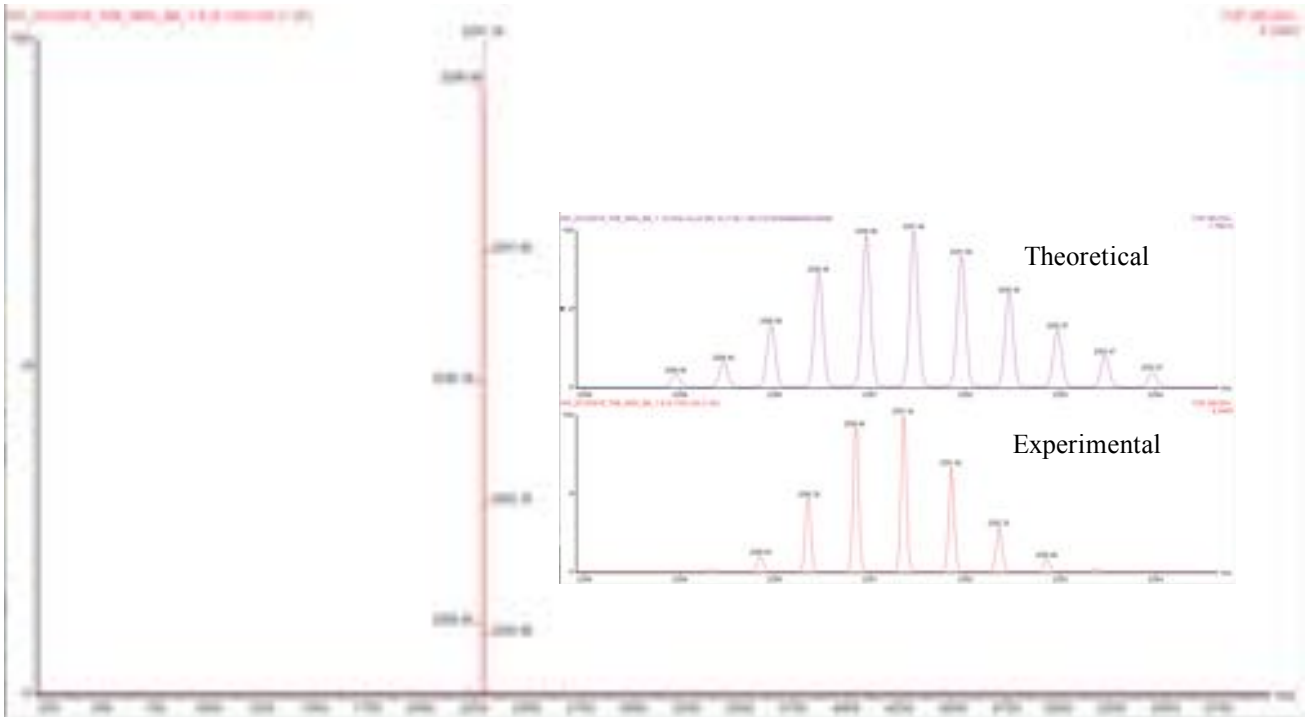

TWIM-MS of $[(\mathbf{1c})_8Ba]^{2+}\bullet(Pic^-)_2$

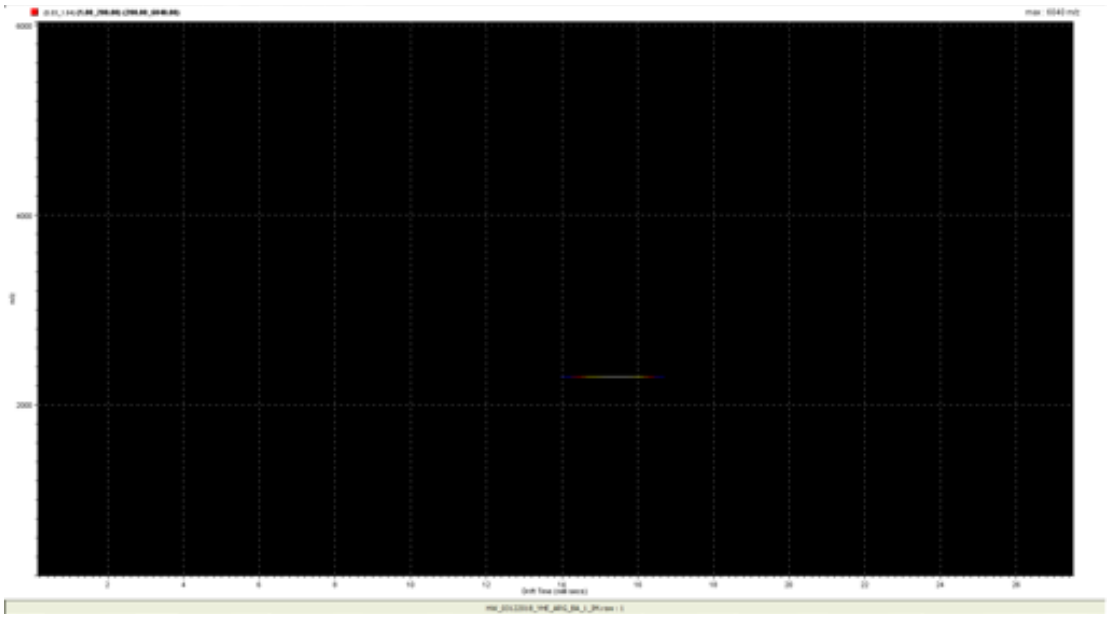

5. ESI-MS of $[(\mathbf{1d})_4Ba]^{2+}\bullet(Pic^-)_2$

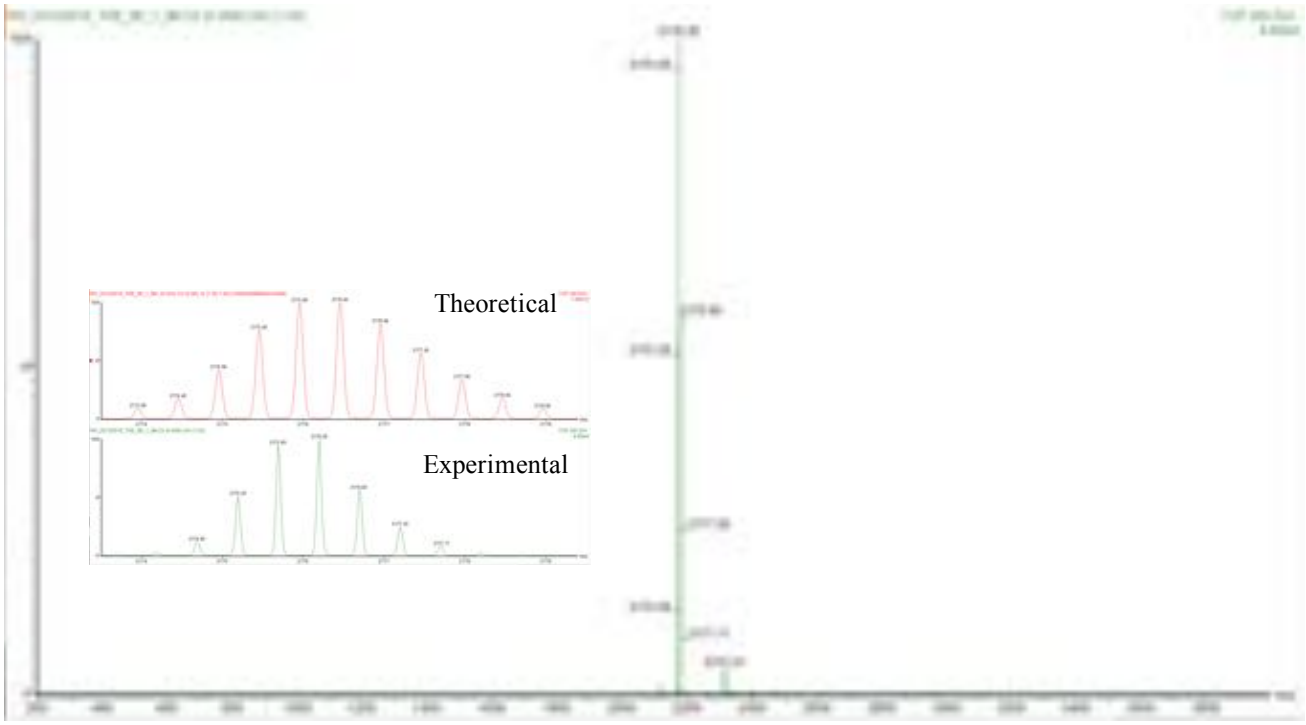

TWIM-MS of $[(\mathbf{1d})_4Ba]^{2+}\bullet(Pic^-)_2$

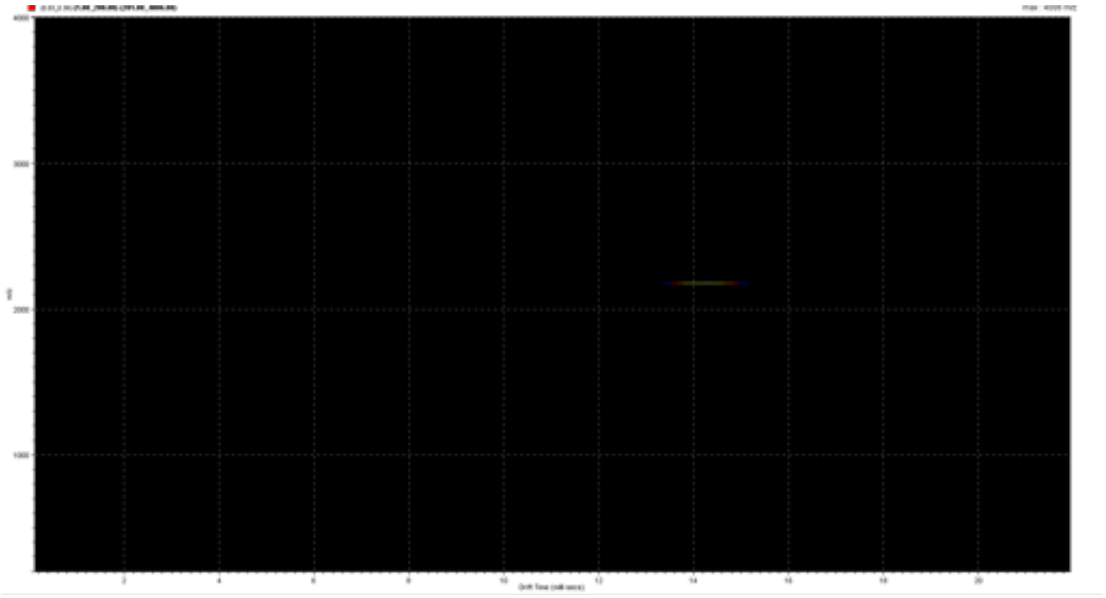

6. ESI-MS of $[(\mathbf{1d})_4K]^+\bullet(Pic^-)$

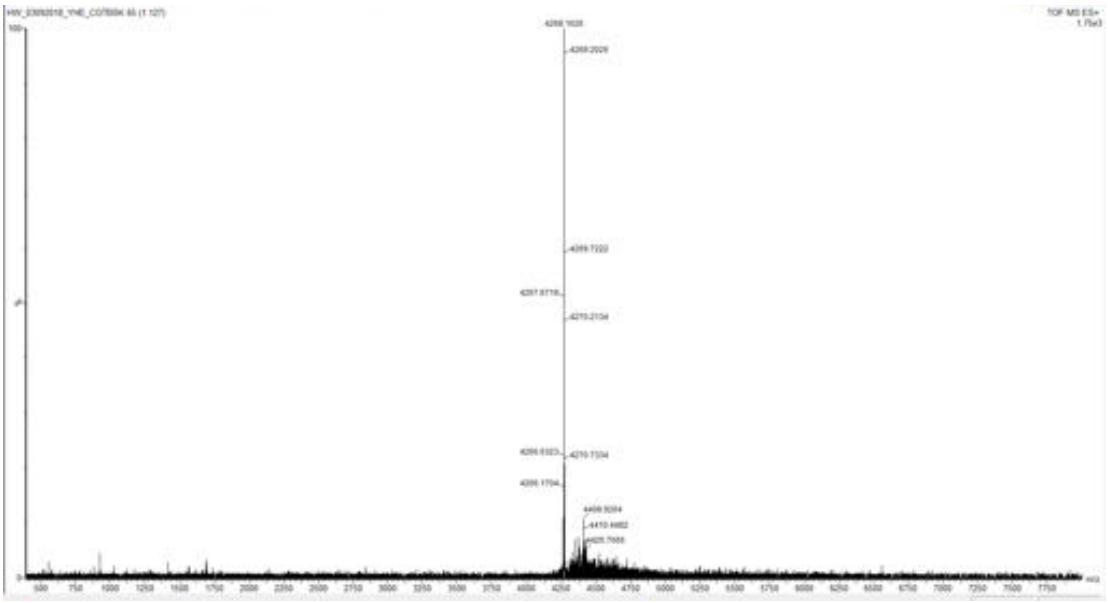

V. Single-Crystal X-Ray Diffraction

The X-ray diffraction data for **HY_II_164_1, HY_III_8_4_8Ph_G_KPF6, HY-8PhGSrPic and HY_264_1_Ba** were measured on Bruker D8 Venture PHOTON 100 CMOS system equipped with a Cu Kα INCOATEC ImuS micro-focus source (λ = 1.54178 Å). The X-ray diffraction data for compound **HY_II_207_6**, **HY_93_3_8PHG_Rb and HY_III_88_2_CGKPIC** were collected using synchrotron radiation (λ = 0.44281 Å) at Advanced Photon Source, Beamline 15-ID-B of ChemMatCARS in Argonne National Lab, Argonne, IL. Indexing was performed using *APEX3* [1] (Difference Vectors method). Data integration and reduction were performed using SaintPlus [2]. Absorption correction was performed by multi-scan method implemented in SADABS [3]. Space groups were determined using XPREP implemented in APEX3 [1]. Structures were solved using SHELXT [4] and refined using SHELXL-2017 [5-6] (full-matrix least-squares on F^2) with help of OLEX2 interface program [7].

General remarks: All crystals diffracted only up to 1.0-1.1 A resolution and severe disorder is present in structural voids. Several TBSO groups, counter anions and solvent molecules are disordered in analyzed structures. Restraints for ADP and geometrical parameters have been used to disordered parts in order to keep the geometry of disordered parts feasible. 2Fo-Fc / Fo-Fc electron density maps in WinCoot [9] were used to place the solvent molecules and to validate the model. Some of electron density “blobs” visible in difference Fourier map in WinCOOT had non-conclusive shapes and were not further modeled. Crystal data and refinement conditions are shown in Tables 1-3.

HY_II_164_1: Based on electron density shape the solvent molecules were assigned as DCM or hexane. The contribution of heavily disordered solvent molecules in structural voids was treated as diffuse using Squeeze procedure implemented in Platon program [10, 11]. Due to disorder the accurate number of solvent molecules is tentative. Crystal data and refinement conditions are shown in Table 1.

HY_III_8_4_8Ph_G_KPF6. Based on electron density shape the solvent molecules were assigned as ACN. Due to disorder the accurate number of solvent molecules and precise orientation is tentative. There seem to be two positions occupied by PF6 counterion with PF6 occupancy of approximately equal 0.5 at each site. One of PF6 ion occupies position close to symmetry element and is heavily disordered. The assignment of this moiety is tentative. The presence of other counterions (eg Cl^-) cannot be 100% ruled out. Some of electron density “blobs” visible in difference Fourier map in WinCOOT had non-conclusive shapes and were not further modeled. Crystal data and refinement conditions are shown in Table 2.

HY_II_207_6: Based on electron density shape the solvent molecules were assigned as hexane and DCM. Due to disorder the accurate number of solvent molecules and precise orientation is tentative. Crystal data and refinement conditions are shown in Table 3.

HY_93_3_8PHG_Rb: Based on electron density shape the solvent molecules were assigned as MeOH or ACN. Diffuse electron density visible in voids could not be modeled reliably. Shape of electron density tentatively suggests the presence of heavily disordered picrate anions. Due to disorder the accurate number of solvent molecules is tentative.

HY-8PhGSrPic: Based on electron density shape the solvent molecules were assigned as Hexane or ACN. Crystal may contain also isomers of hexane due to use of Hexanes as crystallization solvent. Diffuse electron density visible in voids could not be modeled reliably. Due to disorder the accurate number of solvent molecules is tentative. Picrate anions are well defined.

HY_III_88_2_CGKPIC: Based on electron density shape the solvent molecules were assigned as DMSO. It is not clear if MeOH and water are also present in the structure as they can partially overlap with disordered DMSO. Solvent forms hydrogen bonds with -NH2 and –OH groups. Due to disorder anions could not be located in the structure.

HY_264_1_Ba: Based on electron density shape the solvent molecules were assigned as ACN. Diffuse electron density visible in voids could not be modeled reliably. Only one of picrate anions was located. The shape of electron density tentatively suggests the presence of heavily disordered picrate anions. Due to disorder the accurate number of solvent molecules is tentative.

Acknowledgements: The single crystal diffraction data for compound **HY_II_207_6**, **HY_93_3_8PHG_Rb and HY_III_88_2_CGKPIC** were collected at Argonne National Laboratory, Advanced Photon Source, Beamline 15-ID-B of ChemMatCARS. ChemMatCARS Sector 15 is principally supported by the Divisions of Chemistry (CHE) and Materials Research (DMR), National Science Foundation, under grant number NSF/CHE-1346572. Use of the PILATUS3 X CdTe 1M detector is supported by the National Science Foundation under the grant number NSF/DMR-1531283. Use of the Advanced Photon Source, an Office of Science User Facility operated for the U.S. Department of Energy (DOE) Office of Science by Argonne National Laboratory, was supported by the U.S. DOE under Contract No. DE-AC02-06CH11357. Science by Argonne National Laboratory, was supported by the U.S. DOE under Contract No. DE-AC02-06CH11357.

[1] Bruker (2016). *APEX3* (Version 2015.9). Bruker AXS Inc., Madison, Wisconsin, USA.
[2] Bruker (2016) SAINT. Data Reduction Software.
[3] Sheldrick, G. M. (1996). *SADABS. Program for Empirical Absorption Correction.* University of Gottingen, Germany.
[4] Sheldrick, G.M. (2015) Acta Cryst. A71, 3-8
[5] Sheldrick, G.M. (1990) Acta Cryst. A46, 467-473
[6] Sheldrick, G. M. (2008). Acta Cryst. A64, 112-122.
[7] Dolomanov, O.V.; Bourhis, L.J.; Gildea, R.J.; Howard, J.A.K.; Puschmann, H., OLEX2: A complete structure solution, refinement and analysis program (2009). J. Appl. Cryst., 42, 339-341
[8] Sheldrick, Acta Cryst. D66 (2010) 479-485.
[9] Emsley P., Lohkamp B., Scott W.G., Cowtan K., Features and Development of Coot, Acta Cryst. (2010), D66, 486-501.
[10] A.L.Spek, Acta Cryst. 2009, D65, 148-155.
[11] R. W. W. Hooft, L. H. Straver , A. L. Spek J. Appl. Cryst. (2008), 41, 96-103

Table 1 Crystal data and structure refinement for HY_II_164_1.	
Identification code	HY_II_164_1
Empirical formula	$C_{228.75}H_{322.25}BaCl_5N_{46}O_{54}Si_8$

Moiety formula	$[Ba(C_{25}H_{35}N_5O_5Si)_8]^{2+}\cdot 2(C_6H_2N_3O_7)^-\cdot 2.5CH_2Cl_2\cdot 2.375C_6H_{14}$
Formula weight	5119.87
Temperature/K	100(2)
Crystal system	monoclinic
Space group	$P2_1$
a/Å	29.5563(8)
b/Å	30.8599(10)
c/Å	33.3264(10)
α/°	90
β/°	90.621(2)
γ/°	90
Volume/Å^3	30395.4(16)
Z	4
ρ_{calc}g/cm^3	1.119
μ/mm^{-1}	2.304
F(000)	10807.0
Crystal size/mm^3	0.110 × 0.110 × 0.030
Radiation	CuKα (λ = 1.54178)
2Θ range for data collection/°	4.934 to 133.196
Index ranges	-33 ≤ h ≤ 31, -36 ≤ k ≤ 36, -39 ≤ l ≤ 39
Reflections collected	248634
Independent reflections	99409 [R_{int} = 0.0946, R_{sigma} = 0.1128]
Data/restraints/parameters	99409/12490/6432
Goodness-of-fit on F^2	1.022
Final R indexes [I>=2σ (I)]	R_1 = 0.1087, wR_2 = 0.2890
Final R indexes [all data]	R_1 = 0.1506, wR_2 = 0.3340
Largest diff. peak/hole / e Å^{-3}	2.69/-1.02
Flack parameter	0.190(2)

Table 2 Crystal data and structure refinement for HY_III_8_4_8Ph_G_KPF6.	
Identification code	HY_III_8_4_8Ph_G_KPF6
Empirical formula	$C_{216.5}H_{304.75}F_6KN_{48.25}O_{40}PSi_8$
Moiety formula	$8(C_{25}H_{35}N_5O_5Si)K(PF6)8.25(CH_3CN)$
Formula weight	4632.11
Temperature/K	100(2)
Crystal system	orthorhombic
Space group	$P2_12_12$
a/Å	43.3567(17)

b/Å	43.6708(16)
c/Å	14.0917(6)
α/°	90
β/°	90
γ/°	90
Volume/Å^3	26681.5(18)
Z	4
ρ_{calc}g/cm^3	1.153
μ/mm^{-1}	1.202
F(000)	9846.0
Crystal size/mm^3	0.110 × 0.050 × 0.010
Radiation	CuKα (λ = 1.54178)
2Θ range for data collection/°	6.272 to 136.954
Index ranges	-52 ≤ h ≤ 51, -52 ≤ k ≤ 52, -16 ≤ l ≤ 16
Reflections collected	317194
Independent reflections	48890 [R_{int} = 0.1095, R_{sigma} = 0.0568]
Data/restraints/parameters	48890/6703/3715
Goodness-of-fit on F^2	1.033
Final R indexes [I>=2σ (I)]	R_1 = 0.0972, wR_2 = 0.2632
Final R indexes [all data]	R_1 = 0.1203, wR_2 = 0.2889
Largest diff. peak/hole / e Å^{-3}	0.81/-0.56
Flack parameter	0.103(4)

Table 3 Crystal data and structure refinement for HY_II_207_6.

Identification code	HY_II_207_6
Empirical formula	$C_{452.15}H_{656.6}Cl_{6.5}K_2N_{86}O_{94}Si_{16}$
Moiety formula	[16($C_{25}H_{35}N_5O_5Si$)2K] 2($C_6H_2N_3O_7$) ·3.25CH_2Cl_2·6.15C_6H_{14}
Formula weight	9559.06
Temperature/K	100(2)
Crystal system	monoclinic
Space group	P2
a/Å	30.320(3)
b/Å	22.277(2)
c/Å	44.399(4)
α/°	90
β/°	104.4610(14)
γ/°	90
Volume/Å^3	29038(4)

Z	2
ρ_{calc}g/cm^3	1.093
μ/mm^{-1}	0.030
F(000)	10192.0
Crystal size/mm^3	0.050 × 0.040 × 0.005
Radiation	synchrotron (λ = 0.44281)
2Θ range for data collection/°	1.626 to 32.338
Index ranges	-37 ≤ h ≤ 37, -27 ≤ k ≤ 27, -53 ≤ l ≤ 55
Reflections collected	734274
Independent reflections	115388 [R_{int} = 0.0638, R_{sigma} = 0.0664]
Data/restraints/parameters	115388/12939/6719
Goodness-of-fit on F^2	1.039
Final R indexes [I>=2σ (I)]	R_1 = 0.0953, wR_2 = 0.2614
Final R indexes [all data]	R_1 = 0.1101, wR_2 = 0.2830
Largest diff. peak/hole / e Å^{-3}	1.22/-0.73
Flack parameter	0.03(3)

Table 4 Crystal data and structure refinement for HY_93_3_8PHG_Rb.	
Identification code	HY_93_3_8PHG_Rb
Empirical formula	$C_{206.75}H_{280}N_{42}O_{42.75}RbSi_8$
Formula weight	4347.90
Temperature/K	100(2)
Crystal system	orthorhombic
Space group	$P2_12_12$
a/Å	43.381(9)
b/Å	43.722(9)
c/Å	14.181(3)
α/°	90
β/°	90
γ/°	90
Volume/Å^3	26896(9)
Z	4
ρ_{calc}g/cm^3	1.074
μ/mm^{-1}	0.057
F(000)	9222.0
Radiation	synchrotron (λ = 0.41328)
2Θ range for data collection/°	2.064 to 26.662
Index ranges	-48 ≤ h ≤ 48, -48 ≤ k ≤ 48, -15 ≤ l ≤ 15

Reflections collected	346504
Independent reflections	38893 [R_{int} = 0.0882, R_{sigma} = 0.0600]
Data/restraints/parameters	38893/6881/2783
Goodness-of-fit on F^2	2.384
Final R indexes [I>=2σ (I)]	R_1 = 0.1474, wR_2 = 0.3511
Final R indexes [all data]	R_1 = 0.1701, wR_2 = 0.3615
Largest diff. peak/hole / e $Å^{-3}$	0.87/-0.60
Flack parameter	0.157(6)

Table 5 Crystal data and structure refinement for HY-8PhGSrPic.	
Identification code	HY-8PhGSrPic
Empirical formula	$C_{236.35}H_{284}N_{46.61}O_{54}Si_8Sr$
Formula weight	4954.17
Temperature/K	100(2)
Crystal system	monoclinic
Space group	$P2_1$
a/Å	29.4434(14)
b/Å	30.9027(14)
c/Å	33.2881(15)
α/°	90
β/°	90.387(2)
γ/°	90
Volume/$Å^3$	30288(2)
Z	4
$\rho_{calc}g/cm^3$	1.086
μ/mm^{-1}	1.138
F(000)	10441.0
Crystal size/mm^3	0.310 × 0.250 × 0.170
Radiation	CuKα (λ = 1.54178)
2Θ range for data collection/°	4.912 to 108.768
Index ranges	-30 ≤ h ≤ 25, -32 ≤ k ≤ 32, -34 ≤ l ≤ 29
Reflections collected	360882
Independent reflections	71854 [R_{int} = 0.0646, R_{sigma} = 0.0578]
Data/restraints/parameters	71854/16575/6077
Goodness-of-fit on F^2	1.437
Final R indexes [I>=2σ (I)]	R_1 = 0.1308, wR_2 = 0.3310
Final R indexes [all data]	R_1 = 0.1608, wR_2 = 0.3598
Largest diff. peak/hole / e $Å^{-3}$	0.95/-1.37

Flack parameter	0.138(4)

Table 6 Crystal data and structure refinement for HY_III_88_2_CGKPIC.	
Identification code	HY_III_88_2_CGKPIC
Empirical formula	$C_{166.3}H_{168}KN_{40}O_{49.15}S_{5.1}$
Formula weight	3715.97
Temperature/K	100(2)
Crystal system	cubic
Space group	I23
a/Å	56.969(16)
b/Å	56.969(16)
c/Å	56.969(16)
α/°	90
β/°	90
γ/°	90
Volume/Å^3	184889(161)
Z	24
ρ_{calc}g/cm^3	0.801
μ/mm^{-1}	0.016
F(000)	46550.0
Radiation	synchrotron (λ = 0.41328)
2Θ range for data collection/°	2.036 to 21.654
Index ranges	-51 ≤ h ≤ 51, -46 ≤ k ≤ 51, -51 ≤ l ≤ 51
Reflections collected	265353
Independent reflections	24224 [R_{int} = 0.1783, R_{sigma} = 0.0899]
Data/restraints/parameters	24224/5791/2525
Goodness-of-fit on F^2	1.970
Final R indexes [I>=2σ (I)]	R_1 = 0.1286, wR_2 = 0.3204
Final R indexes [all data]	R_1 = 0.1698, wR_2 = 0.3403
Largest diff. peak/hole / e Å^{-3}	0.71/-0.49
Flack parameter	0.11(15)

Table 7 Crystal data and structure refinement for HY_264_1_Ba_0m.	
Identification code	HY_264_1_Ba_0m
Empirical formula	$C_{222.52}H_{296}BaN_{43.76}O_{51.5}Si_8$
Formula weight	4770.02

Temperature/K	100(2)
Crystal system	monoclinic
Space group	$P2_1$
a/Å	28.10(5)
b/Å	36.715(2)
c/Å	29.3334(18)
α/°	90
β/°	98.061(3)
γ/°	90
Volume/Å^3	29964(51)
Z	4
ρ_{calc}g/cm^3	1.057
μ/mm^{-1}	1.898
F(000)	10070.0
Radiation	CuKα (λ = 1.54178)
2Θ range for data collection/°	4.696 to 117.966
Index ranges	-31 ≤ h ≤ 31, -40 ≤ k ≤ 34, -32 ≤ l ≤ 32
Reflections collected	163061
Independent reflections	63603 [R_{int} = 0.0646, R_{sigma} = 0.0825]
Data/restraints/parameters	63603/21808/6115
Goodness-of-fit on F^2	1.299
Final R indexes [I>=2σ (I)]	R_1 = 0.1184, wR_2 = 0.3060
Final R indexes [all data]	R_1 = 0.1504, wR_2 = 0.3391
Largest diff. peak/hole / e Å^{-3}	1.02/-1.31
Flack parameter	0.184(3)

Supplemental References

(1) Shi, X.; Fettinger, J. C.; Davis, J. T. *J. Am. Chem. Soc.* **2001,** *123*, 6738-6739.

(2) Münzel, M.; Szeibert, C.; Glas, A. F.; Globisch, D.; Carell, T. *J. Am. Chem. Soc.* **2011,** *133*, 5186-5189.

(3) Ishiyama, T.; Murata, M.; Miyaura, N. *J. Org. Chem.* **1995,** *60*, 7508-7510.

(4) Mboyi, C. D.; Gaillard, S.; Mabaye, M. D.; Pannetier, N.; Renaud, J.-L. *Tetrahedron* **2013,** *69*, 4875-4882.

(5) Western, E. C.; Daft, J. R.; Johnson, E. M.; Gannett, P. M.; Shaughnessy, K. H. *J. Org. Chem.* **2003,** *68*, 6767-6774.